IERS TECHNICAL NOTE 7

The IERS extragalactic Celestial Reference Frame and its tie with HIPPARCOS

E.F. Arias
Observatorio Astronomico de La Plata / Central Bureau of IERS

M. Feissel
Observatoire de Paris / Central Bureau of IERS

J.-F. Lestrade
Observatoire de Paris / Central Bureau of IERS

December 1991

Central Bureau of IERS - Observatoire de Paris
61, avenue de l'Observatoire
F-75014 PARIS - France

IERS Technical Notes

This series of publications gives technical information related to the IERS activities, e.g. reference frames, excitation of the Earth rotation, computational or analysis aspects, models, etc. It also contains the description and results of the analyses performed by the IERS Analysis Centres for the Annual Report global analysis.

Back issues

No 1 : C. Boucher and Z.Altamimi. The initial IERS Terrestrial Reference Frame.

No 2 : Earth orientation and reference frame determinations, atmospheric excitation functions, up to 1988 (Annex to the IERS Annual Report for 1988). *[No longer available, superseded by N.T. No 5].*

No 3 : D.D. McCarthy (ed). IERS Standards (1989)

No 4 : C. Boucher and Z. Altamimi. Evaluation of the realizations of the Terrestrial Reference System done by the BIH and IERS (1984-1988).

No 5: Earth orientation and reference frame determinations, atmospheric excitation functions, up to 1989 (Annex to the IERS Annual Report for 1989). *[Superseded by N.T. No 8].*

No 6 : C. Boucher and Z. Altamimi. ITRF89 and other realizations of the IERS Terrestrial Reference System for 1989.

No 7 : E.F. Arias, M. Feissel and J.-F. Lestrade. The IERS extragalactic Celestial Reference Frame and its tie with HIPPARCOS.

No 8: Earth orientation and reference frame determinations, atmospheric excitation functions, up to 1990 (Annex to the IERS Annual Report for 1990).

Future issues

No 9 : C. Boucher and Z. Altamimi. ITRF90 and other realizations of the IERS Terrestrial Reference System for 1990.

THE IERS CELESTIAL REFERENCE FRAME AND ITS TIE WITH HIPPARCOS

CONTENTS

	page
IERS Technical Notes	ii
Abstract	2
The celestial system and frame of IERS	3
Introduction	3
Internal consistency and precision of the frame	4
Definition and maintenance of the system	4
Physical properties and observational history of the fiducial objects	6
Precision and consistency of VLBI frames	27
Introduction	27
Analysis of four 1990 extragalactic reference frames	28
Analysis of four 1991 extragalactic reference frames	41
Analysis of RSC(IERS) 91 C 01	46
Comparison of two methods of combination	50
Connection of the Hipparcos frame	59
The Hipparcos mission	59
Link objects between the Hipparcos and VLBI frames	59
Modelling of the link	60
Simulation of Hipparcos data	63
Accuracy of the link	66
Conclusion	70
References	72

ABSTRACT

This Technical Note gives a presentation of analyses of VLBI extragalactic reference frames performed in the framework of the International Earth Rotation service (IERS), in the course of the maintenance of its conventional celestial frame. These studies are a part of the global analysis of celestial frames, terrestrial frames and Earth orientation made at the Central Bureau of IERS. They are based on results obtained by the Jet Propulsion Laboratory (JPL), the NASA Goddard Space Flight Center (GSFC), the NOAA National Geodetic Survey (NGS), and the US Naval Observatory (USNO), as a part of programs of observation and analysis of Earth rotation, crustal dynamics, deep space navigation, astrometry.

In Section 1 the definition of the IERS celestial reference system and its relationship with the 1991 IAU Resolution A4 on Reference Systems are described. The 1991 realization of the IERS celestial reference system, RSC(IERS) 91 C 01, is studied in terms of internal consistency and precision. Finally the physical properties and the observational history of the 396 extragalactic objects it contains are analysed in some detail.

Section 2 is devoted to the comparison of celestial frames obtained from independent observation programs by GSFC, JPL, NGS and USNO. Two sets of four catalogues ("1990" and "1991") are compared under complementary viewpoints. The catalogues available in 1990 are analysed considering only the 39 objects common to the four data sets; the dependence on geometrical and physical parameters of the discrepancies of coordinates for the same object in the various frames is studied. It is shown that outside the regions of the sky where the network geometry induces slight deformations, the uncertainty on the coordinates is ±0.0002". The regional deformations are further studied with the 1991 versions of the frames derived by the same four institutes.

Section 2 is concluded by the description of the combination algorithm by which the IERS Celestial Reference Frame is maintained, and a comparison with a frame recently compiled by JPL from a combination at the level of the observations.

Section 3 gives an estimation of the expected accuracy of the link of the Hipparcos frame to an extragalactic frame and its time evolution based on VLBI observations of radio stars.

1 - THE CELESTIAL SYSTEM AND FRAME OF IERS

Introduction

The celestial reference frame of IERS is based on the positions of compact extragalactic objects measured by VLBI. It is maintained on the basis of the analyses of several observation programs for the study of Earth rotation, crustal deformations, astrometry, and for deep space navigation. We present hereafter its latest realization, which is a combination of the individual frames obtained independently by two groups. The GSFC frame (Ma *et al.*, 1991), includes 334 objects observed with various networks: the International Radio Interferometric Surveying (IRIS), the NASA Crustal Dynamic Project (CDP), the Navy VLBI Network (NAVNET), and in the Naval Research Laboratory (NRL) reference frame program. The JPL frame (Steppe *et al.*, 1991) gives the positions of 241 objects observed with Deep Space Network. The two frames have 179 objects in common. The combination is based on a three rotation angle model applied to a selection of radio sources common to the individual frames. The initial definition of the system and the maintenance process is described by Arias and Feissel (1990); the connection to the conventional terrestrial system of IERS at the level of 0.001" is studied by Feissel (1991).

The distribution on the sky of the latest realization (IERS, 1991) of the IERS celestial reference system is shown on figure 1; the declination interval covered is from -84° to +85°.

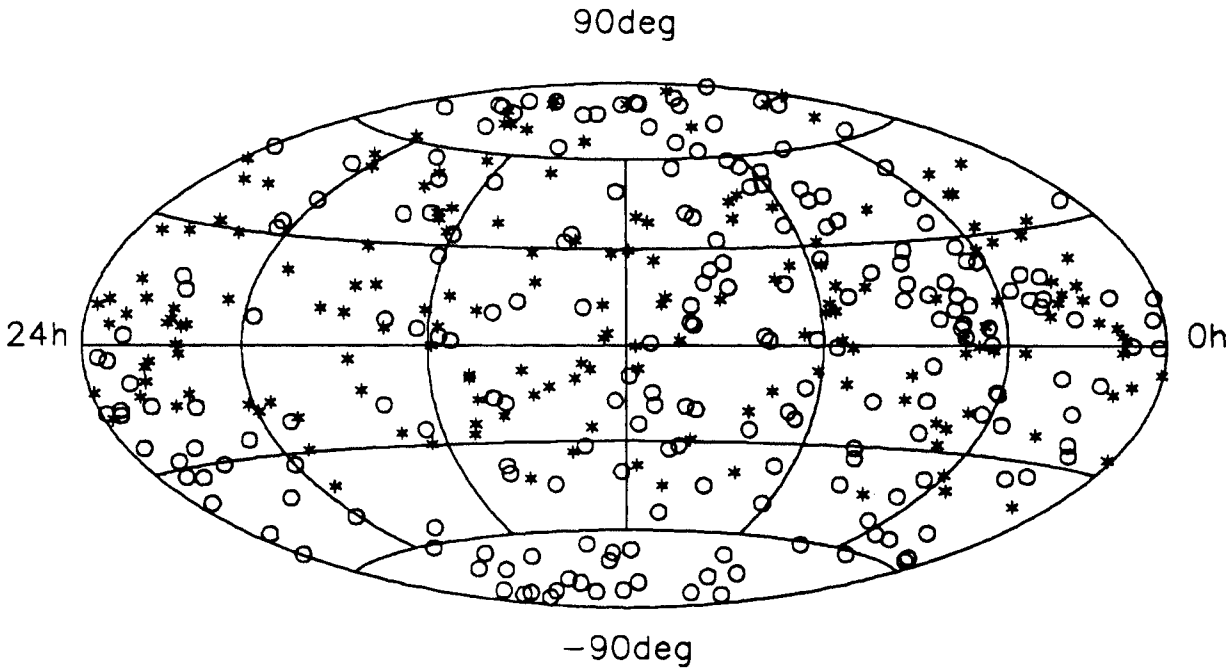

Figure 1. Distribution of the 396 extragalactic radio sources of RSC(IERS)91 C 01. The asterisks show the objects observed independently in two programs (DSN, and IRIS/CDP/NAVNET/NRL).

The observational history and the physical properties of the sources are described in section 2, this volume. The redshifts span the interval 0.1-2.5 quite evenly. The total flux is in general over 1 Jansky. The spectral indices are between -0.8 and +1.4. The distribution in optical magnitudes has a peak around the 18th magnitude. A part of the IERS sources has been mapped at S and X bands (e.g. Charlot 1990). The primary sources mapped show no significant structure at the angular scale of 0.001".

Internal consistency and precision of the frame

It is well known that the use of the conventional IAU 1976 Precession and IAU 1980 Theory of Nutation in the analysis of VLBI observations would give rise to systematic errors in the source positions, and to misorientation of the axes of the frames, both at the level of a few milliarcseconds. Therefore the common practice in catalogue work is to estimate additional parameters which describe the motion of the celestial pole relative to its conventional position, either by estimating celestial pole offsets for each session, or by estimating a precession correction and the residual amplitudes of some of the nutation terms, as allowed by the length and time density of the series of observations analysed. Sovers (1991a) studies in detail the effects of these procedures on the resulting source positions. In the combination performed by the Central Bureau of IERS, only individual frames obtained by one of these procedures are used. The slight offsets between the poles of the catalogues, that are due to inconsistent fixing of the celestial pole offsets at some reference day, are accounted for by the adjustment of rotation angles; they have no influence on the consistency of the individual frames with the combined one.

The noticeably different network geometries of the various observing programs are expected to cause regional deformations in the derived celestial frames. From detailed comparisons of large JPL and GSFC catalogues, Sovers (1990) concludes that the only systematic difference between the two catalogues is an increase of right ascension differences for lower declinations, amounting to 0.001" to 0.002" over the entire range of declinations.

A detailed analysis of the internal consistency and precision of the frame is given in section 2, this volume.

Definition and maintenance of the system

The IERS celestial reference system is barycentric through the appropriate modelling of observations by the analysis centres which contribute individual catalogues. The condition that the sources have no proper motion is also applied by the analysis centres; however, checks are regularly performed to insure the validity of this constraint (Ma and Shaffer, 1991) to avoid spurious motions of some sources.

The direction of the axes of the IERS celestial reference system is illustrated on Figure 2, which represents estimated positions of the FK5 and IERS polar axes relative to the mean celestial pole at J2000.0, and estimated relative positioning of the FK5 and IERS right ascension origins. The estimated parameters are rotation angles A_1, A_2, A_3, around three axes in the directions $\alpha = 0^h$, $\delta = 0$; $\alpha = 6^h$, $\delta = 0$; $\delta = 90°$. A_1, A_2 are plotted in a plane tangent to the celestial sphere at the celestial pole; A_3 is plotted in a plane tangent to the celestial sphere in the vicinity of the equinox.

The Ox axis was implicetely defined in the initial realization (Arias *et al.*, 1988b) by the adoption of the right ascensions of 23 radio sources in catalogues obtained by the GSFC, the JPL, and the NGS. These catalogues had been compiled by fixing the right ascension of 3C273B to the usual (Hazard *et al.* 1971) conventional FK5 value (12h 29m 6.6997s at J2000.0). The figure shows the positions of the IERS and FK5 origins relative to the dynamical equinox at J2000.0. The uncertainty on the FK5 origin of right ascensions is derived from the quadratic sum of the accuracies given by Fricke, (1982) (±0.045") and Schwann, (1988) (±0.07"/cy), considering a mean epoch of

1955 for the proper motions in right ascensions. Comparing VLBI and LLR Earth orientation and terrestrial frames shows that the IERS origin of right ascensions is consistent with the dynamical equinox of the JPL ephemeris DE200 within 0.01" (Finger and Folkner 1992, Charlot 1991).

The Oz axis points in the direction to the mean pole at J2000.0 as defined by the IAU conventional models for precession and nutation. As a result of the inaccuracy of the conventional models, the Oz axis of the IERS celestial system is shifted from the expected position of the mean pole at J2000.0 by about 0.01" in longitude sin ε and 0.001" in obliquity. In the figure, the coordinate axes are centered at the mean celestial pole at J2000. P_{IERS} is an estimation of the IERS polar axis derived from VLBI analyses (e.g. Steppe *et al.*, 1991); the various VLBI estimations agree within a few milliarcseconds (radius of the circle around P_{IERS}). The area of probable position of the FK5 pole is obtained by first considering that the systematic part is dominated by a correction of -0.25"/cy to the precession constant imbedded in the FK5 System, and second by adopting Fricke's (1982) estimation of the accuracy of the FK5 equator (±0.02"), and Schwan's (1988) estimation of the limit of the residual rotation (±0.07"/cy), taking the epochs of observations from Fricke *et al.*, (1988). If one assumes that the error in the precession rate is absorbed by the proper motions of stars, the circle has to be centered at P_{J2000}, keeping the same radius.

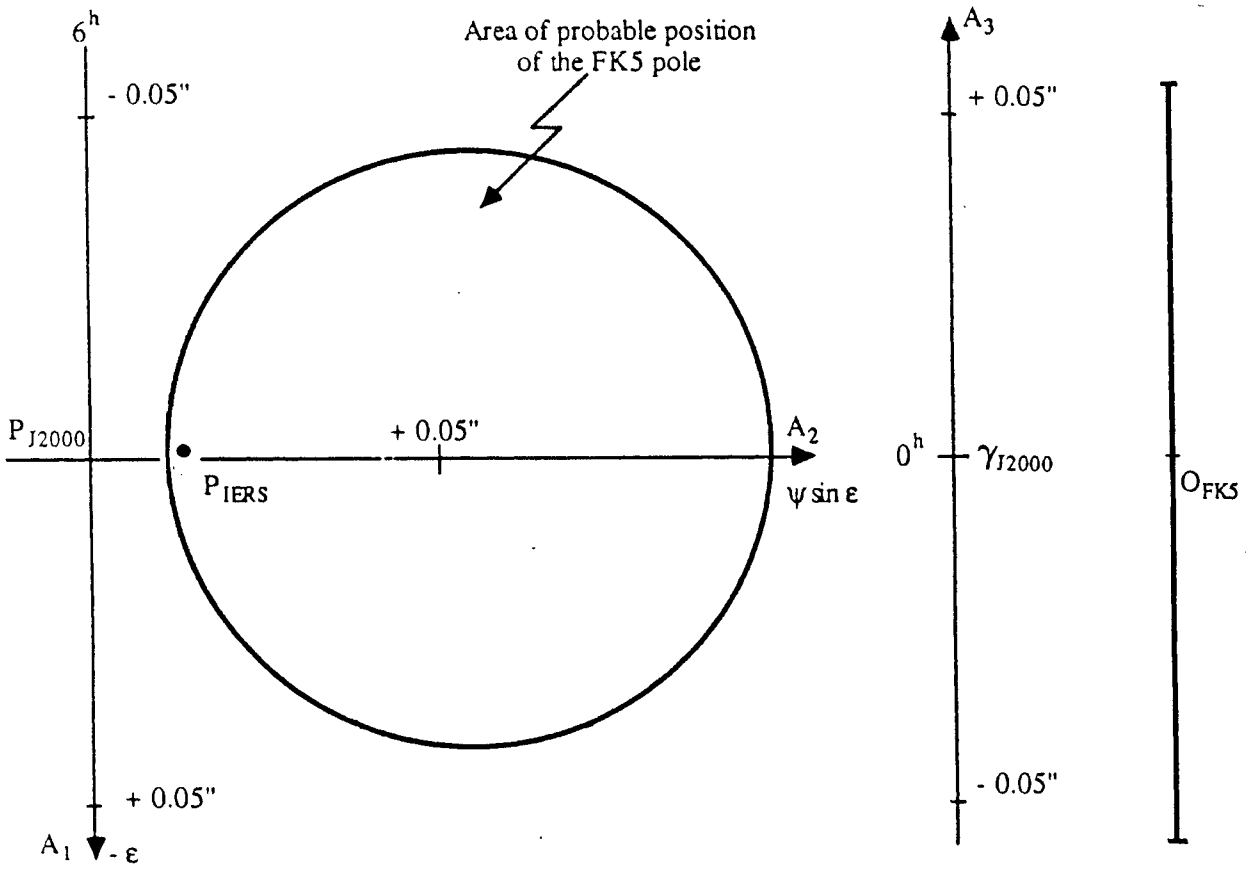

Figure 2. Direction of the axes of the IERS and FK5 celestial systems relative to the mean pole and equinox at J2000.0.

The new astrometric techniques and the availability of large computers used to analyze data raise the question of how one should understand the conventional character of the celestial frame. In practice, it can be understood in two ways:

- the source coordinates themselves are considered conventional, *i.e.*, their numerical values are fixed for some time (years); this is the FKn philosophy,

- the axes of the system are considered conventionally as fixed to their initial directions, but improved or additional source coordinates available at the time of analysis are provided to the users; this is required for space navigation, Earth orientation programs, geodetic applications, linkage of celestial frames, etc. The system maintenance method applied by the Central Bureau of IERS is along these lines; it should be mentioned that such a procedure is made possible by the high model standardization in the operation of IERS, and by the fact that the implementation of an extragalactic celestial frame implies much less geophysical and astronomical modelling than does the FK series of catalogues. This approach was also retained in the IAU resolutions on reference systems, adopted in August 1991 (see Table 1).

New realizations of the IERS celestial reference system are produced whenever justified by the progress in the observations or in the modelling. The successive realizations produced up to now have maintained the initial definition of the axes within 0.0001"; the coordinates of the 57 primary sources have changed by less than 0.0006" (rms).

At its 1991 General Assembly, the International Astronomical Union has made recommendations on the future conventional celestial system for astronomical research, listed in Table 1. The analyses of the IERS celestial system presented in section 2, this volume, and of its tie with the HIPPARCOS celestial frame (section 3) should help to make clear the contribution of IERS to the future conventional celestial reference system.

Physical properties and observational history of the fiducial objects

The physical properties of the 396 radio sources in RSC(IERS)91 C 01 can be investigated on the basis of a VLBI survey published by Preston *et al.* (1985). The survey was conducted by performing 2.29 GHz VLBI observations over the full sky. The result is a catalogue of 1398 objects with the following information : redshift, total flux, spectral index, optical identification and visual magnitude. The characteristics of the IERS sources are listed in Tables 2 (p. 10) and 3 (p. 14), together with the numbers of observations and formal uncertainties of the coordinates.

Figures 3a through 3d (pages 19-22) show the histograms of the optical identifications, visual magnitudes, redshifts and total radio flux of sources in the last realisation of IERS celestial reference frame.

The distribution of visual magnitudes of IERS objects (Figure 3b, Table 5) is similar to the one in the survey, with a peak around the 18th magnitude. The total radio fux (Figure 3c, Table 6) is in general over 1 Jansky, while the survey has a larger proportion of weaker radio sources. The redshifts (Figure 3d, Table 7) are quite evenly distributed in the interval 0.1-2.5.

Table 1. IAU Resolution A4: recommendations VI and VII from the Working Group on Reference Systems (1991)

RECOMMENDATION VI

considering,

the desirability of implementing a conventional celestial barycentric reference system based upon the observed positions of extragalactic objects, and,

noting,

the existence of tentative reference frames constructed by various institutions and combined by the International Earth Rotation Service (IERS) into a frame used for Earth rotation series,

recommends,

1. that intercomparisons of these frames be extensively made in order to assess their systematic differences and accuracy,
2. that an IAU Working Group consisting of members of Commissions 4, 8, 19, 24, 31 and 40, the IERS, and other pertinent experts, in consultation with all the institutions producing catalogs of extragalactic radio sources, establish a list of candidates for primary sources defining the new conventional reference frame, together with a list of secondary sources that may later be added to or replace some of the primary sources, and,

requests,

1. that such a list be presented to the XXIInd General Assembly (1994) as a part of the definition of a new conventional reference system,
2. that the objects in this list be systematically observed by all VLBI and other appropriate astrometric programs.

Note for Recommendation VI

This recommendation essentially describes the first part of the work that must be done to prepare the realization of the reference system defined by Recommendations I and II. The choice of objects must be made in the first place by considering their observability by VLBI, but special care should be taken to include a large proportion of extragalactic radio sources with well identified optical counterparts.

Table 1. (cont.)

RECOMMENDATION VII

considering,

a) that the new conventional celestial barycentric reference frame should be as close as possible to the existing FK5 equator and equinox and the dynamical equinox which are referred to J2000.0,

b) that it should be accessible to astrometry in visual as well as in radio wavelengths,

recommends,

1. that the principal plane of the new conventional celestial reference system be as near as possible to the mean equator at J2000.0 and that the origin in this principal plane be as near as possible to the dynamical equinox of J2000.0,

2. that the positions of the extragalactic objects selected in accordance with Recommendation VI and representing the reference frame be computed initially for the equator and equinox J2000.0 using the best available values of the celestial pole offset with respect to the IAU expressions for precession and nutation,

3. that a great effort be made to compare reference frames of all types, in particular the FK5, solar system and extragalactic reference frames,

4. that observing programs be undertaken or continued in order to relate planetary positions to radio and optical objects, and to determine the relationship between catalogs of extragalactic source positions and the best catalogs of star positions, in particular the FK5 and Hipparcos catalogs.

Table 1. (cont.)

Notes for Recommendation VII

1. *This recommendation specifies the choice of the coordinate axes that will be adopted in the final reference frame and describes the work to be done before such a frame can be constructed. Although the considerations call for visual and radio wavelengths for the primary catalog, other observable wavelengths are not excluded. Positions of objects observed in other wavelengths should also be referred to the same system.*

2. *The objective set by this recommendation is that there should be no discontinuity in the positions of stars when the present FK5 frame is replaced by the extragalactic reference frame. This means that the position of the extragalactic objects should be in the FK5 system for J2000.0. It is acknowledged that the best values of precession and nutation must be used in order to avoid introducing spurious proper motions into the positions of extragalactic objects. The final transfer to the preferred equinox and principal plane will be done by applying a rotation at J2000.0.*

3. *The dynamical equinox in this recommendation is defined as the intersection of the mean equator and the ecliptic. The latter is defined as the uniformly rotating plane of the orbit of the Earth-Moon barycenter averaged over the entire period for which the ephemerides are valid. Since it is ephemeris dependent, the choice of the equinoctial point will be made using the most accurate and generally available ephemerides of the solar system at the time.*

4. *The definition given to the reference system by Recommendations I and II implies the stability in time of the system of coordinates realized by the celestial reference frame. The directions of the coordinate axes should not be changed even if at some later date the realization of the dynamical equinox or CEP are improved. Similarly, modifications to the set of extragalactic objects realizing the reference system should be made in such a way that the directions of the axes are not changed. This means that once the coordinate axes have been specified, in the way described in the first part of the recommendation, the connection between the definition of the conventional reference system and the peculiarities of the Earth's kinematics will have been severed.*

5. *As long as the relationship between the optical and the extragalactic radio frames is not sufficiently accurately determined, the FK5 catalog shall be considered as a provisional realization of the celestial reference system in optical wavelengths.*

Table 2. Characteristics of the objects in the IERS Celestial Reference Frame. Objects observed by at least two programs.

OBJECT	Tp (1)	Redsh.	Flux (Jy)	SP	m_v	GSFC soln Nobs	JPL soln Nobs	IERS σ_α (2)	IERS σ_δ (3)
0003-066	G	0.347	1.69	0.0	19.7	12	3	0.49	13.28
0008-264	Q	1.096	0.58	0.3	19.0	8	40	0.97	0.68
0016+731	Q	-	1.50	0.2	18.2	1583	11	0.81	0.24
0048-097	B	-	1.30	0.8	17.3	694	25	0.16	0.31
0104-408	Q	-	-	0.6	19.0	65	119	0.19	1.11
0106+013	Q	2.107	3.90	0.5	18.4	16716	273	0.16	0.27
0111+021	A	0.047	-	-0.2	16.5	46	37	1.00	1.28
0112-017	Q	1.365	-	-0.2	17.4	44	37	0.13	0.60
0113-118	Q	0.670	-	0.1	18.3	3	67	8.74	2.00
0119+041	Q	0.637	0.90	-0.1	19.5	5206	31	0.16	0.30
0133+476	Q	0.860	2.10	0.5	18.0	654	192	0.21	0.24
0146+056	Q	2.345	-	0.8	19.0	17	13	0.22	1.70
0149+218	Q	1.320	1.40	-0.2	18.0	55	15	0.10	0.59
0201+113	G	-	1.30	0.0	19.5	100	18	0.21	0.38
0202+149	Q	-	3.20	-0.4	21.9	1069	135	0.12	0.80
0202+319	Q	1.466	1.60	0.1	18.0	81	3	0.37	0.52
0212+735	Q	-	2.30	-0.1	19.0	30517	374	2.64	1.08
0224+671	Q	-	1.20	0.3	19.5	741	223	2.06	1.20
0229+131	Q	2.065	2.00	-0.5	17.7	14699	30	0.16	0.24
0234+285	Q	1.207	-	-	18.5	16667	472	0.17	0.24
0235+164	Q	0.524	2.10	0.6	19.0	1128	307	0.16	0.24
0237-233	Q	2.223	-	-0.7	16.6	26	3	1.83	8.83
0239+108	Q	-	1.80	0.0	20.0	28	83	0.07	0.93
0256+075	A	-	0.70	0.7	18.0	39	33	0.23	0.22
0300+470	L	-	-	-	18.0	10938	347	0.19	0.24
0309+411	G	-	0.60	0.1	18.0	13	12	0.93	0.22
0316+413	A	0.017	24.80	1.0	12.0	592	38	1.22	1.97
0326+277	Q	1.533	-	-	-	11	10	0.61	0.07
0332-403	Q	1.445	-	0.5	18.5	18	49	0.10	0.14
0333+321	Q	1.258	2.30	-	17.5	84	124	0.25	0.30
0336-019	Q	0.852	2.70	0.4	18.4	223	75	0.16	0.28
0400+258	Q	2.109	1.40	0.0	18.0	47	8	0.71	0.38
0402-362	Q	1.417	-	0.5	17.2	94	121	1.23	0.07
0406+121	Q	-	-	0.5	22.0	15	97	0.13	0.64
0420-014	Q	0.915	1.00	0.3	17.8	12466	500	0.16	0.25
0430+052	A	0.033	6.40	0.1	15.0	119	44	0.69	0.41
0434-188	B	2.702	1.30	0.3	20.0	150	108	0.18	0.30
0440-003	Q	0.850	-	-0.5	19.2	45	16	0.12	1.17
0451-282	Q	2.560	2.30	0.1	19.0	5	20	1.82	0.39
0454-234	Q	1.009	-	0.3	18.5	3429	3	0.95	8.70
0458-020	Q	2.286	2.00	0.1	18.4	160	3	2.47	5.13
0500+019	-	-	2.00	-0.5	-	20	13	0.62	0.24
0454+844	Q	-	1.30	0.3	16.5	32	84	16.12	0.43
0511-220	Q	-	1.30	0.1	19.5	5	11	2.12	0.73
0528+134	Q	-	-	0.5	20.0	20694	148	0.16	0.24

Table 2. (cont.)

OBJECT	Tp (1)	Redsh.	Flux (Jy)	SP	m_v	GSFC soln Nobs	JPL soln Nobs	IERS σ_α (2)	IERS σ_δ (3)
0537-441	Q	0.894	-	0.1	15.5	88	147	2.29	0.49
0552+398	Q	2.365	3.40	-	18.0	42112	724	0.16	0.24
0605-085	Q	-	-	0.2	18.0	61	16	0.02	1.25
0607-157	Q	0.324	1.00	-0.4	18.0	7	13	0.21	3.31
0657+172	-	-	-	-	-	175	25	0.60	1.42
0723-008	Q	0.127	2.10	-0.4	18.0	72	82	0.14	1.42
0727-115	-	-	-	0.1	-	5948	632	0.17	0.28
0735+178	L	-	2.00	0.1	14.9	84	97	0.41	1.23
0736+017	Q	0.191	2.90	-0.1	16.5	69	22	0.24	1.79
0738+313	Q	0.635	1.90	0.2	17.0	118	17	2.27	3.32
0742+103	-	-	3.90	-0.1	-	3918	336	0.16	0.26
0745+241	Q	-	-	0.5	19.0	304	54	0.46	1.38
0748+126	Q	0.889	2.00	0.5	17.8	25	68	0.38	2.23
0754+100	L	-	-	0.2	14.5	27	16	0.46	1.31
0805-077	Q	-	1.10	-0.4	19.5	19	10	0.35	2.04
0814+425	Q	-	1.60	-0.4	18.5	888	162	0.19	0.26
0823+033	Q	-	1.42	0.9	18.0	695	213	0.16	0.26
0827+243	Q	0.939	1.30	-	17.5	19	18	0.26	1.53
0836+710	Q	-	4.40	-0.3	16.5	39	17	2.58	2.65
0851+202	L	0.306	-	1.3	14.0	31084	573	0.16	0.25
0859-140	Q	1.327	2.90	-0.4	16.6	17	21	0.81	3.00
0859+470	Q	1.402	2.20	-0.1	18.7	223	42	0.48	1.59
0917+449	Q	2.180	-	0.6	19.0	16	2	1.43	0.21
0920-397	Q	-	2.10	-0.2	19.0	17	6	1.69	1.45
0923+392	Q	0.699	4.20	1.0	17.8	36367	532	0.16	0.24
0925-203	Q	0.348	-	-0.2	16.4	19	12	1.40	1.18
1004+141	Q	2.707	0.81	-0.1	19.0	18	18	0.53	1.38
1034-293	L	-	1.30	0.5	18.0	1654	217	0.73	2.46
1055+018	Q	0.890	2.87	0.4	18.0	3606	356	0.16	0.27
1104-445	Q	1.598	-	0.1	18.2	123	141	0.36	0.33
1111+149	Q	0.869	-	0.1	18.0	37	25	0.14	1.00
1116+128	Q	2.118	1.74	-0.3	19.3	19	11	0.07	1.70
1123+264	Q	2.341	0.70	-	17.5	234	137	0.16	0.25
1128+385	Q	-	0.90	-0.2	16.0	26	84	0.12	1.33
1144+402	Q	-	0.90	-0.2	18.5	1816	3	0.23	0.34
1144-379	Q	-	-	1.2	16.2	29	222	0.58	0.72
1145-071	Q	-	0.97	0.2	18.5	11	13	0.45	0.48
1148-001	Q	1.982	2.51	-0.4	17.6	41	25	0.98	1.40
1150+812	Q	-	1.20	-0.1	18.5	173	5	2.53	1.99
1156+295	Q	0.729	1.30	-	15.6	3759	1	0.23	0.34
1219+285	L	-	1.47	-	16.5	108	1	0.55	1.61
1222+037	Q	0.957	0.96	0.1	19.0	93	60	0.21	0.48
1226+023	Q	0.158	-	0.0	12.9	17252	296	0.23	0.29
1228+126	G	- 4	-	-0.6	9.6	31	16	0.93	1.21
1243-072	Q	0.267	0.72	0.6	18.0	20	14	0.38	0.93

Table 2. (cont.)

OBJECT	Tp (1)	Redsh.	Flux (Jy)	SP	m_v	GSFC soln Nobs	JPL soln Nobs	IERS σ_α (2)	IERS σ_δ (3)
1244-255	Q	0.633	1.36	0.9	17.0	62	121	1.48	2.06
1253-055	Q	0.538	11.80	0.4	17.8	1506	155	1.04	2.49
1302-102	Q	0.286	1.03	0.1	14.9	12	19	0.44	0.64
1308+326	L	0.996	-	-	19.0	4620	304	0.16	0.26
1313-333	Q	2.210	1.23	0.5	20.0	47	49	0.43	1.60
1334-127	Q	-	1.94	0.2	18.5	3089	272	0.19	0.32
1342+662	Q	-	-	0.1	20.0	11	35	2.84	0.98
1342+663	Q	-	-	0.1	18.8	44	171	2.19	1.61
1354+195	Q	0.720	1.80	-0.1	16.0	901	151	0.16	0.29
1354-152	Q	-	1.17	0.1	18.5	148	20	1.32	2.37
1404+286	G	0.077	1.70	0.9	14.0	24885	22	0.20	0.31
1406-076	Q	1.494	1.30	0.2	20.0	10	11	0.71	0.81
1418+546	L	-	1.00	0.4	14.5	1499	237	0.23	0.29
1424-418	Q	0.308	2.22	0.7	17.5	93	1	33.88	12.02
1435-218	Q	1.194	-	0.2	17.9	3	1	1.42	50.70
1502+106	Q	1.833	2.03	0.6	19.5	6411	193	0.16	0.31
1504+377	-	-	1.10	0.2	-	11	3	5.43	4.00
1504-166	Q	0.876	2.20	-0.4	18.5	31	64	0.86	2.00
1510-089	Q	0.361	3.14	0.3	16.5	697	253	0.19	0.32
1511-100	Q	-	0.88	0.4	18.5	19	16	1.05	0.46
1514-241	L	0.049	1.90	-0.1	15.0	14	10	1.17	0.96
1519-273	Q	-	0.99	0.2	18.5	61	189	0.22	0.47
1538+149	L	-	1.50	-	15.5	22	2	0.19	5.76
1548+056	Q	-	2.28	0.3	18.0	4241	23	0.19	0.32
1555+001	Q	1.770	0.58	0.2	19.3	57	101	0.09	0.13
1606+106	Q	-	1.00	1.1	18.5	32	2	0.07	14.54
1611+343	Q	1.401	-	0.1	17.5	7671	110	0.16	0.30
1624+416	-	-	1.50	-0.3	-	23	1	4.39	14.54
1622-297	-	-	2.20	0.2	-	24	1	2.75	4.51
1633+382	Q	1.814	2.10	0.8	18.0	8075	214	0.17	0.30
1637+574	Q	0.745	1.40	0.4	17.0	2746	4	2.27	0.07
1638+398	Q	-	1.10	0.1	18.5	412	129	1.21	0.24
1642+690	Q	-	1.70	-0.1	20.5	1478	6	3.24	0.03
1641+399	Q	0.595	7.60	0.4	16.0	27450	468	0.16	0.30
1656+053	Q	0.879	1.61	0.5	16.5	143	22	0.32	0.35
1657-261	-	-	1.10	-0.2	-	46	43	1.31	0.55
1717+178	Q	-	1.00	0.6	18.5	19	26	0.01	0.16
1730-130	Q	0.902	-	-0.1	18.5	3250	275	0.19	0.33
1738+476	Q	-	0.92	0.1	17.5	23	97	1.47	0.49
1739+522	Q	1.375	-	0.6	18.5	10064	6	0.22	0.33
1741-038	Q	-	5.60	0.3	18.5	12475	285	0.18	0.32
1743+173	Q	1.725	0.90	0.1	19.5	21	1	0.37	3.86
1749+701	L	0.760	1.10	0.3	17.0	41	115	2.81	0.62
1749+096	L	-	1.07	-0.2	17.0	2735	55	0.18	0.32
1751+288	Q	-	1.10	-	20.0	41	1	3.88	9.61

Table 2. (cont.)

OBJECT	Tp (1)	Redsh.	Flux (Jy)	SP	m_v	GSFC soln Nobs	JPL soln Nobs	IERS σ_α (2)	IERS σ_δ (3)
1803+784	G	-	2.60	0.3	13.0	37196	21	6.71	0.74
1807+698	A	0.050	3.10	-0.3	14.2	41	253	3.81	0.42
1821+107	Q	1.360	-	0.5	16.0	65	47	0.33	0.50
1845+797	A	0.057	7.30	-0.6	15.0	29	5	10.48	1.00
1908-201	-	-	2.30	-	-	11	35	0.39	2.22
1921-293	Q	0.352	-	-	17.5	3098	165	1.76	0.31
1923+210	-	-	-	-	-	157	44	0.29	0.81
1928+738	Q	0.360	3.00	0.0	15.5	596	9	3.84	0.90
1933-400	Q	-	-	0.3	19.0	15	9	2.06	0.79
1936-155	Q	1.657	1.30	0.2	19.4	1	16	1.02	1.46
1954+513	Q	1.230	1.40	-0.1	18.5	156	5	0.80	1.36
1958-179	Q	0.650	1.12	0.1	17.5	270	129	0.20	0.33
2008-159	Q	1.180	0.60	1.0	18.0	24	24	0.20	2.31
2021+614	Q	-	2.26	0.1	19.0	34	115	1.20	1.04
2030+547	-	-	1.40	-	-	25	17	1.28	1.76
2029+121	Q	-	1.10	0.7	18.5	30	33	0.22	1.25
2113+293	Q	-	1.12	-	19.5	182	100	0.19	0.30
2121+053	Q	1.878	2.47	1.1	17.5	12494	36	0.18	0.31
2128+048	-	-	-	-0.5	-	10	1	1.37	39.87
2128-123	Q	0.501	1.69	0.1	16.0	339	26	0.18	0.32
2131-021	L	0.557	2.20	0.2	19.0	18	32	0.09	1.29
2134+004	Q	1.936	6.50	0.8	18.0	8594	121	0.64	0.92
2144+092	Q	-	0.78	0.2	18.6	100	1	0.21	4.52
2145+067	Q	0.990	3.10	0.5	16.5	3670	307	0.16	0.30
2149+056	-	-	1.06	0.3	-	19	78	0.64	1.91
2155-152	L	-	1.80	0.1	17.5	81	53	0.79	0.57
2200+420	L	0.070	4.20	-0.1	14.5	20559	192	0.20	0.27
2201+315	Q	0.297	2.02	0.2	14.5	159	3	0.27	4.55
2216-038	Q	0.901	1.62	0.7	16.4	6564	96	0.19	0.32
2223-052	Q	1.404	5.20	0.2	18.4	28	93	0.27	0.85
2227-088	Q	1.562	1.30	0.5	18.0	15	20	0.07	1.49
2230+114	Q	1.037	-	-0.5	17.3	736	132	0.16	0.29
2234+282	Q	0.795	0.91	-	19.0	10436	166	0.18	0.28
2243-123	Q	0.630	-	-0.2	17.3	82	130	0.19	0.34
2251+158	Q	0.859	10.50	0.8	16.1	19520	263	0.18	0.29
2253+417	Q	1.476	1.50	-0.3	18.8	104	57	0.21	1.12
2254+074	L	-	0.88	0.9	16.5	37	14	0.19	0.62
2318+049	Q	0.633	-	-0.2	19.0	50	31	0.34	1.46
2319+272	G	0.120	1.10	-	15.5	23	3	0.29	0.70
2328+107	Q	1.498	1.05	-0.1	18.1	57	2	0.09	0.73
2344+092	Q	0.677	1.90	-0.2	16.0	20	3	0.17	0.26
2345-167	Q	0.600	-	1.3	18.0	626	74	0.21	0.32
2351+456	G	-	-	-0.1	19.9	18	1	16.50	11.39
2355-106	Q	-	-	0.5	18.0	106	42	0.01	0.71

(1) Type of object: Q :Quasar; G: Galaxy; L: BL Lac; B: Blue object; A: Other.
(2) Unit: 0.0001s
(3) Unit: 0.001"

Table 3. Characteristics of the objects in the IERS Celestial Reference Frame.
Objects observed by one program.

OBJECT	Tp (1)	Redsh.	Flux (Jy)	SP	m_v	GSFC solution Nobs	σ_α (2)	σ_δ (3)	JPL solution Nobs	σ_α (2)	σ_δ (3)
0007+106	Q	0.089	-	-	15.4	19	0.5	0.9			
0013-005	A	-	-	-	19.8				15	0.2	0.5
0014+813	Q	-	1.00	-0.2	16.5	13	29.1	0.6			
0019+058	Q	-	-	0.2	19.5				52	0.3	0.8
0026+346	Q	-	1.80	-0.3	-	22	1.4	1.5			
0047-579	Q	1.797	-	0.4	18.5	2	1.9	3.3			
0056-572	Q	-	-	0.5	18.0	1	7.9	10.5			
0056-001	Q	0.720	2.20	-0.4	17.3	26	0.5	1.5			
0118-272	Q	-	1.00	0.2	16.5	9	0.9	0.6			
0119+115	G	-	1.80	0.3	19.0				29	0.2	0.3
0135-247	Q	0.831	1.49	0.4	16.9	21	0.5	0.3			
0138-097	Q	-	0.90	0.9	18.0	18	0.5	0.4			
0150-334	Q	0.610	1.00	-0.1	16.5	11	0.9	0.7			
0153+744	Q	-	2.10	-0.3	16.0	38	4.6	0.4			
0159+723	-	-	-	0.2	-	20	4.9	0.6			
0202-172	Q	1.740	1.20	0.0	18.0	26	0.4	0.3			
0208-512	Q	1.003	-	-0.2	17.5	139	0.3	0.2			
0220-349	-	-	-	0.0	-	18	0.7	0.4			
0221+067	Q	-	1.40	0.4	20.0				11	0.3	0.4
0230-790	Q	-	-	0.5	18.5	5	26.3	4.7			
0238-084	A	- 5	-	1.5	12.0	25	0.6	0.8			
0241+622	Q	0.044	-	-	15.7	3	21.5	7.0			
0252-549	Q	0.537	-	0.1	18.0	1	1.5	11.5			
0250+178	Q	-	-	0.2	18.5				12	0.4	1.0
0259+121	-	-	-	-	-				1	6.1	64.8
0306+102	L	-	1.30	0.7	20.0				14	0.3	0.4
0308-611	Q	-	-	0.7	18.5	45	1.3	0.4			
0317+188	G	-	-	-0.1	19.0				11	0.2	0.3
0319+121	Q	-	1.40	-0.3	19.0	29	0.3	0.8			
0334-546	Q	-	-	0.2	20.0	1	11.7	12.6			
0338-214	Q	0.048	-	0.2	18.0	16	0.7	0.4			
0342+147	-	-	-	-	-				28	0.3	0.5
0355+508	-	-	6.80	1.0	-	4934	0.2	0.1			
0403-132	Q	0.571	4.00	0.1	17.2	12	0.4	0.4			
0406-127	Q	1.563	-	0.1	18.5				9	0.2	0.5
0409+229	Q	1.213	1.70	-0.4	18.7				13	0.2	0.4
0414-189	Q	1.536	1.00	0.2	18.0	23	0.4	0.4			
0420+417	Q	-	1.70	-	-				15	0.3	0.7
0422+004	L	-	0.80	0.4	16.0	13	0.4	1.0			
0423+233	-	-	-	-	-				11	0.2	0.3
0425+048	Q	-	-	-1.3	20.0				27	1.1	1.5
0426-380	Q	-	1.44	0.2	19.0	27	0.4	0.3			
0426+273	-	-	-	-	-				14	0.2	0.4
0431-512	Q	0.557	-	-0.3	18.0	4	13.1	5.1			
0438-436	Q	2.852	-	0.0	18.8				42	1.1	0.9

Table 3. (cont.)

OBJECT	Tp (1)	Redsh.	Flux (Jy)	SP	m_v	GSFC solution Nobs	σ_α (2)	σ_δ (3)	JPL solution Nobs	σ_α (2)	σ_δ (3)
0440+345	-	-	-	-	-				13	0.4	0.5
0446+112	G	-	1.80	-	20.0				19	0.3	0.6
0454-810	-	-	-	0.2	-	10	24.5	0.9			
0457+024	Q	2.384	1.30	-0.2	18.0	45	0.3	0.9			
0458+138	-	-	-	0.5	-				9	1.1	1.6
0459+060	Q	-	-	-0.5	19.5				9	0.3	0.6
0502+049	B	-	0.60	0.5	19.0				13	1.0	1.5
0506+101	B	-	4.10	0.2	19.5				21	0.3	0.4
0507+179	-	-	0.70	-	-				26	0.3	0.5
0522-611	Q	1.400	-	-0.1	18.5	4	4.0	1.5			
0530-727	-	-	-	-	-	39	2.8	0.4			
0528-250	Q	2.805	-	-0.2	17.7	22	0.5	0.3			
0529+075	Q	-	1.10	-	19.0	13	3.8	29.0			
0537-158	Q	0.947	-	-0.1	18.0				6	0.5	1.7
0536+145	-	-	-	-	-				30	0.3	0.4
0539-057	Q	-	-	1.4	20.0	10	0.4	1.1			
0544+273	-	-	-	-	-				18	0.5	0.7
0556+238	-	-	-	-	-				42	0.1	0.3
0600+177	-	-	-	-	-				28	0.3	0.4
0611+131	-	-	-	-	-				9	0.1	0.5
0609+607	-	-	-	-	-	60	0.9	0.3			
0615+820	Q	-	1.30	0.0	17.5	12	26.5	1.0			
0629-418	Q	1.416	-	0.5	19.3	16	1.5	0.7			
0637-752	Q	0.651	-	0.1	15.8	175	2.0	0.2			
0637-337	-	-	-	0.4	-	8	1.9	0.6			
0642+214	G	0.245	1.80	-0.7	19.5				16	0.3	0.5
0642+449	Q	3.402	1.20	-0.8	18.5	34	0.4	0.3			
0646-306	-	-	0.90	0.2	-	29	0.4	0.3			
0648-165	-	-	-	-	-	25	0.3	0.3			
0650+371	Q	1.982	1.00	0.4	18.0				1	15.2	15.4
0707+476	Q	-	0.80	-0.3	16.0	31	0.6	0.4			
0710+439	G	-	2.00	-0.2	19.8				1	15.6	16.8
0711+356	Q	1.620	1.90	-0.3	19.0	74	0.4	0.5			
0716+714	L	-	0.70	0.1	11.0	280	0.9	0.2			
0722+145	B	-	5.30	0.0	19.0				17	0.3	0.5
0718+792	-	-	1.00	0.0	-	39	10.3	0.5			
0738-674	-	-	-	-	-	1	28.4	9.5			
0743-006	Q	-	-	0.6	17.5	18	0.3	0.9			
0743+259	-	-	0.60	-	-				16	0.3	0.6
0749+540	Q	-	-	-0.3	18.5	19	1.1	0.7			
0804+499	Q	0.351	1.30	0.5	17.5	62	0.4	0.2			
0809-493	-	-	-	-0.3	-	5	7.0	3.4			
0808+019	L	-	0.39	0.4	17.5	11	0.3	1.0			
0812+367	Q	1.025	1.20	0.0	18.0	39	0.4	0.5			
0818-128	L	-	0.90	-0.1	15.5	15	0.5	0.3			

Table 3. (cont.)

OBJECT	Tp (1)	Redsh.	Flux (Jy)	SP	m_v	GSFC solution Nobs	σ_α (2)	σ_δ (3)	JPL solution Nobs	σ_α (2)	σ_δ (3)
0820+560	Q	1.409	1.70	-0.1	18.0	101	0.5	0.2			
0823-223	Q	-	-	0.3	17.5	12	0.8	1.7			
0826-373	-	-	2.30	-	-	18	0.8	0.6			
0828+493	Q	-	0.50	-0.3	18.5	63	0.8	0.4			
0834-201	Q	2.752	3.30	-0.1	19.0	19	0.5	1.1			
0833+585	Q	2.101	-	1.3	18.0	38	1.3	0.3			
0839+187	Q	0.259	2.20	0.2	16.5	20	0.4	0.7			
0906+015	Q	1.018	0.76	-0.2	17.5	46	0.4	1.1			
0912+029	Q	-	0.68	-0.3	18.5				16	0.5	0.7
0919-260	Q	2.300	1.20	0.2	19.0	287	0.1	0.2			
0917+624	Q	-	1.60	0.2	19.5	87	0.7	0.2			
0952+179	Q	1.472	1.00	-0.3	18.0				7	0.3	3.0
0953+254	Q	0.712	1.30	1.3	17.5	153	0.1	0.2			
0955+326	Q	0.533	0.70	-0.3	15.8	21	0.4	0.5			
0954+658	Q	-	0.90	0.4	18.5	1622	0.4	0.1			
0959-443	Q	0.021	-	-0.1	17.0	6	4.7	2.6			
1012+232	Q	0.565	-	-0.3	17.5				20	0.3	0.4
1020+400	Q	-	1.20	-0.3	17.5	13	0.7	0.6			
1022+194	Q	0.828	1.04	0.7	17.5				14	0.2	0.5
1030+415	Q	1.120	0.80	0.3	18.2	26	0.6	0.5			
1032-199	Q	2.198	-	0.1	19.0	8	0.6	0.5			
1031+567	Q	-	1.80	-0.3	20.3	11	2.8	1.1			
1038+064	Q	1.270	1.64	-0.4	16.5				68	0.3	0.6
1040+123	Q	1.029	2.38	-0.7	17.3				13	0.2	0.5
1039+811	Q	-	-	0.4	16.5	20	10.2	0.4			
1042+071	B	-	-	0.0	18.5				14	0.3	0.7
1045-188	Q	-	-	0.3	19.0	6	0.7	0.6			
1044+719	-	-	1.00	0.1	-				15	1.0	0.5
1048-313	-	-	0.50	-0.1	-	22	0.5	0.4			
1053+815	G	-	0.60	-0.4	18.5	40	10.4	0.4			
1057-797	-	-	-	0.6	-	174	4.4	0.2			
1101-325	Q	0.354	0.80	-0.4	16.3	2664	6.0	84.7			
1101-536	Q	1.598	-	-	18.2	2	2.2	4.6			
1124-186	A	-	0.60	0.5	18.5	100	0.1	0.3			
1127-145	Q	1.187	-	0.2	16.9				60	0.5	0.8
1130+009	Q	-	0.33	0.0	19.0	27	0.5	1.6			
1143-245	Q	1.950	1.10	-0.2	18.0	27	0.5	0.4			
1148-671	-	-	-	-0.6	-	5	11.4	2.5			
1156-094	A	-	0.87	-0.2	-				9	4.8	6.3
1206-399	Q	0.966	-	-0.2	16.1	9	4.6	1.4			
1213-172	-	-	1.20	0.3	-	11	0.4	0.7			
1216+487	Q	1.073	0.70	0.2	18.5	41	0.6	0.4			
1221+809	Q	-	-	-0.3	19.0	54	11.4	0.5			
1221-829	-	-	-	-0.8	-	41	63.6	4.0			
1236-684	-	-	-	-0.5	-	6	16.1	2.9			

Table 3. (cont.)

OBJECT	Tp (1)	Redsh.	Flux (Jy)	SP	m_v	GSFC solution Nobs	σ_α (2)	σ_δ (3)	JPL solution Nobs	σ_α (2)	σ_δ (3)
1252+119	Q	0.871	1.80	0.2	16.6	54	0.4	0.6			
1251-713	-	-	-	0.2	-	9	5.5	0.7			
1255-316	Q	1.924	1.58	0.1	18.7	25	0.5	0.4			
1315+346	B	1.050	-	-0.1	19.0				8	0.3	1.0
1323+321	G	-	3.60	-0.6	19.0	5	5.3	9.5			
1334-649	-	-	-	0.0	-	5	12.4	2.4			
1349-439	L	0.053	-	0.6	17.5				47	1.4	1.1
1357+769	Q	-	-	0.7	19.0	24	6.0	0.5			
1413+135	G	-	0.90	-0.1	20.0	20	0.4	0.9			
1430-178	Q	2.331	1.19	-0.1	19.5				27	0.6	1.0
1435+638	Q	2.060	1.60	-0.2	15.0	42	1.6	0.4			
1442+101	Q	3.530	2.01	-0.6	17.8	16	0.7	1.2			
1443-162	-	-	-	-	-				8	0.4	0.8
1445-161	A	-	1.01	-0.5	20.5				12	0.4	0.8
1448+762	G	-	1.00	0.5	20.0	21	8.4	0.6			
1451-375	Q	0.314	1.40	0.4	16.2	6	2.7	2.3			
1451-400	-	-	-	-0.2	-	14	1.0	0.6			
1532+016	Q	1.420	1.19	0.3	18.5				20	0.3	0.7
1547+507	Q	-	-	0.1	18.5	32	0.7	0.4			
1546+027	Q	0.412	0.79	0.4	18.0	49	0.3	0.8			
1540-828	-	-	-	0.1	-	32	43.3	3.3			
1549-790	G	-	-	-0.2	20.7	9	15.5	0.7			
1600+335	-	-	2.70	-	-				2	0.9	4.2
1607+268	Q	-	3.10	-0.9	19.0	9	12.3	31.3			
1614+051	Q	3.208	0.63	0.4	19.5				16	0.3	0.7
1610-771	Q	1.710	-	0.8	19.0	137	3.1	0.2			
1619-680	-	-	-	0.0	-	3	4.3	1.8			
1622-253	G	-	-	-0.1	21.3	2273	0.1	0.2			
1652+398	L	0.034	-	0.0	13.8	55	0.3	0.3			
1655+077	Q	-	1.63	0.4	19.5				34	0.3	0.7
1706-174	A	-	-	-	17.5				43	0.5	1.0
1727+502	G	0.055	0.23	-	16.5	1	70.7	41.9			
1732+389	G	-	-	0.8	19.5	60	0.4	0.3			
1758-651	-	-	-	0.1	-	5	15.3	3.5			
1815-553	-	-	-	-0.1	-	140	0.5	0.3			
1826+796	-	-	-	-	-	26	9.7	0.7			
1823+568	Q	-	1.60	0.2	18.4	309	0.3	0.2			
1831-711	Q	1.356	-	-0.2	17.5	18	3.2	0.6			
1842+681	Q	-	1.20	-0.4	17.9	34	1.7	0.3			
1856+736	-	-	-	-	-	24	4.4	0.6			
1903-802	Q	-	-	0.2	19.0	4	26.2	1.0			
1920-211	-	-	-	-	-				44	0.3	0.8
1925-610	-	-	-	-0.1	-	3	2.7	2.3			
1935-692	Q	3.170	-	-	18.8	3	7.4	1.6			
1947+079	Q	-	1.00	0.0	18.0	40	0.3	0.9			

Table 3. (cont.)

OBJECT	Tp (1)	Redsh.	Flux (Jy)	SP	m_v	GSFC solution Nobs	σ_α (2)	σ_δ (3)	JPL solution Nobs	σ_α (2)	σ_δ (3)
2000-330	Q	3.780	1.10	0.8	19.0	8	2.5	1.1			
2007+777	Q	-	1.20	0.9	16.5	84	3.3	0.2			
2005+403	Q	1.736	4.90	-	19.5	15	2.1	2.0			
2005-489	A	-	-	0.2	16.0	5	4.2	2.4			
2017+743	-	-	-	-	-	27	5.4	0.4			
2021+317	-	-	-	-	-	31	0.4	0.4			
2023+336	-	-	-	-	-	8	2.8	3.6			
2037+511	Q	1.690	5.00	-	20.0	1597	0.2	0.1			
2037-253	Q	1.570	0.90	0.3	18.5	9	0.6	0.4			
2051+745	-	-	-	-	-	12	11.8	0.8			
2059-786	-	-	-	-1.3	-	2	56.4	1.5			
2106-413	Q	-	-	0.2	20.0	10	1.3	0.7			
2109-811	G	-	-	0.2	20.0	5	74.5	4.1			
2126-158	Q	3.270	0.90	0.1	17.3	3	0.3	1.1			
2136+141	Q	2.427	1.19	0.0	18.5	87	0.2	0.3			
2142-758	Q	1.139	-	-0.1	17.4	2	23.0	2.0			
2149-307	Q	2.340	1.35	-0.2	17.5	20	0.5	0.3			
2146-783	-	-	-	-0.1	-	6	39.9	2.1			
2150+173	G	-	1.10	0.4	21.0	38	0.3	0.6			
2210-257	Q	1.833	0.90	0.1	19.5	5	5.3	1.7			
2229+695	G	-	-	0.4	19.6				16	1.1	0.5
2233-148	A	-	-	0.3	19.5	6	0.5	0.6			
2245-328	Q	2.268	-	-0.2	18.6				67	0.5	0.8
2252-090	-	-	-	0.1	-				1	29.8	44.7
2254+024	Q	2.090	-	0.2	18.0				21	0.4	0.7
2255-282	Q	0.926	-	0.4	16.7	1953	0.1	0.1			
2312-319	Q	0.284	-	-0.3	18.5	13	0.9	0.6			
2320-035	Q	1.410	0.79	-0.1	18.0				95	0.2	0.5
2325-150	Q	2.465	1.10	0.2	19.0	7	0.6	0.7			
2326-477	Q	1.302	-	0.0	17.0	57	0.3	0.5			
2329-162	Q	1.153	1.20	-0.2	18.5	8	0.5	0.5			
2329-384	Q	1.195	-	-0.2	16.2	12	0.9	0.5			
2331-240	Q	0.048	0.90	0.0	17.0	4	7.6	8.0			
2335-027	Q	1.072	0.65	0.2	19.3				13	0.3	0.6
2351-154	Q	2.665	-	-0.2	17.0				14	0.2	0.6
2352+495	G	0.237	2.30	-0.3	19.0	56	0.6	0.4			
2355-534	Q	1.006	-	0.4	17.8	30	0.6	0.5			

(1) Type of object: Q: Quasar; G: Galaxy; L: BL Lac; B: Blue object; A: Other
(2) Unit: 0.0001s
(3) Unit: 0.001"

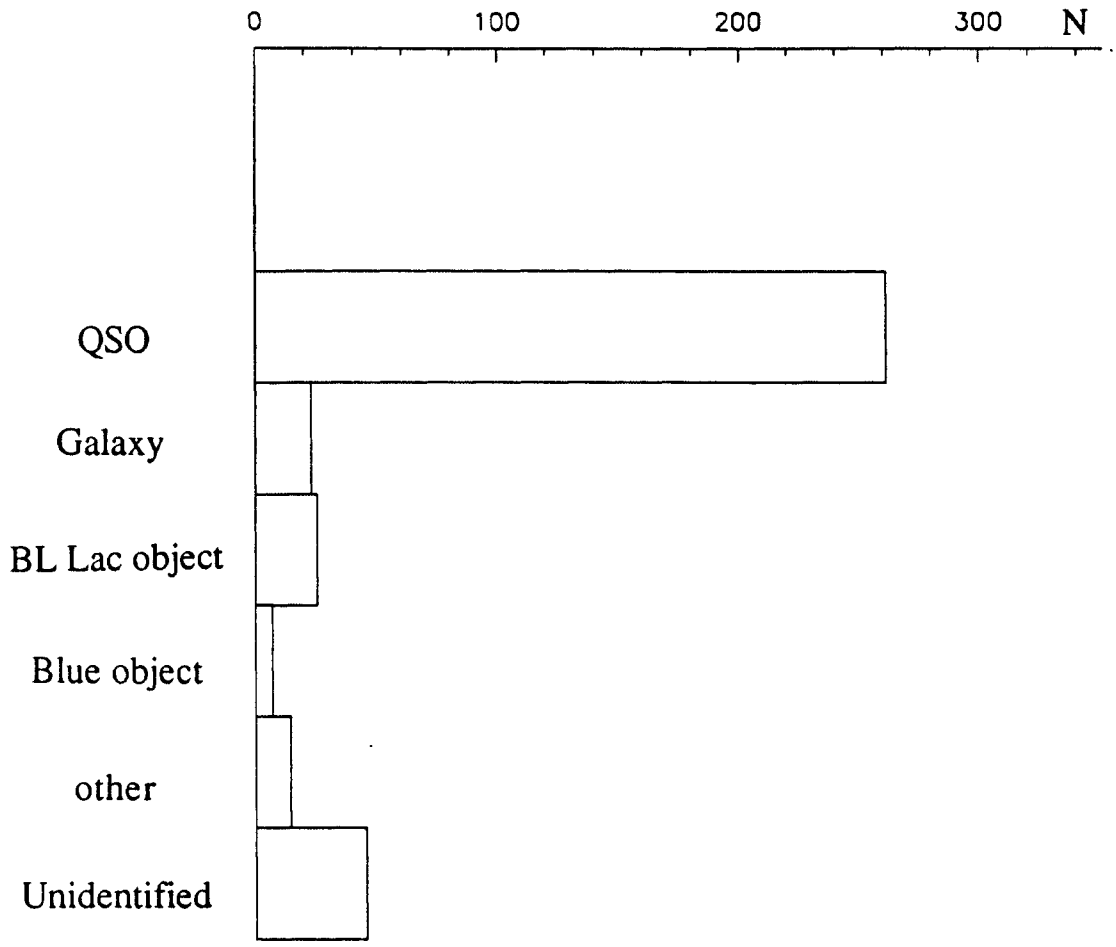

Figure 3a. Optical identification of extragalactic radio sources in RSC(IERS) 91 C 01.

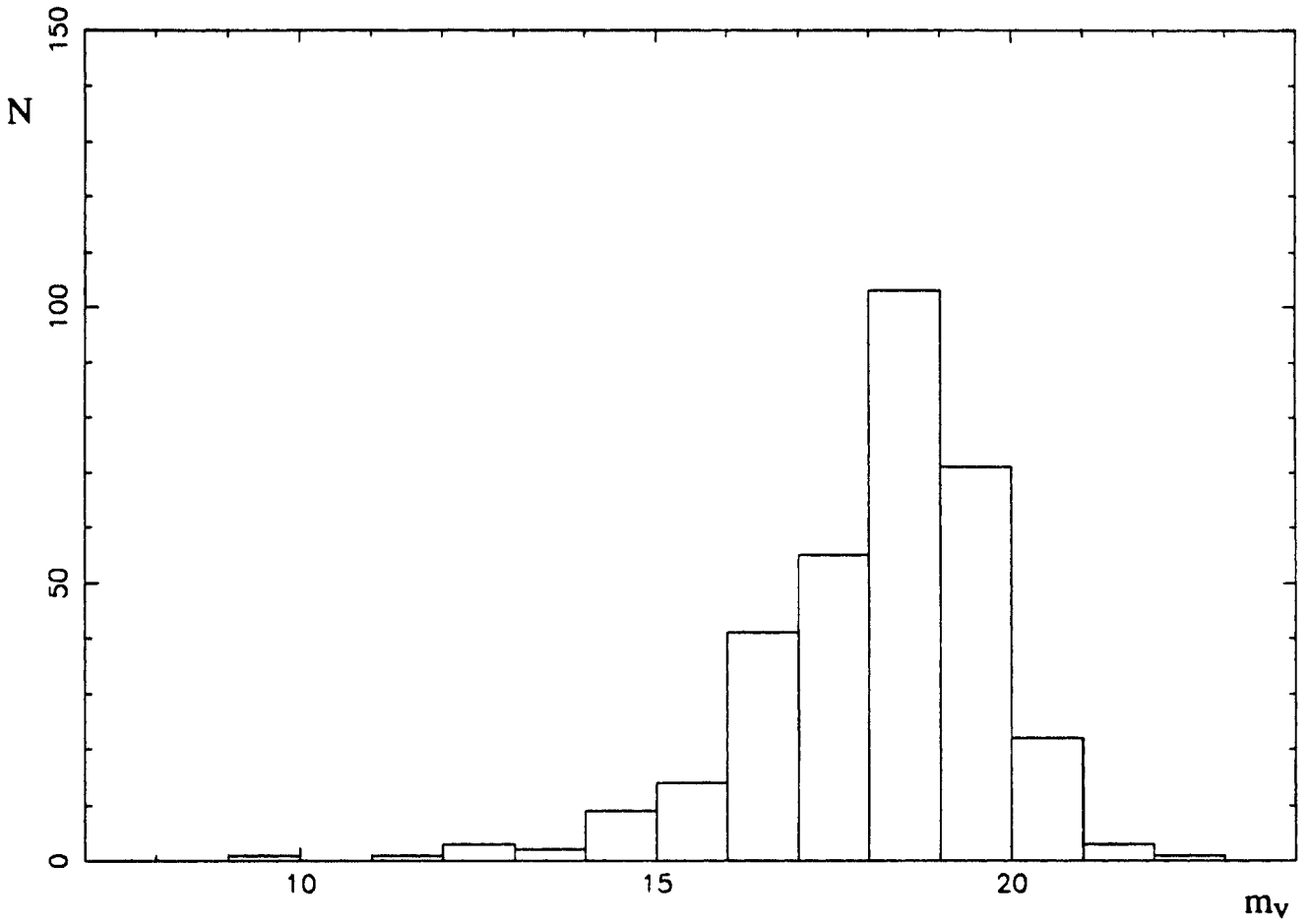

Figure 3b. Visual magnitudes of the optical counterparts of radio sources in RSC(IERS) 91 C 01 (total of 326 values).

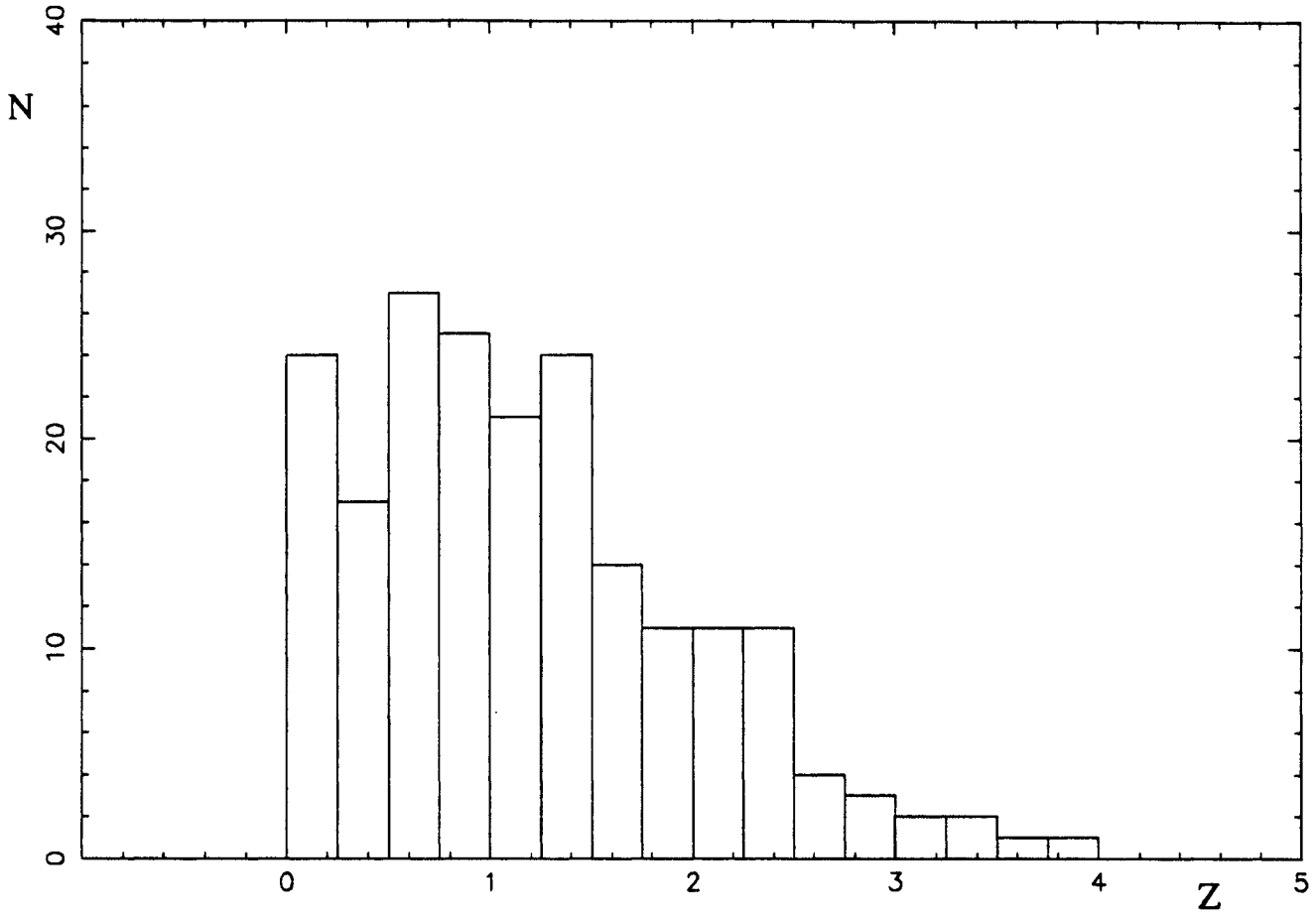

Figure 3c. Redshift of extragalactic radio sources in RSC(IERS) 91 C 01 (total of 198 values).

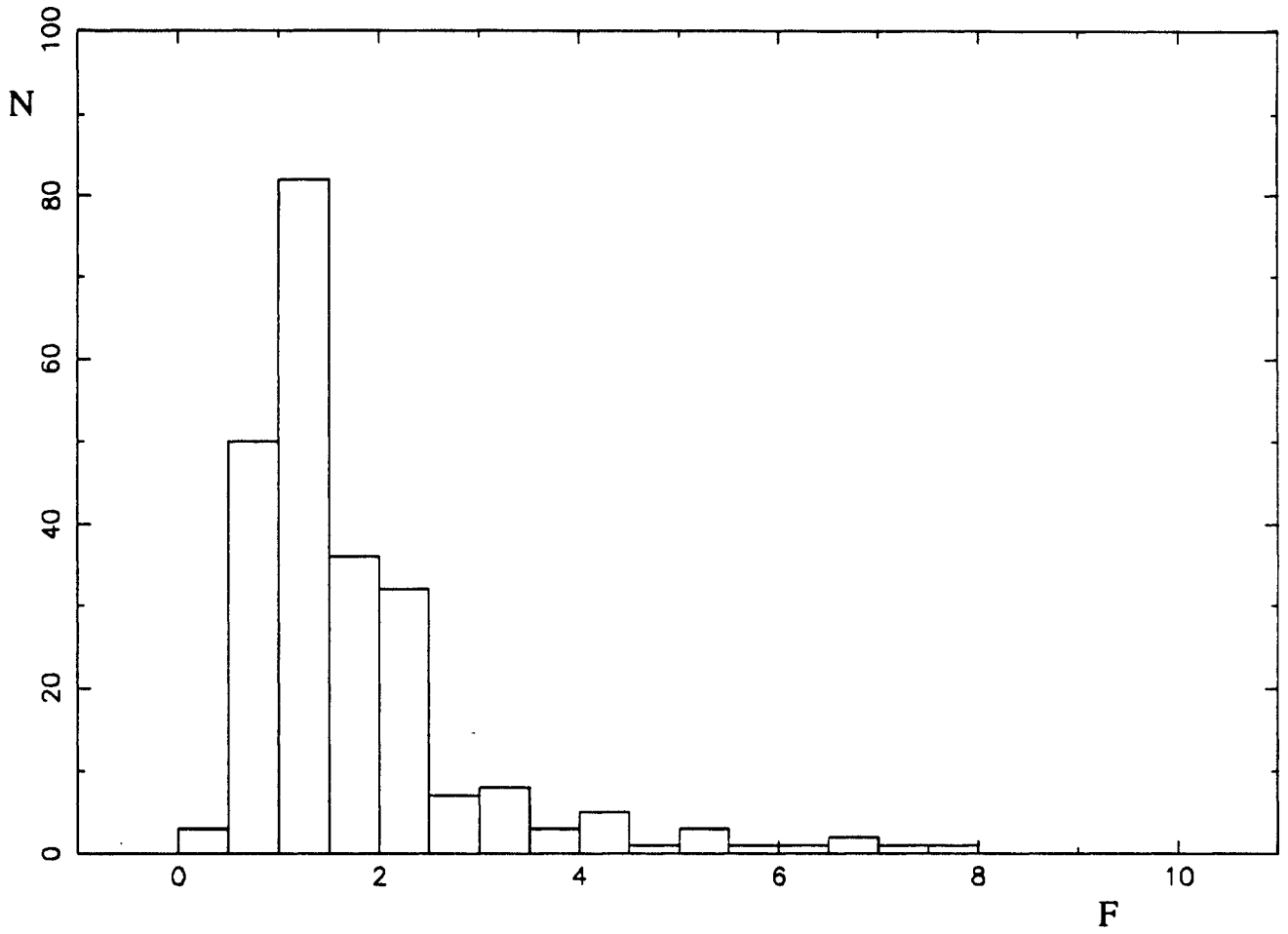

Figure3d. Total flux (Jy) of extragalactic radio sources in RSC(IERS) 91 C 01 (limited to 9.5 Jy; total of 239 values).

Table 4 presents the statistics on the optical identification of radio sources in the IERS frame and in the 917 objects detected in the complete sky survey by Preston *et al.* The distribution of the IERS sources according to their optical classes is similar to the distribution in the survey. Concerning the optical identification of IERS primary sources, 78% of them are quasars, 10% are BL Lac objects and 4% are galaxies. 61% of the quasars selected for the HIPPARCOS/HST link are included in IERS celestial reference frame RSC (IERS) 91 C 01.

Table 4. Optical identifications of the radio sources in the IERS Celestial Reference Frame and in the VLBI survey by Preston *et al.* (1985).

Optical identification (%)	IERS sources (%)	Detected in the survey
Quasar	69	59
Galaxy	7	11
BL Lac	8	7
Stellar objects	4	6
Other/unidentified	12	8
Empty fields		9

Table 5. Distribution of the visual magnitudes of sources in the IERS Celestial Reference Frame

Magnitude range	Number of objects (%)
10 - 12	2
12 - 14	2
14 - 16	6
16 - 18	42
18 - 20	42
20 - 22	6

Table 6. Distribution of the total radio flux of sources in the IERS Celestial Reference Frame.

Flux density (Jy)	Number of objects (%)
0 - 1	22
1 - 2	49
2 - 4	21
4 - 6	4
> 6	4

Table 7. Distribution of redshifts of sources in the IERS Celestial Reference Frame.

Redshift	Number of objects (%)
0 - 1	53
1 - 2	27
2 - 3	17
3 - 4	3

We have also looked at the number of observations of IERS sources in the individual frames of JPL and GSFC contributing to RSC (IERS) 91 C 01. Figures 4a and 4b show the histograms for the number of observations (delay, delay rate) of sources in RSC (JPL) 91 R 01 and in RSC (GSFC) 91 R 04. The total number of sources in each frame is 241 and 334 respectively. The histogram for the number of observations of sources in the last realisation of IERS frame (both individual VLBI frames together) is plotted in Figure 5.

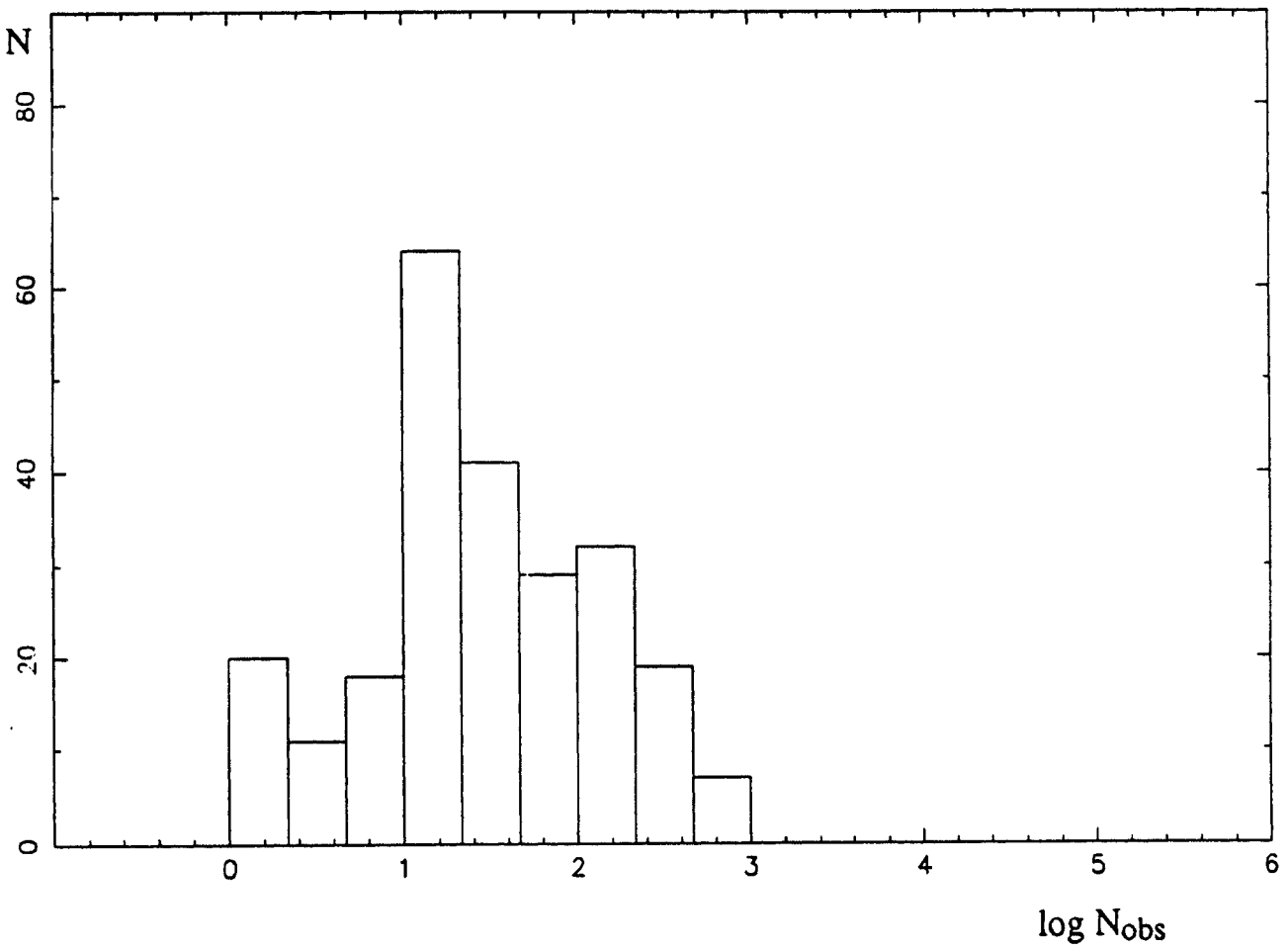

Figure 4a. Number of observations of extragalactic radio sources in RSC (JPL) 91 R 01. The total number of sources in the frame is 241.

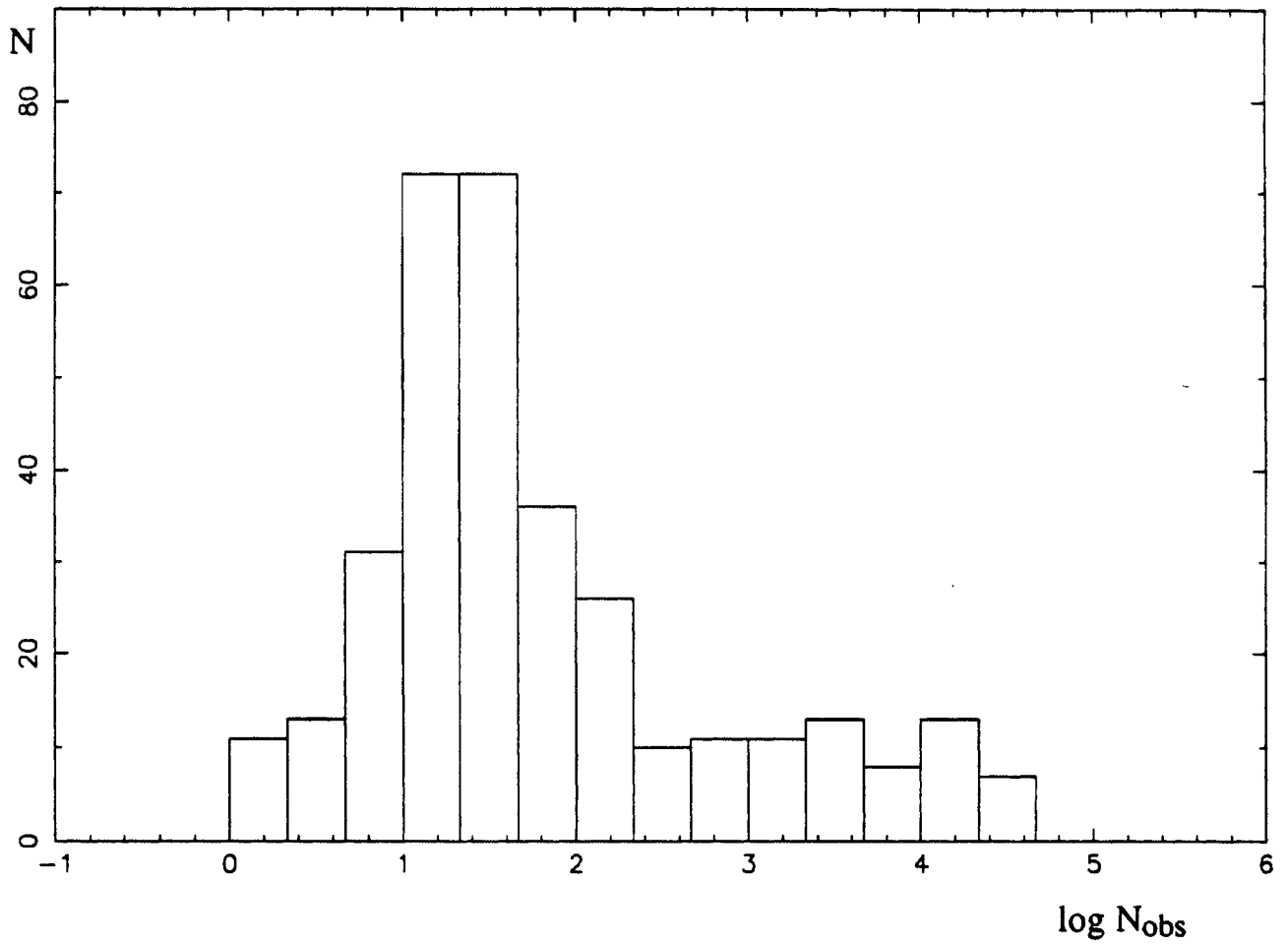

Figure 4b.Number of observations of extragalactic radio sources in RSC (GSFC) 91 R 04. The total number of sources in the frame is 334.

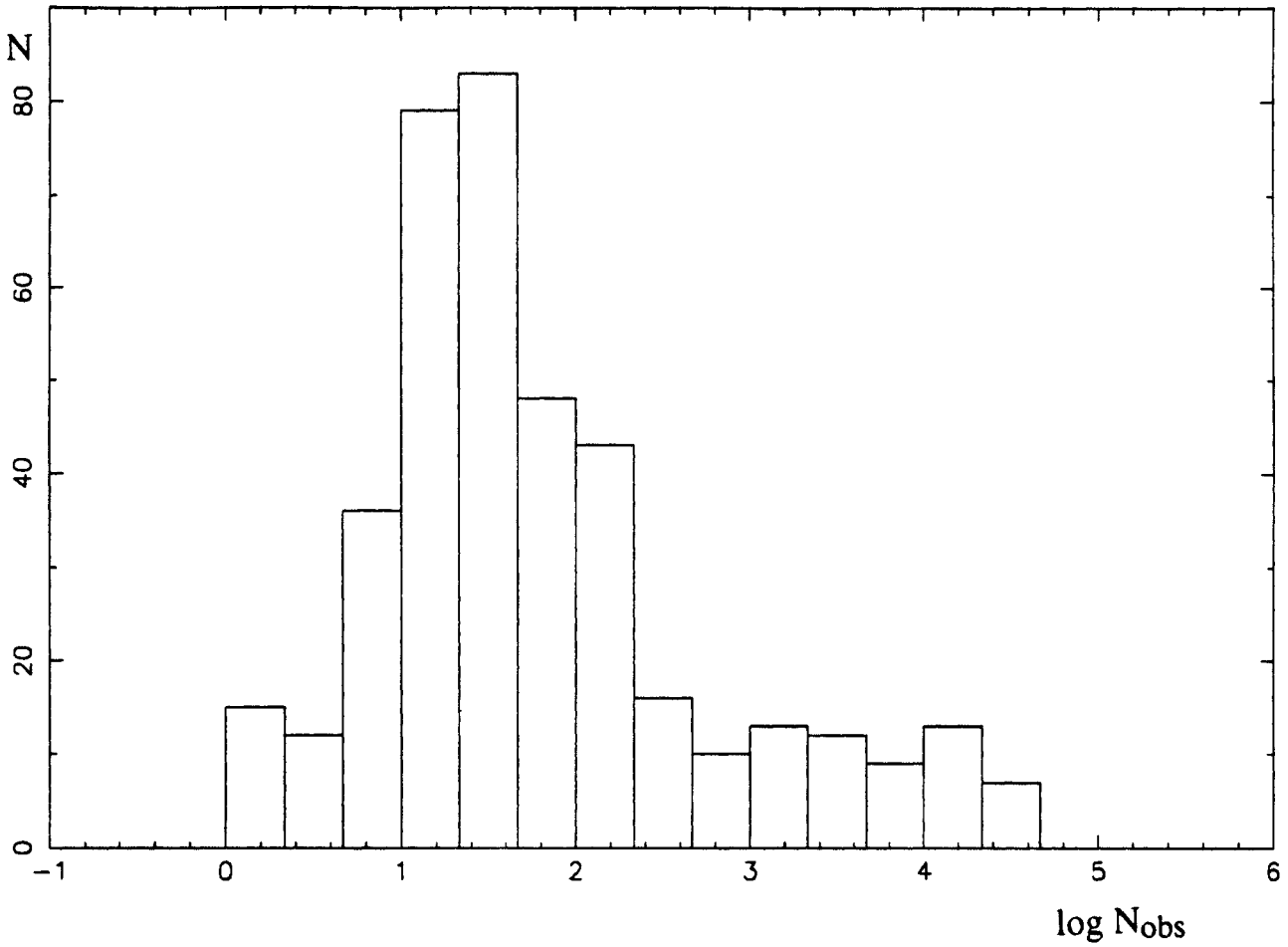

Figure 5. Number of observations of extragalactic radio sources in RSC (IERS) 91 R 01. The total number of sources in the frame is 396.

2 - PRECISION AND CONSISTENCY OF VLBI FRAMES

Introduction

This section reports on the results of analyses and comparisons of extragalactic VLBI reference frames obtained by the IERS Analysis Centres from independent (or quasi-independent) observation programs, in order to estimate their accuracy and consistency. After a detailed study of these two sets of frames, an internal analysis of the compiled IERS celestial frame is presented. The catalogues analysed in this section are listed in table 8.

Table 8. The VLBI extragalactic reference frames compared; rotation angles (A_1, A_2, A_3) to rotate a version of a frame to the next one of the same laboratory.

Name	Label		Nb of objects	A_1	A_2	A_3	Reference
				----------(0.001")----------			
G90	RSC(GSFC)	90 R 01	72	-0.02	+0.26	-0.05	Ma and Caprette, 1990
G91	RSC(GSFC)	91 R 03	234	±0.04	±0.04	±0.03	Ma and Caprette, 1991
J90	RSC(JPL)	90 R 02	197	-0.63	-0.04	+0.32	Steppe *et al.*, 1990
				±0.06	±0.06	±0.04	Steppe *et al.*, 1991
J91	RSC(JPL)	91 R 01	241	-0.05	-0.33	-0.12	
				±0.10	±0.09	±0.07	
	RSC(JPL)	90 R 03	216				Sovers, 1991b
N90	RSC(NGS)	90 R 01	70	+0.33	-0.43	+0.01	Carter and Robertson, 1990
N91	RSC(NGS)	91 R 01	77	±0.09	±0.09	±0.08	Carter and Robertson, 1991
U90	RSC(USNO)	90 R 05	80	+0.65	+1.78	+0.39	Eubanks *et al.*, 1991a
U91	RSC(USNO)	91 R 02	80	±0.03	±0.03	±0.03	Eubanks *et al.*, 1991b
	RSC(IERS)	88 C 01	228	-0.15	-0.24	+0.21	Arias *et al.*, 1988
				±0.10	±0.10	±0.07	
	RSC(IERS)	89 C 01	209	-0.09	-0.08	+0.00	IERS, 1989
				±0.13	±0.13	±0.09	
	RSC(IERS)	90 C 01	228	+0.03	+0.06	+0.00	IERS, 1990
				±0.05	±0.04	±0.04	
	RSC(IERS)	91 C 01	396				IERS, 1991

The celestial frames studied are based on independent observations, except in two cases :
- G90 and N90 are partially based on common observations; the comparison between these two frames was not considered in the analyses,
- a small proportion of the N91 observations are also used for G91, while N91 uses none of the remaining part of G91 observations ; this slight redundancy was neglected in the comparisons.

Successive versions of the frames obtained by a given institute differ mainly in that more recent observations are accumulated in the second version - less than 10% in general ; otherwise they are based on analysis schemes that are consistent for each analysis centre. For what concerns the direction of the pole and of the origin of right ascensions, the consistency is maintained in general within a fraction of one milliarcsecond.

In order to investigate the regional deformations of the frames, or to derive statistical properties of the individual source coordinates, it is necessary first to account for the slight misalignments of

the various frames which result from the diversity of the implementation of the celestial system definitions. As there is a general tendency to match the IERS axes, the mutual misalignments between the frames studied here are smaller than 0.003".

The relative orientation between two celestial frames is obtained by computing differential rotations about the three coordinate axes on the basis of differences of coordinates of common objects. A source common to the two frames and in the direction of unit vector $\vec{D}$ has two sets of coordinates, one in frame 1 and one in frame 2. Provided that there exists no relative deformations between the frames, and that they only differ by a rotation, the transformation between the two celestial reference frames can be written as:

$$\vec{D}_2 = M \vec{D}_1 \qquad (1)$$

where the rotation matrix M is

$$M = \begin{bmatrix} 1 & A_3 & -A_2 \\ -A_3 & 1 & A_1 \\ A_2 & -A_1 & 1 \end{bmatrix}$$

A_1, A_2, A_3 are the infinitesimal rotation angles about x,y and z axes respectively, which express the rotation of frame 2 to frame 1. In each frame, the x-axis is in the direction of the origin of right ascensions, the z-axis points to the celestial pole and the y-axis completes a direct triad.

The differences between the equatorial coordinates of a source common to two frames are, to the first order with respect to A_1, A_2, and A_3:

$$\alpha_1 - \alpha_2 = A_1 \cos\alpha_2 \sin\delta_2 / \cos\delta_1 + A_2 \sin\alpha_2 \sin\delta_2 / \cos\delta_1 - A_3 \cos\delta_2 / \cos\delta_1 \qquad (2)$$

$$\delta_1 - \delta_2 = -A_1 \sin\alpha_2 + A_2 \cos\alpha_2 \qquad (3)$$

The three unknowns A_1, A_2 A_3 are estimated by a least squares fit for a selection of sources common to the two frames. The equations are weighted according to the uncertainties of the coordinates, with a lower limit of 0.00025" on each individual value. Earlier studies have shown that the use of added variance or scaling factors of the formal uncertainties is not necessary.

Analysis of four 1990 VLBI extragalactic reference frames

This section gives the results of statistical analyses of four VLBI frames which were available for the compilation of RSC(IERS) 90 C 01, published in the IERS Annual Report for 1989. The analyses are based on the differences of coordinates in the five pairs of independent catalogues, after taking out relative rotation angles. The latter, listed in table 9, are estimated by restricting the set of common sources considered to those which had been retained as primary in the compilation of RSC(IERS) 90 C 01, *i.e.*, whose coordinates were the most consistent in the various frames (see p.46).

Table 9. Relative orientations of the four 1990 individual frames. N is the number of common sources considered, σ is the rms post-fit residual. Units for A_1, A_2, A_3 and σ: 0.001".

Frame 1-Frame 2	N	A_1	A_2	A_3	σ
U90 - G90	30	-0.33	+0.28	-0.33	0.49
		±0.11	±0.10	±0.09	
G90 - J90	28	-1.86	-2.97	+0.36	0.35
		±0.09	±0.08	±0.06	
N90 - J90	27	-1.87	-1.30	+0.27	0.43
		±0.12	±0.11	±0.08	
N90 - U90	27	+0.28	+0.31	+0.36	0.53
		±0.12	±0.12	±0.11	
U90 - J90	36	-1.91	-2.61	+0.06	0.48
		±0.11	±0.10	±0.07	

Number of observations and formal uncertainties

Figure 6 shows the relationship between the formal uncertainty of the source coordinates and the number of observed delays for the three catalogues for which this information was available(G90, J90, U90). The formal uncertainty follows a law in $N^{-0.5}$ (slope = -1 on the graph) for a $50 < N < 3000$. For larger N it meets a floor at 0.06 mas in $\alpha.\cos\delta$ and 0.13 mas in declination, in the case of GSFC.

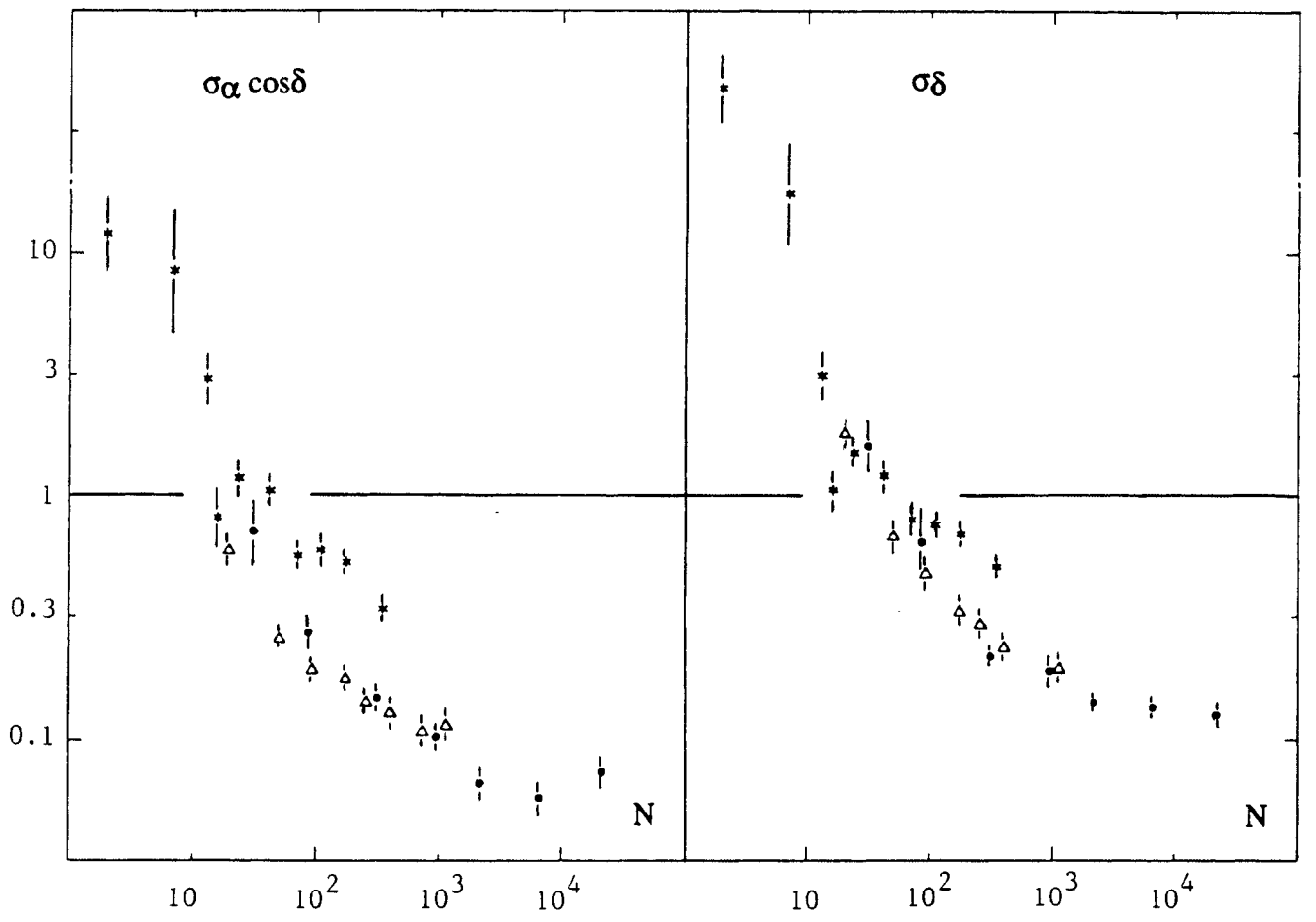

Figure 6. Formal uncertainties of source coordinates as a function of the number of observations.
Unit: 0.001"
- • GSFC (G90, 72 sources)
- * JPL (J90, 197 sources)
- Δ USNO (U90, 80 sources)

Consistency of the coordinates of 39 objects common to the four catalogues

In this section, we consider the residual differences in right ascension and in declination of the 39 sources which are common to the four catalogues, obtained by removing the two-by-two rotation angles of table 9. The mean differences of the source coordinates in a given catalogue with respect to the other three (or two) are listed in table 10. The estimated uncertainty of the mean differences per source ranges from 0.2 to 0.5 mas in general. The data are summarized in table 11.

Table 10. Mean coordinate residual differences, one catalogue - the others

Source	R.A. *cosδ 0.001"				Declination 0.001"			
	GSFC	JPL	NGS	USNO	GSFC	JPL	NGS	USNO
0048-097	0.16	-0.49	0.18	0.26	0.32	-1.32	0.52	0.76
	0.13	0.77	0.15	0.16	0.19	1.32	0.30	0.42
	0.57	0.78	0.58	0.49	1.00	1.36	1.02	0.89
0106+013	-0.03	0.06	-0.08	0.01	-0.67	-0.67	-0.36	1.35
	0.03	0.40	0.03	0.16	0.14	0.53	0.20	0.25
	0.31	0.41	0.31	0.28	0.44	0.57	0.46	0.42
0119+041	-0.23	0.35	-0.12	-0.11	2.95	-4.22	0.65	1.82
	0.18	0.75	0.10	0.07	0.35	1.28	0.30	0.12
	0.56	0.76	0.54	0.45	0.97	1.31	0.96	0.79
0212+735	-0.05	-0.01	-0.31	0.26	0.03	0.01	0.19	-0.16
	0.11	0.45	0.22	0.20	0.12	0.37	0.20	0.20
	0.37	0.49	0.41	0.36	0.32	0.41	0.36	0.32
0229+131	0.03	-0.32	0.09	0.23	-0.45	0.46	-0.69	0.30
	0.04	0.41	0.07	0.28	0.13	0.95	0.20	0.43
	0.35	0.44	0.36	0.37	0.75	0.99	0.76	0.71
0234+285	0.23	0.19	0.18	-0.46	-0.20	-0.16	-0.26	0.47
	0.07	0.35	0.13	0.09	0.12	0.38	0.20	0.12
	0.26	0.36	0.29	0.24	0.31	0.41	0.35	0.28
0235+164	0.15	-0.18	0.59	-0.31	-0.64	0.85	-1.51	0.58
	0.11	0.42	0.14	0.09	0.34	0.38	0.40	0.11
	0.32	0.44	0.33	0.28	0.44	0.49	0.49	0.39
0300+470	0.29	0.19	0.10	-0.45	-0.20	-0.15	-0.05	0.32
	0.09	0.40	0.18	0.09	0.13	0.39	0.20	0.12
	0.30	0.42	0.34	0.27	0.32	0.42	0.35	0.29
0420-014	-0.37	0.23	-0.40	0.28	-1.25	0.98	-1.83	1.08
	0.03	0.33	0.03	0.09	0.14	0.43	0.20	0.11
	0.24	0.33	0.24	0.21	0.34	0.46	0.37	0.31
0528+134	-0.02	0.42	0.16	-0.51	-0.91	0.48	-1.49	1.12
	0.04	0.35	0.07	0.09	0.13	0.42	0.20	0.10
	0.26	0.36	0.26	0.23	0.33	0.45	0.36	0.30
0552+398	0.08	0.19	0.07	-0.29	-0.09	-0.29	-0.10	0.41
	0.08	0.23	0.15	0.09	0.12	0.34	0.20	0.13
	0.19	0.26	0.23	0.19	0.28	0.37	0.33	0.27
0727-115	-0.95	0.80	-0.20	-0.03	-1.34	1.07	-1.76	1.00
	0.06	0.41	0.06	0.10	0.15	0.52	0.20	0.21
	0.30	0.42	0.30	0.26	0.42	0.55	0.44	0.39

Line 1: Average difference with the other three (two) catalogues
Line 2: Formal uncertainty in the catalogue
Line 3: Formal uncertainty of the difference (derived from the quadratic combination of the formal uncertainties of the catalogues considered in the differences)

Table 10. (cont.) Mean coordinate residual differences, one catalogue - the others

Source	R.A. *cosδ 0.001"				Declination 0.001"			
	GSFC	JPL	NGS	USNO	GSFC	JPL	NGS	USNO
0742+103	0.05	-0.08	0.73	-0.44	-1.09	0.73	-1.63	1.07
	0.06	0.30	0.10	0.10	0.19	0.39	0.40	0.10
	0.23	0.31	0.24	0.21	0.34	0.47	0.49	0.36
0851+202	-0.27	0.20	0.06	-0.06	-0.04	-0.53	-0.37	0.80
	0.04	0.28	0.07	0.11	0.12	0.37	0.20	0.09
	0.22	0.29	0.22	0.20	0.29	0.40	0.34	0.27
0923+392	-0.04	-0.16	-0.08	0.23	-0.22	0.03	-0.25	0.28
	0.08	0.23	0.12	0.14	0.12	0.26	0.20	0.09
	0.21	0.26	0.23	0.21	0.23	0.30	0.28	0.22
1034-293	-0.77	1.54	0.34	-1.25	-0.04	1.55	0.47	-1.83
	0.18	0.89	0.16	0.20	0.24	0.78	0.30	0.62
	0.67	0.91	0.66	0.57	0.74	0.89	0.77	0.80
1055+018	-0.28	1.00	0.38	-1.06	-1.27	0.08	-1.30	1.63
	0.03	0.30	0.04	0.15	0.15	0.44	0.30	0.27
	0.24	0.31	0.24	0.23	0.39	0.51	0.47	0.42
1253-055	-0.97	2.02	-0.14	-1.28	0.05	1.08	-0.40	-0.85
	0.09	0.42	0.15	0.12	0.22	0.72	0.40	0.27
	0.32	0.44	0.34	0.29	0.59	0.78	0.68	0.56
1308+326	0.12	0.06	-0.02	-0.12	-0.27	0.04	-0.26	0.32
	0.06	0.24	0.10	0.14	0.13	0.49	0.20	0.16
	0.21	0.26	0.22	0.21	0.39	0.52	0.42	0.35
1334-127	-0.50	1.16	0.04	-0.86	-0.84	0.49	-0.38	0.32
	0.10	0.47	0.10	0.16	0.20	0.77	0.30	0.42
	0.37	0.49	0.37	0.33	0.65	0.83	0.69	0.65
1404+286	0.29	-0.14	0.37	-0.30	0.39	-0.79	0.58	0.14
	0.05	0.29	0.09	0.16	0.13	0.67	0.20	0.20
	0.24	0.31	0.25	0.24	0.51	0.69	0.53	0.46
1418+546	-0.03	0.12	-0.60	0.29	-0.25	0.35	-0.67	0.26
	0.16	0.36	0.23	0.15	0.18	0.56	0.30	0.16
	0.32	0.40	0.36	0.30	0.45	0.60	0.51	0.41
1502+106	0.02	0.10	0.55	-0.48	-0.62	-0.05	0.17	0.35
	0.04	0.28	0.06	0.16	0.15	0.70	0.20	0.27
	0.23	0.30	0.24	0.23	0.55	0.73	0.57	0.51
1548+056	0.09	-0.34	0.41	0.01	-0.89	-0.38	-0.14	1.07
	0.04	0.37	0.04	0.12	0.14	0.81	0.20	0.29
	0.28	0.38	0.28	0.25	0.62	0.84	0.64	0.57
1611+343	0.06	0.02	-0.16	0.04	-0.14	0.27	-0.40	0.09
	0.15	0.31	0.12	0.11	0.20	0.76	0.20	0.21
	0.28	0.34	0.26	0.24	0.59	0.79	0.59	0.51
1633+382	-0.31	0.53	-0.39	-0.06	-0.40	0.56	-0.45	0.01
	0.07	0.29	0.13	0.13	0.12	0.69	0.20	0.21
	0.24	0.31	0.26	0.23	0.52	0.71	0.55	0.47
1730-130	-0.33	0.90	-0.60	-0.28	0.48	-1.72	1.73	0.25
	0.07	0.45	0.10	0.16	0.16	0.96	0.20	0.48
	0.34	0.46	0.35	0.31	0.78	1.01	0.78	0.75
1741-038	0.10	0.08	0.22	-0.29	-0.49	-0.41	0.69	0.28
	0.03	0.39	0.04	0.10	0.15	0.88	0.20	0.31
	0.29	0.40	0.29	0.25	0.68	0.91	0.69	0.61
1749+096	0.05	-0.23	0.23	0.04	-0.28	-0.69	0.69	0.42
	0.04	0.35	0.06	0.12	0.14	0.93	0.20	0.30
	0.26	0.36	0.27	0.24	0.71	0.96	0.72	0.63
1803+784	-0.05	0.03	-0.29	0.19	-0.10	0.19	-0.27	0.06
	0.11	0.88	0.22	0.10	0.12	0.73	0.20	0.17
	0.64	0.89	0.66	0.54	0.54	0.75	0.57	0.47

Table 10. (cont.) Mean coordinate residual differences, one catalogue - the others

Source	R.A. *cosδ 0.001"				Declination 0.001"			
	GSFC	JPL	NGS	USNO	GSFC	JPL	NGS	USNO
1921-293	0.81	0.11	-0.44	-0.35	-2.04	1.89	-0.63	-0.11
	0.09	0.73	0.14	0.14	0.20	1.08	0.30	0.44
	0.53	0.74	0.54	0.45	0.85	1.13	0.88	0.79
1923+210	0.34	0.14	-1.70	0.76	0.62	0.44	-1.54	0.18
	0.39	0.38	0.41	0.22	1.09	0.72	1.10	0.30
	0.50	0.52	0.51	0.45	1.22	1.16	1.23	1.03
2121+053	-0.25	0.15	-0.03	0.03	-0.88	0.30	0.05	0.26
	0.04	0.39	0.04	0.13	0.13	0.71	0.20	0.24
	0.29	0.40	0.29	0.26	0.55	0.74	0.57	0.49
2128-123	0.39	0.75	-0.25	-0.84	-2.06	-0.86	-1.12	2.98
	0.32	0.45	0.41	0.28	0.32	0.85	0.40	0.87
	0.49	0.56	0.56	0.49	0.92	1.03	0.95	1.04
2145+067	-0.31	0.18	-0.17	0.14	-1.09	0.55	-0.36	0.41
	0.04	0.39	0.04	0.10	0.13	0.68	0.20	0.21
	0.29	0.40	0.29	0.25	0.52	0.70	0.54	0.47
2200+420	-0.26	-0.28	-0.22	0.60	-0.23	-0.17	-0.29	0.52
	0.09	0.47	0.13	0.10	0.12	0.49	0.20	0.13
	0.35	0.48	0.36	0.30	0.38	0.51	0.41	0.34
2216-038	0.15	-0.07	0.02	-0.04	-1.83	1.59	-0.79	0.15
	0.04	0.45	0.04	0.10	0.15	0.84	0.30	0.24
	0.33	0.45	0.33	0.28	0.64	0.87	0.69	0.57
2234+282	-0.30	-0.34	0.00	0.54	-0.31	-0.28	-0.06	0.54
	0.08	0.44	0.11	0.09	0.13	0.49	0.20	0.13
	0.33	0.45	0.34	0.28	0.38	0.51	0.41	0.34
2345-167	0.63	-0.71	-0.11	0.36	-1.14	1.28	0.09	-0.58
	0.14	0.69	0.17	0.16	0.18	0.96	0.30	0.42
	0.52	0.71	0.53	0.45	0.76	1.01	0.80	0.72

Table 11. Statistics of the average differences of coordinates in one catalogue with the other three (two). Unit: 0.001"

RSC	Right ascension*cosδ				Declination			
	1	2	3	4	1	2	3	4
G90	-0.06	0.37	0.36	1.05	-0.45	0.95	0.60	1.65
J90	0.21	0.58	0.48	1.25	0.07	1.04	0.77	1.15
N90	-0.04	0.41	0.37	1.16	-0.35	0.84	0.63	1.67
U90	-0.14	0.49	0.32	1.61	0.46	0.89	0.56	1.76

1: arithmetic mean of the differences
2: rms difference
3: rms formal uncertainty of the differences
4: rms ratio of difference/formal uncertainty

Figure 7 is similar to figure 6, the plotted values being the residual position differences of table 10 (line 1). The residual position differences in right ascension follow roughly a law in $N^{-0.5}$, while in the case of the declinations the accumulation of observations does not diminish the dispersion in the same proportion.

Figures 8a and 8b give the plots of the formal uncertainty and of the residual position differences as a function of right ascension and of declination. The most striking feature is the clear degradation of the residual position differences in declination for decreasing declinations, which is not echoed in full size by a similar trend in the formal uncertainties.

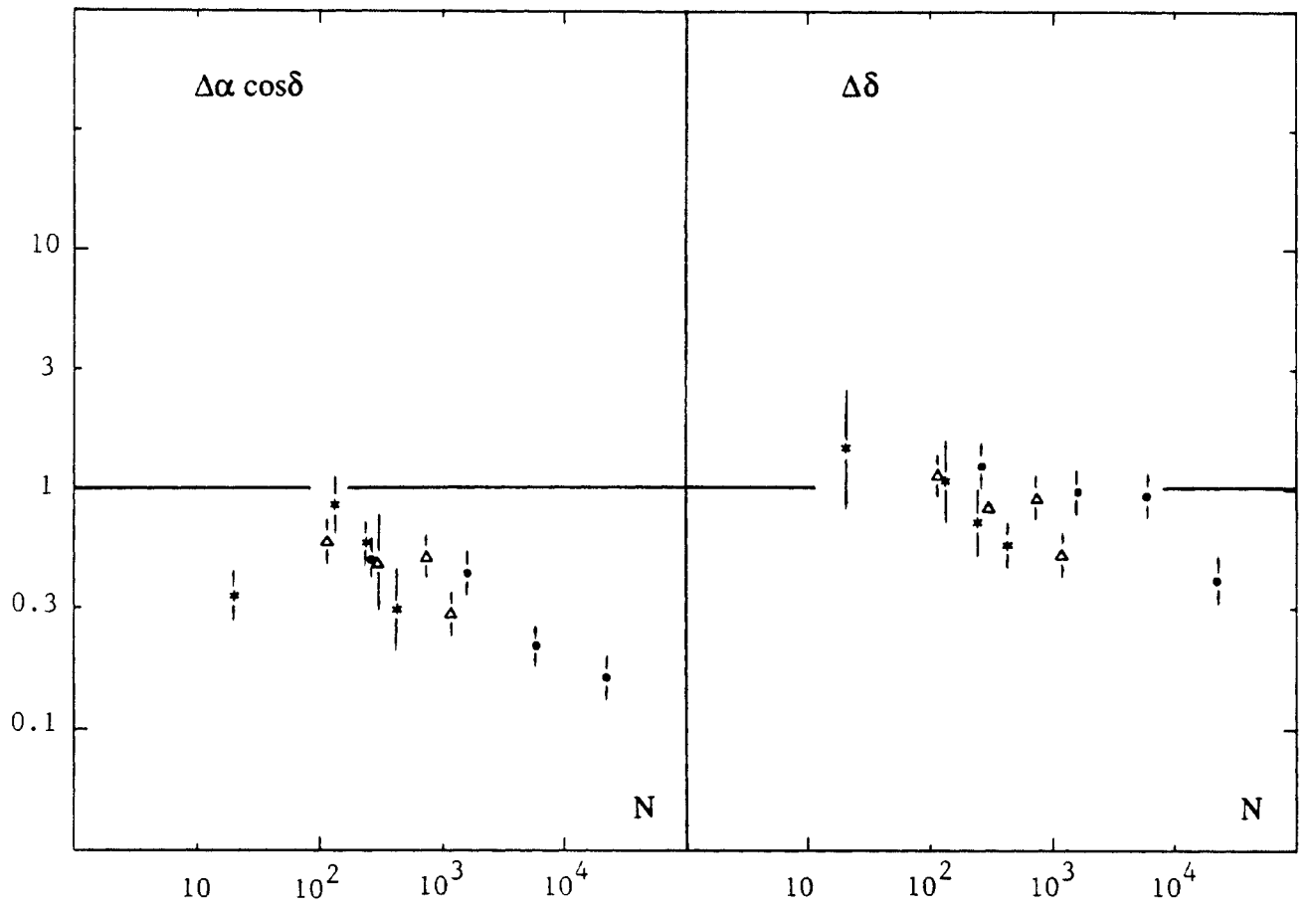

Figure 7. 39 sources common to the four catalogues: mean residual position differences of the coordinates in one catalogue with respect to the other ones, after taking out the relative rotations, as a function of the number of observations. Unit: 0.001"

• GSFC (G90)
* JPL (J90)
Δ USNO (U90)

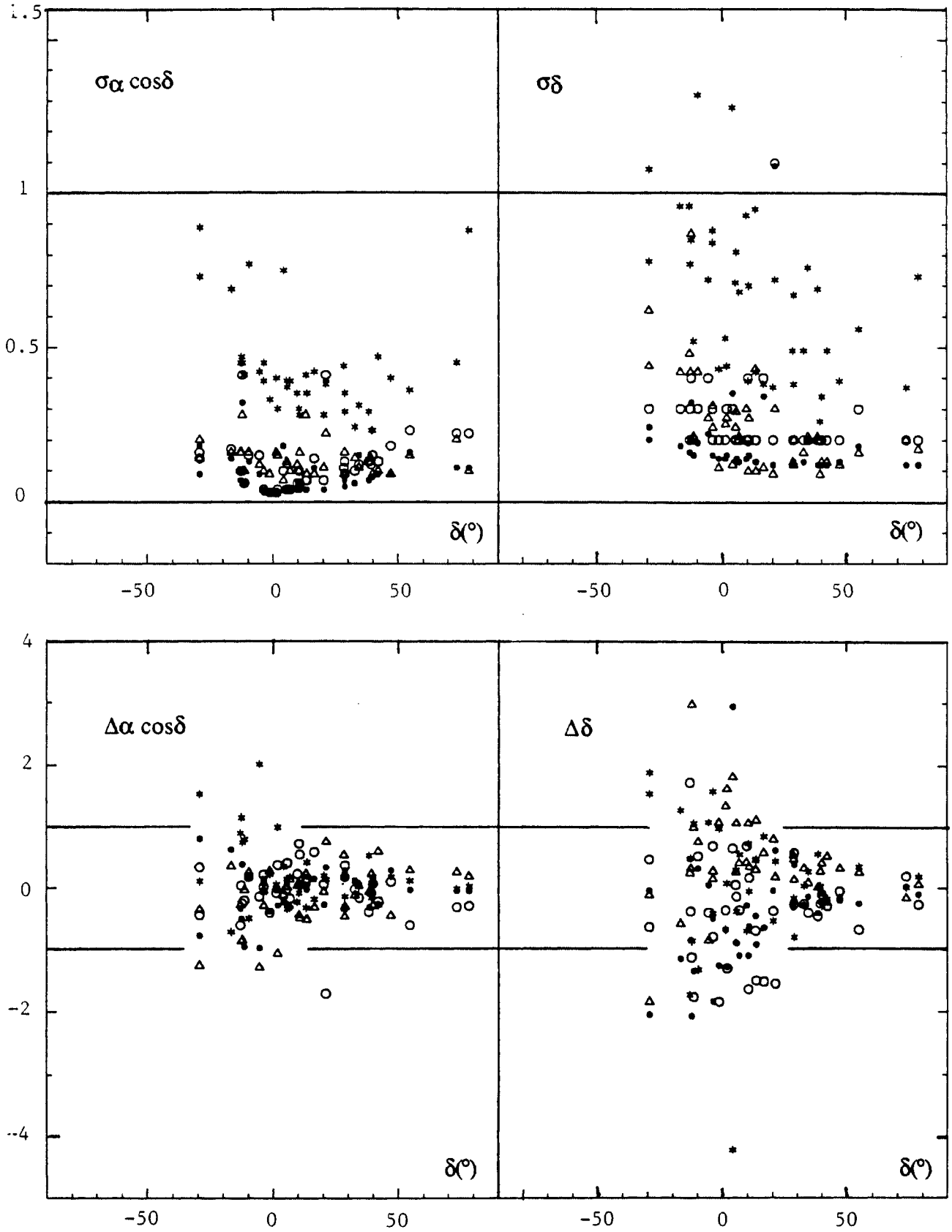

Figure 8a. 39 sources common to four catalogues : formal uncertainties (upper part) and residual position differences (lower part) as a function of declination . Unit: 0.001"
Catalogues G90 (•), J90 (*), N90 (o), U90 (Δ).

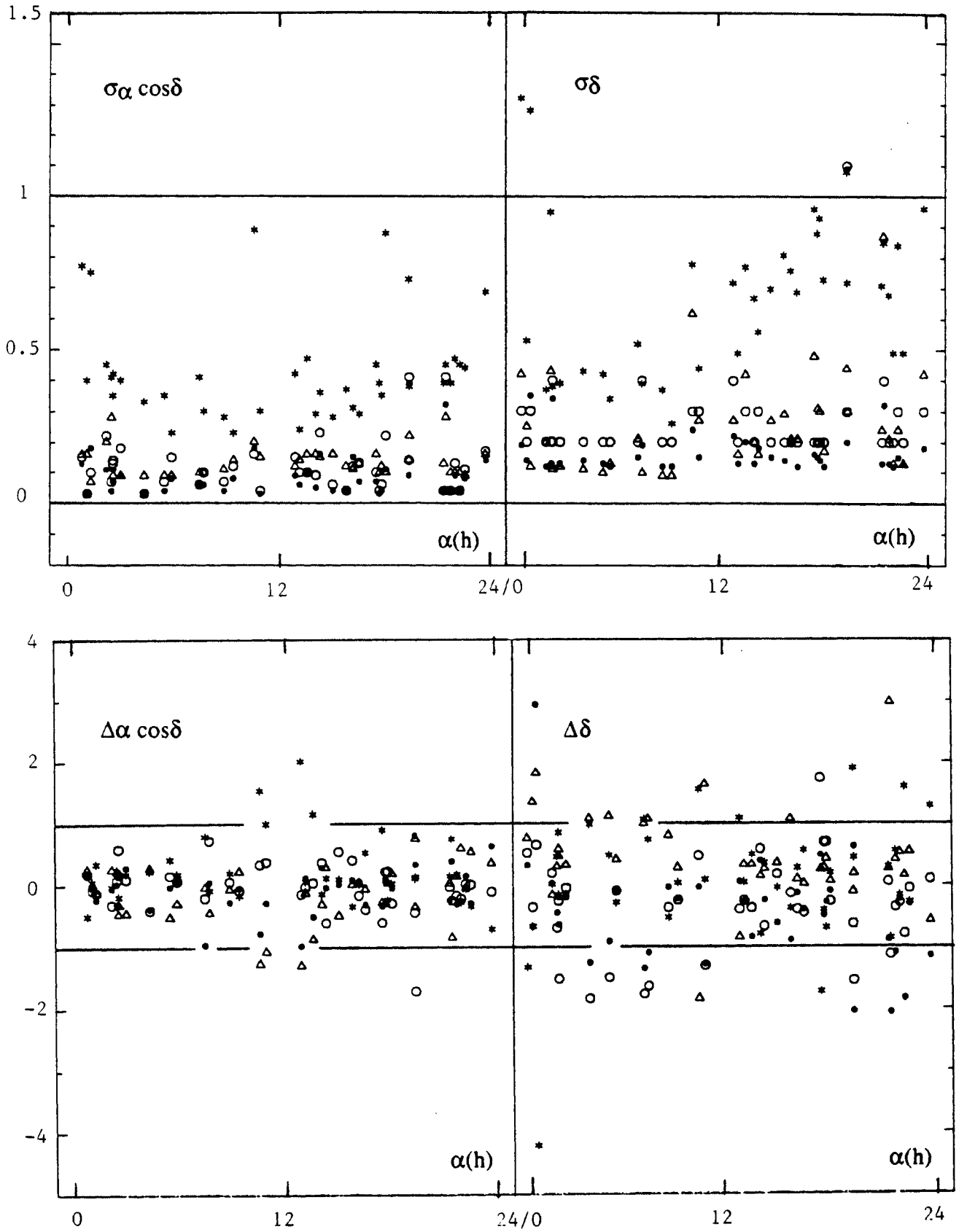

Figure 8b. 39 sources common to four catalogues : formal uncertainties (upper part) and residual position differences (lower part) as a function of right ascension. Unit: 0.001".
Catalogues G90 (•), J90 (*), N90 (o), U90 (Δ).

Using the five sets of residual position differences between pairs of independent catalogues after taking out the relative rotations, we consider two classes of sources, according to their declinations. From figures 8a and 8b, we split the sets of sources at declination 0° for the right ascension residual position differences and declination +20° for the declination residual position differences. Having thus defined four classes with homogeneous behaviours, we perform the three corner hat method : for a given class, the observed variance of the residual position differences in a pair of catalogues is equal to the sum of the intrisic true variances of the positions in each of the two catalogues. By forming all possible triangles between independent catalogues, the true precision of the source coordinates is estimated (see table 12). In the best case, the true uncertainty of the coordinates is about 0.2 mas ; in the worst case, the true uncertainty is still under 1 mas.

Table 12. Estimated position uncertainty of sources observed in four programs.
Unit : 0.001"

	Class:	$\delta \geq 0$	$\delta \geq 20°$	$\delta < 0$	$\delta < 20°$
Cat.	Coordinate:	$\alpha \cos\delta$	δ	$\alpha \cos\delta$	δ
	Nb sources:	27	15	12	24
G90		0.20	0.23	0.34	0.81
J90		0.24	0.23	0.67	0.85
N90		0.27	0.28	0.18	0.85
U90		0.33	0.31	0.42	0.67

Possible systematic effects related to physical characteristics in the 39 objects common to G90, J90, N90, U90.

The influence of various physical characters of the source, as given by Preston *et al.* (1985), is investigated.

Figures 9-12 show the average position differences behaviour as a function of

- the type of object,
- the total flux,
- the redshift,
- the spectral index defined by Preston *et al.* (1985, p.1599).

In order to disantangle the low declination effect, the plots of raw residual differences are complemented with plots where they are corrected by a simple empirical function of declination. As there is no particular correlation of low declinations with any of the physical characteristics considered here, we conclude from the second series of plots that there is no obvious influence of the physical characteristics of the objects on the dispersion of the source coordinates.

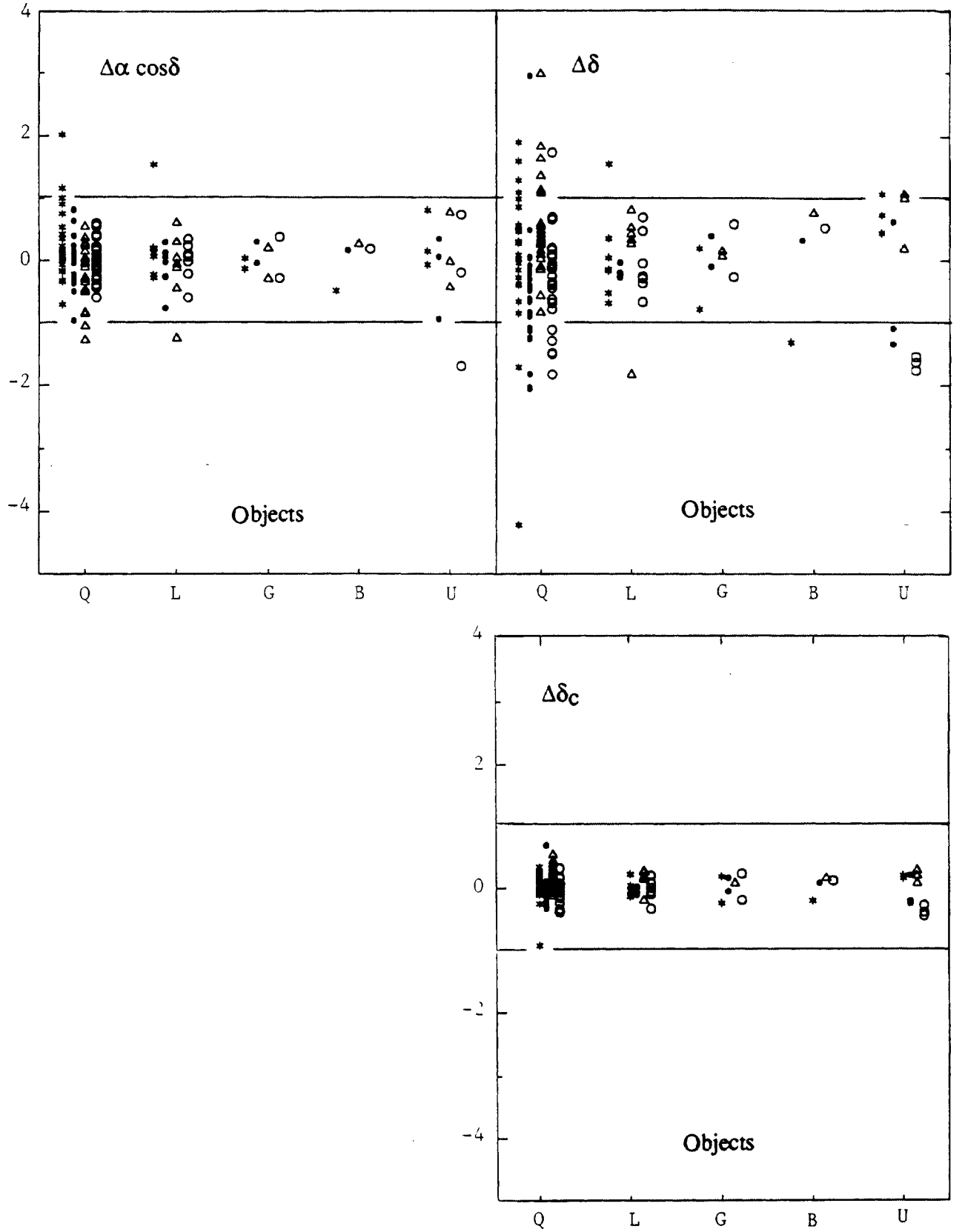

Figure 9. Coordinate residual position differences as a function of the type of object.
Q : quasar ; BL : B Lac object ; G : galaxy ; B : Blue object ; U : unknown.
Upper part : raw residual position differences ; lower part : residual declination differences corrected for an effect in declination. Unit: 0.001".
Catalogues G90 (•), J90 (*), N90 (o), U90 (Δ).

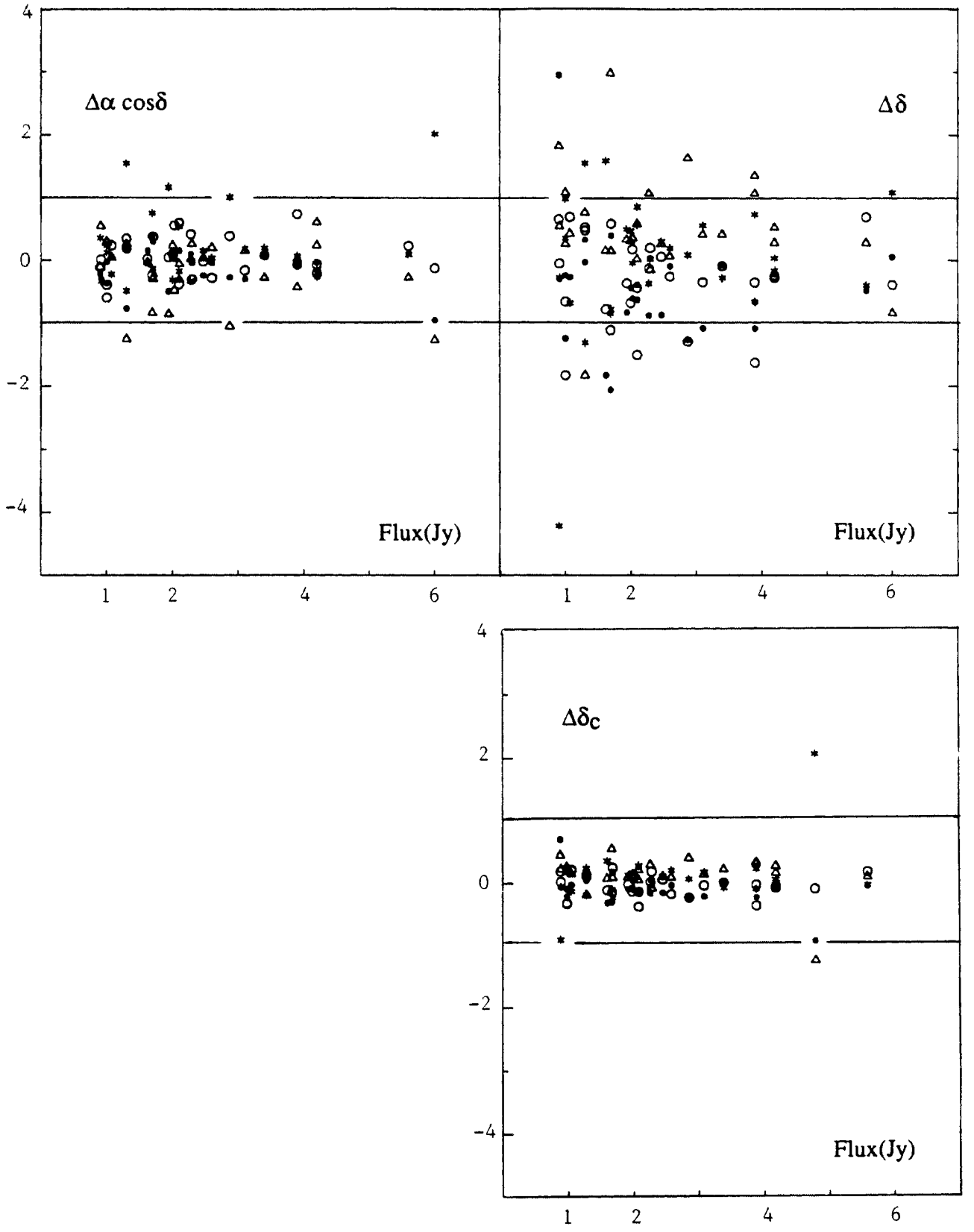

Figure 10. Coordinate residual position differences as a function of total flux.
Upper part : raw residual position differences ; lower part : residual declination differences corrected for an effect in declination. Unit: 0.001".
Catalogues G90 (•), J90 (*), N90 (o), U90 (Δ).

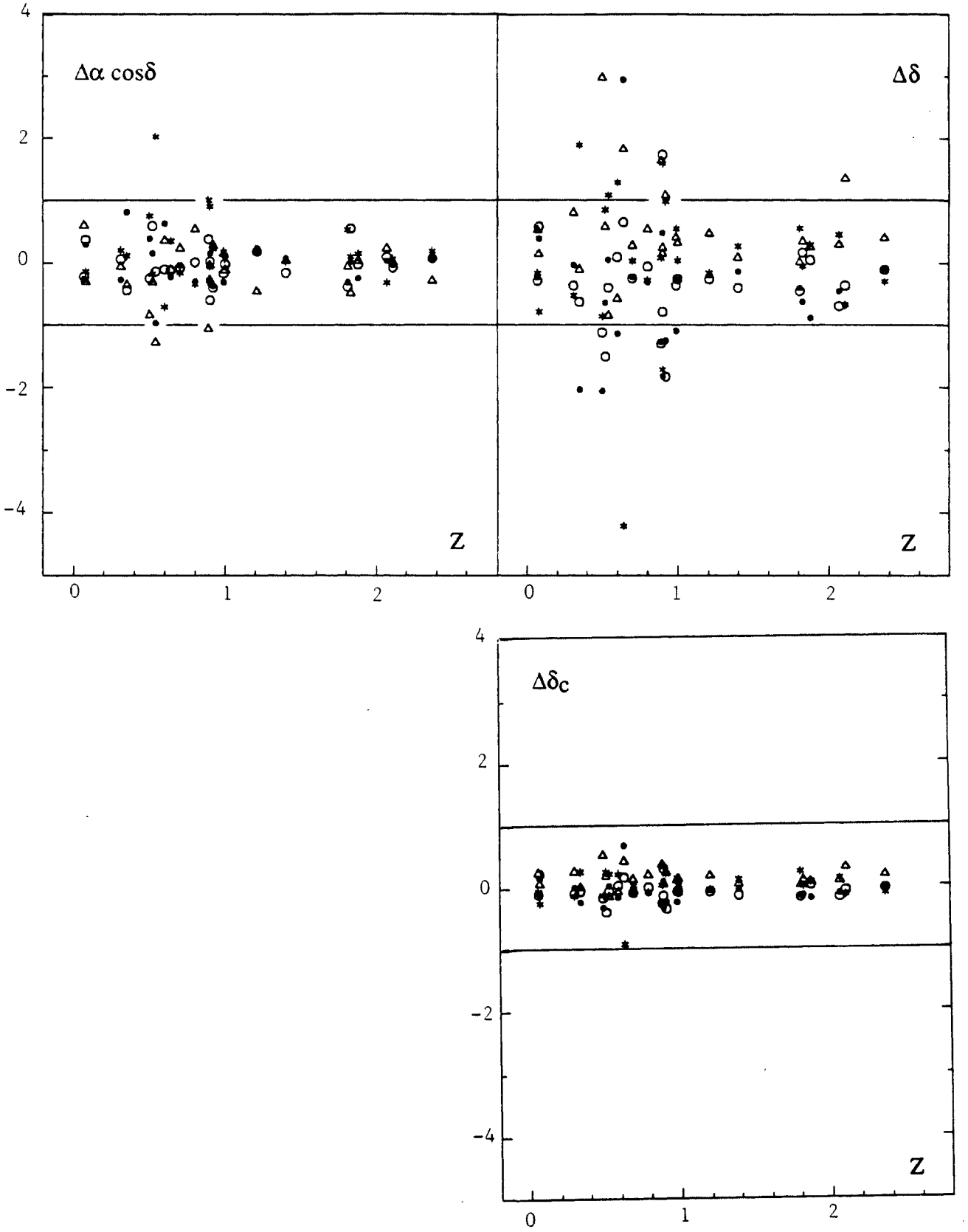

Figure 11. Coordinate residual position differences as a function of redshift
Upper part : raw residual position differences ; lower part : residual declination differences corrected for an effect in declination. Unit: 0.001".
Catalogues G90 (•), J90 (*), N90 (o), U90 (Δ).

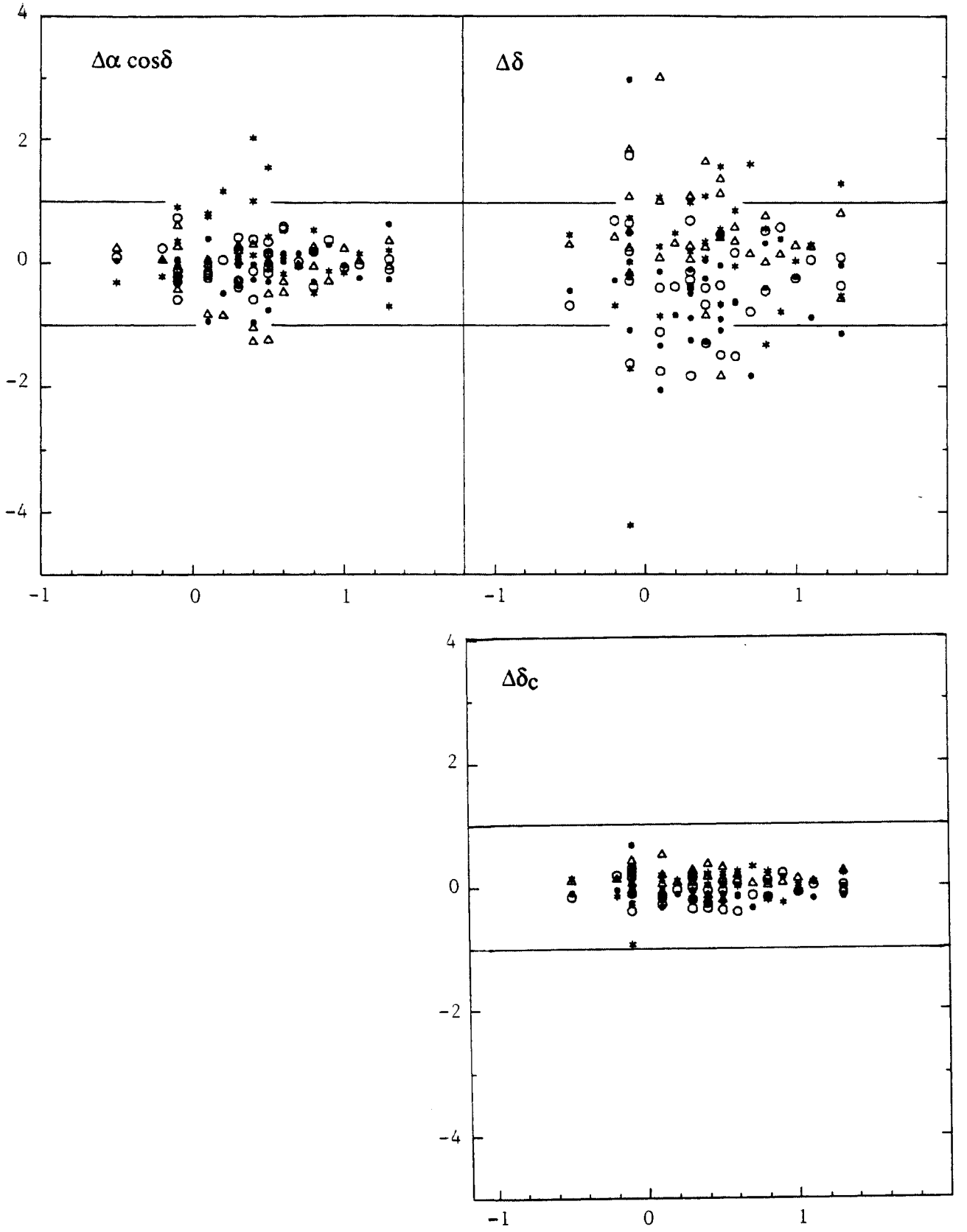

Figure 12. Coordinate residual position differences as a function of spectral type.
Upper part : raw residual position differences ; lower part : residual declination differences corrected for an effect in declination. Unit: 0.001".
Catalogues G90 (•), J90 (*), N90 (o), U90 (Δ).

Comparison of four 1991 VLBI extragalactic reference frames

Analyses of four VLBI extragalactic reference frames submitted to IERS in 1991 are presented here. They have been obtained in the 1991 global solutions at the Goddard Space Flight Center (GSFC), at the Jet Propulsion Laboratory (JPL), at the US National Geodetic Survey (NGS) and at the US Naval Observatory (USNO).

In order to assess the astrometric quality of the four individual frames we have performed comparisons two by two to evaluate the relative orientations between axes and to determine the existence of relative regional deformations.

Table 13 presents the four individual VLBI frames compared. In all cases the pole of the celestial reference frame is fixed by the standard J 2000.0 precession and the IAU 1980 Theory of nutation. In the four solutions, corrections to the position of the celestial pole given by the models are adjusted simultaneously with the astrometric and geodetic parameters. In this process, each series of the celestial pole offsets, $d\psi$ and $d\varepsilon$, is referred to an arbitrary value at some epoch, which gives rise to small offsets in the effective poles of the various frames.

Table 13. Individual VLBI axtragalactic reference frames compared in the analyses.

Frame			Number of objects	Declination interval	Observational data
G91	RSC(GSFC)	91 R 03	234	-81°, +85°	CDP
J91	RSC(JPL)	91 R 01	241	-45°, +85°	DSN
N91	RSC(NGS)	91 R 01	77	-81°, +79°	POLARIS/IRIS (CDP)
U91	RSC(USNO)	91 R 02	80	-41°, +79°	NAVNET

The origin of right ascensions is fixed a priori in the VLBI solutions. In RSC(GSFC) 91 R 03 the conventional right ascension of 3C273B is used to define the origin on the equator. In RSC(NGS) 91 R 01, the radio source coordinates are adjusted by fixing the mean of the right ascensions of nine radio sources to values which were obtained in previous adjustments referred to conventional right ascension of 3C273B. JPL and USNO frames are aligned as closely as possible to the IERS Celestial Reference Frame. In RSC(JPL) 91 R 01 the right ascension and declination of 0851+202 and the declination of 0234+285, both of which are primary sources in the IERS frame, are held fixed at their values in RSC(IERS) 89 C 01. The NAVNET reference frame is obtained in a two step process; in the first step the right ascension of the source 2216-038 is fixed at the value given in RSC RSC(IERS) 90 C 01; the right ascension and declination of 0202+149 and the declination of 0742+103 are fixed in a second step to the values obtained in the first one. In all frames, the standard errors are the values obtained from the adjustment, and they can be interpreted as the limit that would be attained in the absence of unmodeled systematic errors.

The relative rotation angles in the four pairs of frames, estimated by a weighted least squares fit over all common sources, are in table 14. In most cases the directions of axes between the 1991 individual realisations of the VLBI celestial reference frame are consistent better than 0.0015" for A_1 and A_2, with uncertainties at the level of 0.0001"; when the effect of inhomogeneous fixing of the levels of $d\psi$, $d\varepsilon$ is taken into account, the largest difference is 0.0004". The origins of right ascensions, arbitrarily fixed in each frame, differ by less than 0.0003", as indicated by the values of the angle A_3.

Table 14. Relative orientations of the four 1990 individual frames. N indicates the number of common sources considered, σ indicates the rms of the post-fit residuals. Units for A_1, A_2, A_3 and σ: 0.001".

Frame 1-Frame 2	N	A_1	A_2	A_3	σ
N91 - G91	73	+0.196 ±0.038	+0.911 ±0.036	+0.003 ±0.033	0.27
U91 - G91	37	+0.461 ±0.095	+1.740 ±0.094	+0.053 ±0.077	0.63
G91 - J91	150	-1.406 ±0.088	-2.823 ±0.084	+0.219 ±0.065	0.35
N91 - J91	62	-1.131 ±0.119	-1.881 ±0.112	+0.232 ±0.088	0.43
N91 - U91	48	-0.289 ±0.101	-0.815 ±0.096	+0.006 ±0.084	0.53
U91 - J91	74	-0.637 ±0.108	-1.065 ±0.099	+0.198 ±0.079	0.48

Relative deformations

The different network geometries might cause regional deformations in the VLBI frames produced by the individual groups. Source positions in the northern hemisphere are somewhat better determined than in the southern hemisphere. The precision of declinations near the equator strongly depends on the length of the North-South baseline components and on the strategies of observation. A lack of sensitivity to this declination range is noticeable with some networks which are predominantly oriented in the East-West direction.

We have investigated the existence of regional deformations between pairs of frames by comparing the positions of common radio sources after removing the relative orientations previously evaluated (table 14). The position differences of the sources common to the pairs of catalogues are shown in figures 13a through 13f. Most of the position differences are smaller than 0.002". However, systematic effects are present in some pairs of frames. Only a few systematic differences larger than 0.0005" between frames elaborated at NGS and GSFC (figure 13a) are observed. The distribution of vectors in figure 13b suggests that there exists a deformation between NGS and JPL frames with a general effect in declination and a smaller effect in right ascension in the interval 20h - 4h. In the comparison between NGS and USNO frames (figure 13c) most vectors are oriented in the North-South direction, representing a systematic effect in declination only. The vectors representing the positions differences of sources common to USNO and GSFC in figure 13d are oriented in the South-North direction, showing a deformation in declination. Vectors seem to follow a random distribution in the comparison USNO - JPL of figure 13e. In figure 13f, the systematic differences at low declinations already noticed in NGS-JPL (figure 13b) are confirmed for the additional sources common to GSFC and JPL.

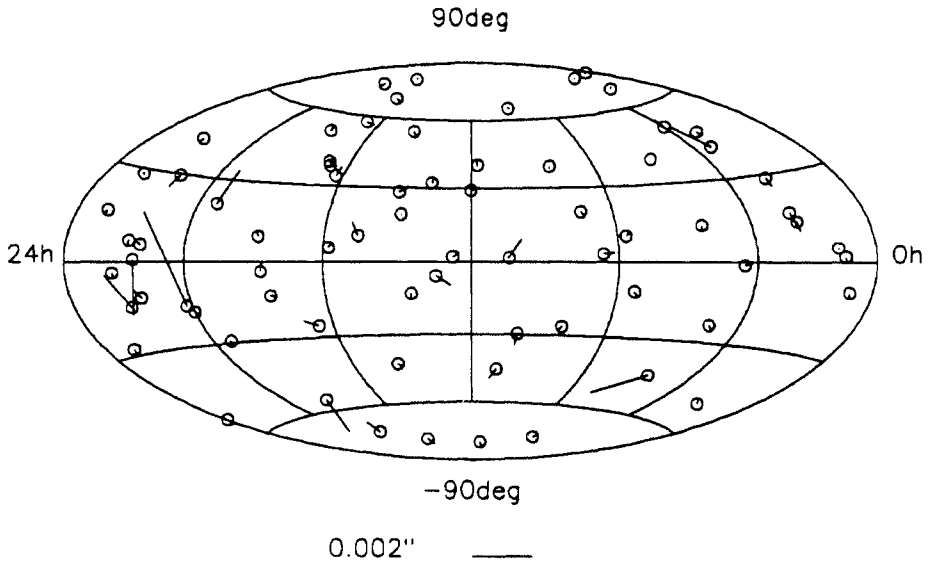

Figure 13a. Position differences of radio sources common to NGS and GSFC frames in Aitoff projection. The solid lines join the NGS positions (circles) to the GSFC positions after removing the global rotations between the two frames. The scale of the vector module is shown in the figure.

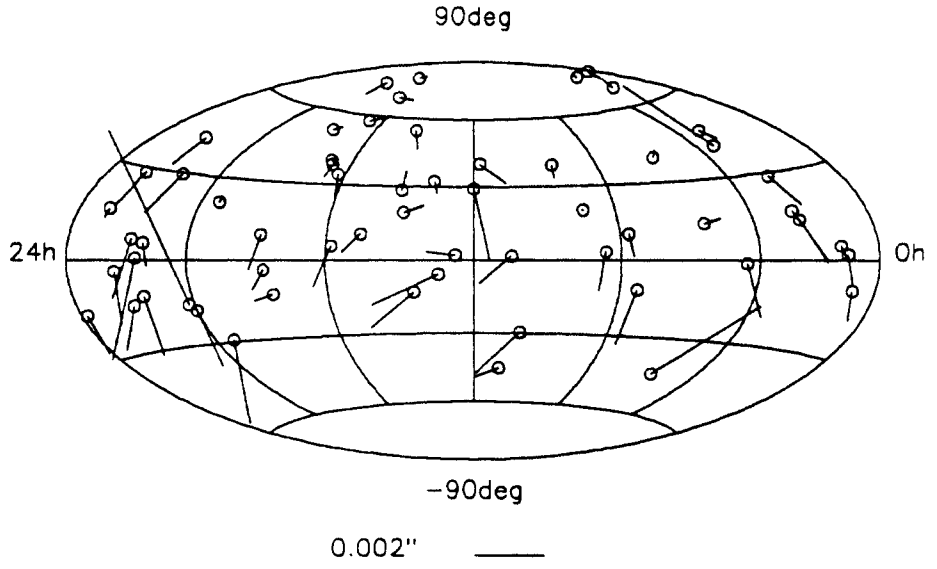

Figure 13b. Position differences of radio sources common to NGS and JPL frames in Aitoff projection. The solid lines join the NGS positions (circles) to the JPL positions after removing the global rotations between the two frames. The scale of the vector module is shown in the figure. Two sources with large position differences are not shown.

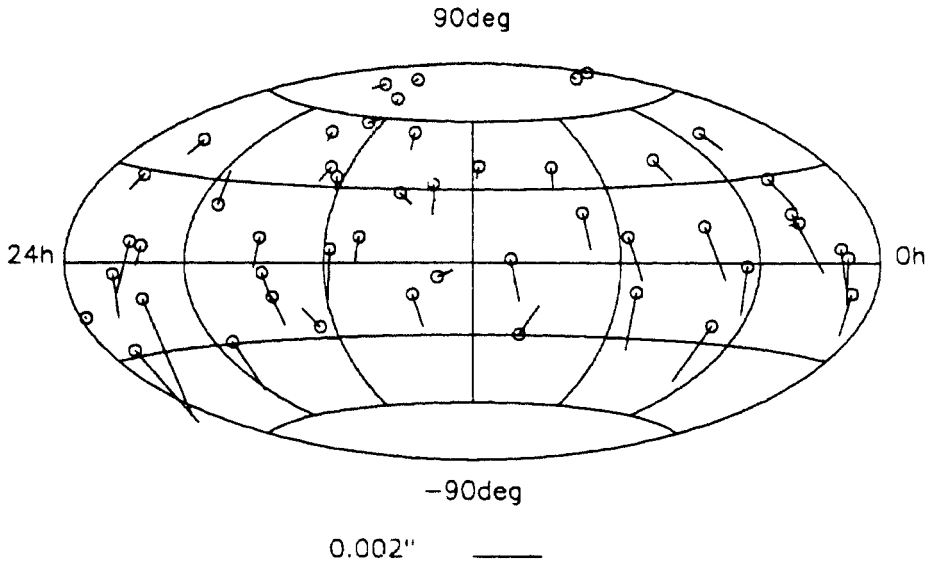

Figure 13c. Position differences of radio sources common to NGS and USNO frames in Aitoff projection. The solid lines join the NGS positions (circles) to the USNO positions after removing the global rotations between the two frames. The scale of the vector module is shown in the figure.

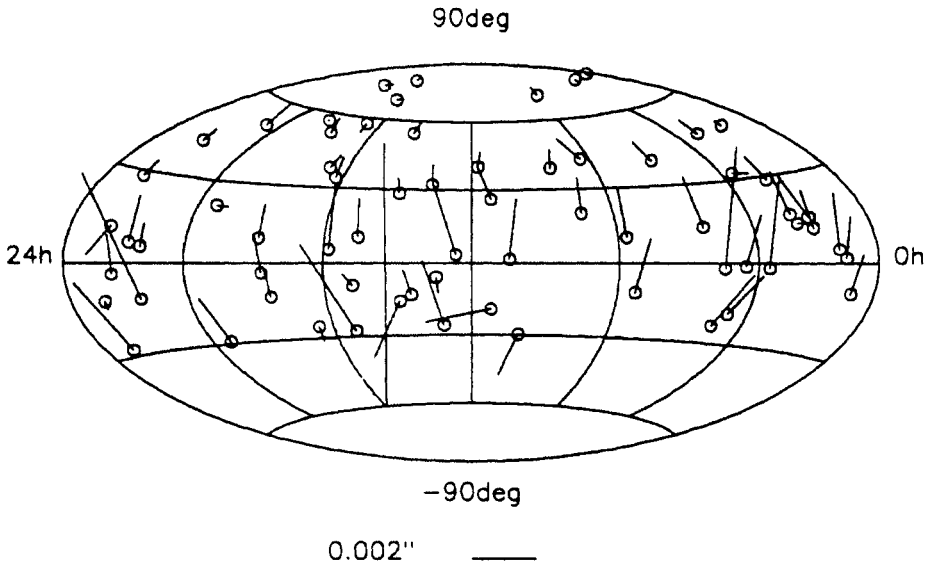

Figure 13d. Position differences of radio sources common to USNO and GSFC frames in Aitoff projection. The solid lines join the USNO positions (circles) to the GSFC positions after removing the global rotations between the two frames. The scale of the vector module is shown in the figure.

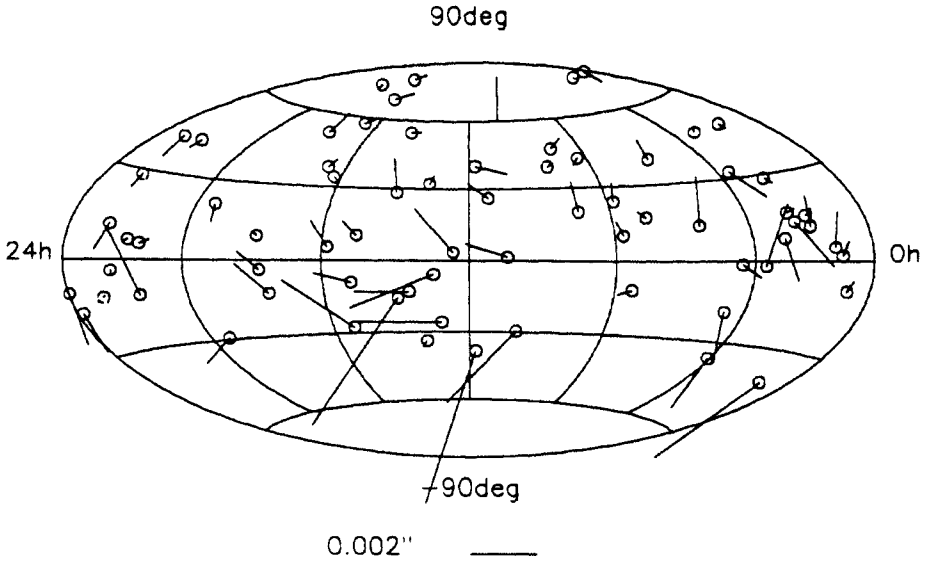

Figure 13e. Position differences of radio sources common to USNO and JPL frames in Aitoff projection. The solid lines join the USNO positions (circles) to the JPL positions after removing the global rotations between the two frames. The scale of the vector module is shown in the figure. Four sources with large position differences are not shown.

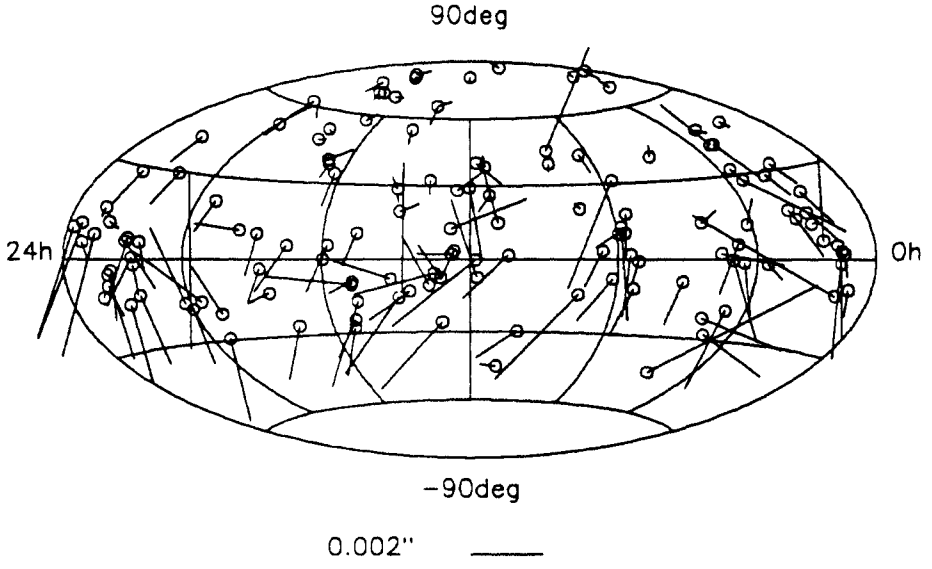

Figure 13f. Position differences of radio sources common to GSFC and JPL frames in Aitoff projection. The solid lines join the GSFC positions (circles) to the JPL positions after removing the global rotations between the two frames. The scale of the vector module is shown in the figure. Fifteen sources with large position differences are not shown.

Analysis of RSC(IERS) 91 C 01

The initial realization of the IERS Celestial Reference Frame, RSC(IERS) 88 C 01, (Arias *et al.*, 1988) included a total of 228 extragalactic radio sources. In the normal process of IERS global analyses, the ICRF is re-evaluated whenever new information is available. This is a maintainance process, in which strict rules are applied, with the aim of insuring the consistency of the direction of axes with the initial definition, while improving the accuracy of the existing sources and extending the frame to new sources.

The adjustment of the celestial reference frame is one part in an algorithm which also embodies maintenace of the terrestrial frame and of consistent series of EOP over the years. This approach makes it possible to compare the corresponding elements in the various individual solutions, thus providing an external check of the consistency of the models used. In the case of the celestial frames, the model for comparisons is a three-angle rotation. The consistency checks are based on a comparison of rotation angles between reference frames with systematic differences between time series of universal time and of the celestial pole offsets (Feissel, 1991). The practical implementation which led to RSC(IERS) 91 C 01, published in the IERS Annual Report for 1990, is described here.

RSC(IERS) 91 C 01 results from the combination of two frames obtained independently by analysis centres at Goddard Space Flight Center (GSFC) and Jet Propulsion Laboratory (JPL).The coordinates of the 334 objects in RSC(GSFC) 91 R 04 are evaluated from data acquired since 1979 by the NASA Crustal Dynamics Project (CDP), POLARIS/IRIS, the USNO NAVNET and the NRL reference frame program. The right ascension origin of the GSFC reference frame is defined by the a priori right ascension of the quasar 3C273B(1226+023). The RSC(JPL) 91 R 01 reference frame (241 objects) is elaborated from the analysis of Deep Space Network (DSN) VLBI observations. The coordinate system is tied to RSC(IERS) 89 C 01 by fixing the right ascension and the declination of 0851+202 and the declination of 0234+285 to their values in that frame. These objects are among the best observed sources in the DSN catalogue, and are primary sources in the IERS Celestial Reference Frame. Both individual reference frames are referred to J2000.0 by means of the standard IAU 1976 precession model and the IAU 1980 Theory of nutation. In their data analysis, radio source positions are obtained in parallel to an adjustment of orrections to the direction of the celestial pole given by the models. The frames have 179 objects in common.

Selection of primary sources of RSC(IERS) 91 C 01

The individual catalogues include well observed pointlike sources, with small uncertainties in their coordinates, and other sources, less observed or having sizeable structure, with coordinates of greater uncertainty. It is therefore necessary to select carefully the *primary sources* to be used in the maintenance of the frame. The 23 primary sources in the initial definition of the IERS frame were selected on the basis of structure, sky coverage, time stability and number of observations (Carter, 1987). In more recent realizations, the selection is based on statistical tests on the actual coordinates in independent programs.

Radio sources common to at least two of the frames used for the maintenance or densification, but not in the primary list, are defined as *secondary sources*, while those belonging to only one individual frame are the *complementary sources*. Neither secondary nor complementary sources are used to define the directions of axes of the combined frame; only their positions relative to it are evaluated.

The primary sources are used to maintain the direction of axes of the celestial reference frame.RSC(IERS) 91 C 01 contains 57 primary sources selected on the basis of statistical analysis performed on the VLBI catalogues described in the previous section (G91, J91, N91, U91).The method of selection of primary sources is as follows.

After solving for the rotation angles A_1, A_2, A_3 between the six pairs of frames, we performed χ^2 tests on the post-fit residuals, for right ascensions and declinations separately, and for both coordinates together. The procedure used a recurrent elimination of sources with the largest position discrepancies until a normal distribution is reached. Table 15 shows, for each pair of catalogues, the χ^2 obtained for the normal distribution, the number of times the rms of the residuals considered as a limit value, and the percentage of objects rejected.

Table 15. Results of the elimination of radio sources to obtain a normal distribution of post-fit residuals.

Frame 1-Frame 2	χ^2			rejected
	α	δ	$\alpha+\delta$	obj.(%)
NGS - GSFC	1.0	1.5	1.6	10
USNO - GSFC	1.9	0.9	1.4	2
GSFC - JPL	1.6	1.3	1.1	19
NGS - JPL	1.5	1.3	1.6	4
NGS - USNO	1.8	1.0	0.9	0
USNO - JPL	1.1	1.2	1.5	8

From the six comparisons of frames, 100 radio sources provide a normal distribution of residuals after taking out the relative orientations between frames. However, we have retained as primary sources only those objects contained at least in three catalogues, resulting in a set of 57 primary sources. These sources are distributed in the declination range $-45° < \delta < +74°$, 41 of them in the northern hemisphere and 16 in the southern hemisphere. The coordinates of the 57 sources in RSC(IERS) 91 C 01 are listed in table 16. 44 objects with post-fit residuals following a normal distribution were not included in the primary list because they belong only to two frames and they permit only one comparison. These objects can be considered good candidates to become primary in the future, provided that they will be included in more than two VLBI solutions. They are evenly distributed in both hemispheres (see table 17).

In the previous realization of the IERS celestial reference frame, RSC (IERS) 90 C 01 (IERS, 1990), the 51 sources retained as primary were those which showed position differences smaller than 0.0015" in all possible comparisons between the four 1990 catalogues of table 8, after taking out the relative orientations. Even if the criteria applied in the selection of primary sources in RSC (IERS) 90 C 01 and in RSC (IERS) 91 C 01 seem formally different, they lead almost to the same set. The residuals of only three primary sources of the previous realisation were rejected by the χ^2 test.

In parallel to the statistical analyses of the object coordinates available from various analysis centres, checks of the size and variability of the radio sources are also performed using maps available in the literature (*e.g.*, Charlot, 1990).

Table 16. Sources used to maintain the axes of RSC(IERS) 91 C 01 (primary sources)

Radio Source Coordinates — RSC(IERS) 91 C 01

SOURCE	RIGHT ASCENSION	DECLINATION	UNCERTAINTY	
	h m s	° ' "	s	"
0016+731	0 19 45.786404	73 27 30.01761	0.000081	0.00024
0048-097	0 50 41.317360	- 9 29 5.20906	0.000016	0.00031
0106+013	1 8 38.771065	1 35 0.31788	0.000016	0.00027
0119+041	1 21 56.861675	4 22 24.73538	0.000016	0.00030
0133+476	1 36 58.594799	47 51 29.10023	0.000021	0.00024
0201+113	2 3 46.657040	11 34 45.41044	0.000021	0.00038
0229+131	2 31 45.894035	13 22 54.71659	0.000016	0.00024
0234+285	2 37 52.405659	28 48 8.99027	0.000017	0.00024
0235+164	2 38 38.930080	16 36 59.27506	0.000016	0.00024
0300+470	3 3 35.242210	47 16 16.27571	0.000019	0.00024
0333+321	3 36 30.107637	32 18 29.34219	0.000025	0.00030
0336-019	3 39 30.937769	- 1 46 35.80314	0.000016	0.00028
0420-014	4 23 15.800691	- 1 20 33.06483	0.000016	0.00025
0434-188	4 37 1.482683	-18 44 48.61213	0.000018	0.00030
0528+134	5 30 56.416725	13 31 55.15023	0.000016	0.00024
0552+398	5 55 30.805599	39 48 49.16540	0.000016	0.00024
0727-115	7 30 19.112469	-11 41 12.59978	0.000017	0.00028
0742+103	7 45 33.059502	10 11 12.69292	0.000016	0.00026
0814+425	8 18 15.999644	42 22 45.41503	0.000019	0.00026
0823+033	8 25 50.338356	3 9 24.52052	0.000016	0.00026
0851+202	8 54 48.874924	20 6 30.64131	0.000016	0.00025
0923+392	9 27 3.013887	39 2 20.85193	0.000016	0.00024
1055+018	10 58 29.605223	1 33 58.82409	0.000016	0.00027
1104-445	11 7 8.694184	-44 49 7.61854	0.000036	0.00033
1123+264	11 25 53.711910	26 10 19.97878	0.000016	0.00025
1144+402	11 46 58.297905	39 58 34.30477	0.000023	0.00034
1156+295	11 59 31.833895	29 14 43.82718	0.000023	0.00034
1222+037	12 24 52.421886	3 30 50.29375	0.000021	0.00048
1226+023	12 29 6.699768	2 3 8.59897	0.000023	0.00029
1308+326	13 10 28.663847	32 20 43.78289	0.000016	0.00026
1334-127	13 37 39.782803	-12 57 24.69244	0.000019	0.00032
1354+195	13 57 4.436638	19 19 7.37243	0.000016	0.00029
1404+286	14 7 0.394398	28 27 14.69019	0.000020	0.00031
1418+546	14 19 46.597378	54 23 14.78700	0.000023	0.00029
1502+106	15 4 24.979786	10 29 39.19905	0.000016	0.00031
1510-089	15 12 50.532932	- 9 5 59.82878	0.000019	0.00032
1519-273	15 22 37.675987	-27 30 10.78429	0.000022	0.00047
1548+056	15 50 35.269253	5 27 10.44862	0.000019	0.00032
1611+343	16 13 41.064232	34 12 47.90897	0.000016	0.00030
1633+382	16 35 15.492952	38 8 4.50064	0.000017	0.00030
1641+399	16 42 58.809925	39 48 36.99405	0.000016	0.00030
1730-130	17 33 2.705772	-13 4 49.54727	0.000019	0.00033
1739+522	17 40 36.977818	52 11 43.40752	0.000022	0.00033
1741-038	17 43 58.856155	- 3 50 4.61603	0.000018	0.00032
1749+096	17 51 32.818573	9 39 0.72885	0.000018	0.00032

Table 16 (Cont.)

Radio Source Coordinates RSC(IERS) 91 C 01

SOURCE	RIGHT ASCENSION	DECLINATION	UNCERTAINTY	
	h m s	° ' "	s	"
1958-179	20 0 57.090431	-17 48 57.67130	0.000020	0.00033
2113+293	21 15 29.413446	29 33 38.36711	0.000019	0.00030
2121+053	21 23 44.517361	5 35 22.09380	0.000018	0.00031
2128-123	21 31 35.261730	-12 7 4.79533	0.000018	0.00032
2145+067	21 48 5.458663	6 57 38.60467	0.000016	0.00030
2200+420	22 2 43.291355	42 16 39.98011	0.000020	0.00027
2216-038	22 18 52.037727	- 3 35 36.87867	0.000019	0.00032
2230+114	22 32 36.408894	11 43 50.90447	0.000016	0.00029
2234+282	22 36 22.470835	28 28 57.41348	0.000018	0.00028
2243-123	22 46 18.231970	-12 6 51.27670	0.000019	0.00034
2251+158	22 53 57.747936	16 8 53.56139	0.000018	0.00029
2345-167	23 48 2.608485	-16 31 12.02074	0.000021	0.00032

Table 17. Candidate primary sources selected in the analysis for RSC(IERS) 91 C 01

Object	Object	Object	Object	Object
0112-017	0637-752	1124-186	1638+398	2223-052
0149+218	0716+714	1128+385	1656+053	2227-088
0202+319	0723-008	1150+812	1657-261	2255-282
0208-512	0735+178	1313-333	1738+476	2355-106
0256+075	0736+017	1342+663	1807+698	
0309+411	0748+126	1406-076	1823+568	
0402-362	0754+100	1504-166	1831-711	
0430+052	0805-077	1514-241	1954+513	
0440-003	0919-260	1555+001	2021+614	
0605-085	0954+658	1622-253	2131-021	

The combination model

The differences between catalogues are expressed in a direct trirectangle coordinate system with the x-axis and z-axis in the respective directions to the origin of right ascensions and pole of the IERS celestial frame. The model currently used considers a three-angle rotation matrix, assuming no systematic local deformation (see p. 28, this volume); the validity of the latter assumption is a part of the examination of the results. There is two steps in the compilation of RSC(IERS) 91 C 01. In step 1 the coordinates of the primary sources in the combined frame and the relative orientations $A_1(i)$, $A_2(i)$, $A_3(i)$ between it and the three individual frames (i=1, 2) are evaluated simultaneously by a weighted least squares adjustment. The directions of axes are constrained to be aligned with the axes of the previous realisation, RSC(IERS) 90 C 01. The consistency of the directions of axes of the successive realizations of the IERS celestial reference system already performed to date is estimated by the rotation angles from one version to the next, listed in table 8. The instability between the successive versions of the frame is presently well under 0.0001". In step 2 the coordinates of secondary and complementary sources in the combined frame are obtained by removing in each individual frame the relative orientation evaluated in step 1.

Comparison of two methods of combination

Recently, Sovers (1991b) produced a celestial frame with 216 objects by combining the 320 000 observations accumulated between 1978.6 and 1990.8 in the Crustal Dynamics Project (178 24-hour sessions, 135 000 observations, 76 objects), the IRIS program (452 24-hour sessions, 168 000 observations, 31 objects), the JPL Radio Reference Frame Development program (78 mainly 24-hour sessions, 10 000 observations, 230 objects), and the Time and Earth Motion Precision Observations program (663 3-hour sessions, 7000 observations, 106 objects). The CDP and IRIS data represent a large number of observations (see pp. 10-18) of relatively few objects made on a wide variety of networks in the northern hemisphere. The JPL data represent a large number of objects, observed with the three Deep Space Network stations which include one station in the southern hemisphere, with fewer observations of each source (see pp. 10-18), on longer baselines and with larger antennas than for CDP and IRIS. This reference frame, JPL 1990-3, is referred to as RSC(JPL) 90 R 03 in the following.

In comparison, RSC(IERS) 91 C 01 contains 396 objects. It was produced from the combination of two frames, obtained by GSFC (Ma and Caprette, 1991) and JPL (Steppe *et al.*, 1991) from two independent sets of observations which largely overlap the above ones. The JPL frame, RSC(JPL) 91 R 01, is based on essentially the above mentioned JPL observations; it contains 241 objects. The GSFC frame, RSC(GSFC) 91 R 04, is based on the CDP and IRIS observations above mentioned, completed up to the end of 1990, plus about 260 000 observations from 533 other sessions from the POLARIS, CDP-IRIS, NAVNET, and NRL astrometry programs. These additional observations concern only partially the sources in RSC(JPL) 90 R 03, they mainly bring new sources in the GSFC frame, which contains 334 objects.

The 216 JPL 1990-3 objects are all present in RSC(IERS) 91 C 01. 153 of them also have coordinates in the JPL and GSFC frames on which the IERS one is based. This offers the opportunity to investigate any significant difference between the two combined frames which may arise from the difference in methods of combination. Indeed it is expected that, as in the present IERS/CB algorithm the full covariance information of the individual frames that are combined is not used, local systematisms due to insufficient networks are not compensated for. The direct combination of observations is thought to be more efficient in this respect. However, as long as the networks do not cover properly the Earth, the local systematims cannot be expected to totally disappear. On the other hand, the comparison of partial frames on which the IERS/CB algorithm is based should be a more efficient tool to evaluate the accuracy of estimated coordinates than the direct combination of networks. It should be noted that for sources with structure size at the mas scale, the differences in resolution of baselines of different lengths can introduce shifts between the effective radiation centres that are observed. As in the frames presently available the source structure effects are not accounted for, inconsistencies can be expected for some sources, in the direct combination method as well as in the indirect one.

The uncertainties on the source coordinates in the two combined frames are derived from the variance information available as an output of the least square fit; they depend on the input covariance matrix of the observables and on the consistency of the data combined. In both cases considered here, the input covariance matrix is diagonal. In the case of the JPL combination, the observables are the delays and delay rates, and session-specific variance is added to account for mismodelling of some observational effects. The number of estimated parameters is about 58 000, including the 432 source coordinates. In the case of the IERS/CB combination, the observables are the differences in source coordinates in the two individual frames, and the only unknowns considered in addition to the 114 source coordinates are the angles which rotate the individual frames to the combined one. The input variance is obtained by adding quadratically the formal uncertainties provided in the individual frames (with a lower value of 0.25 mas for each). The formal uncertainty of the estimated coordinates reflect the consistency of the coordinates in the individual frames that are combined, taking into account the global relative orientations. Figure 14 shows the relationship between the formal uncertainties of the

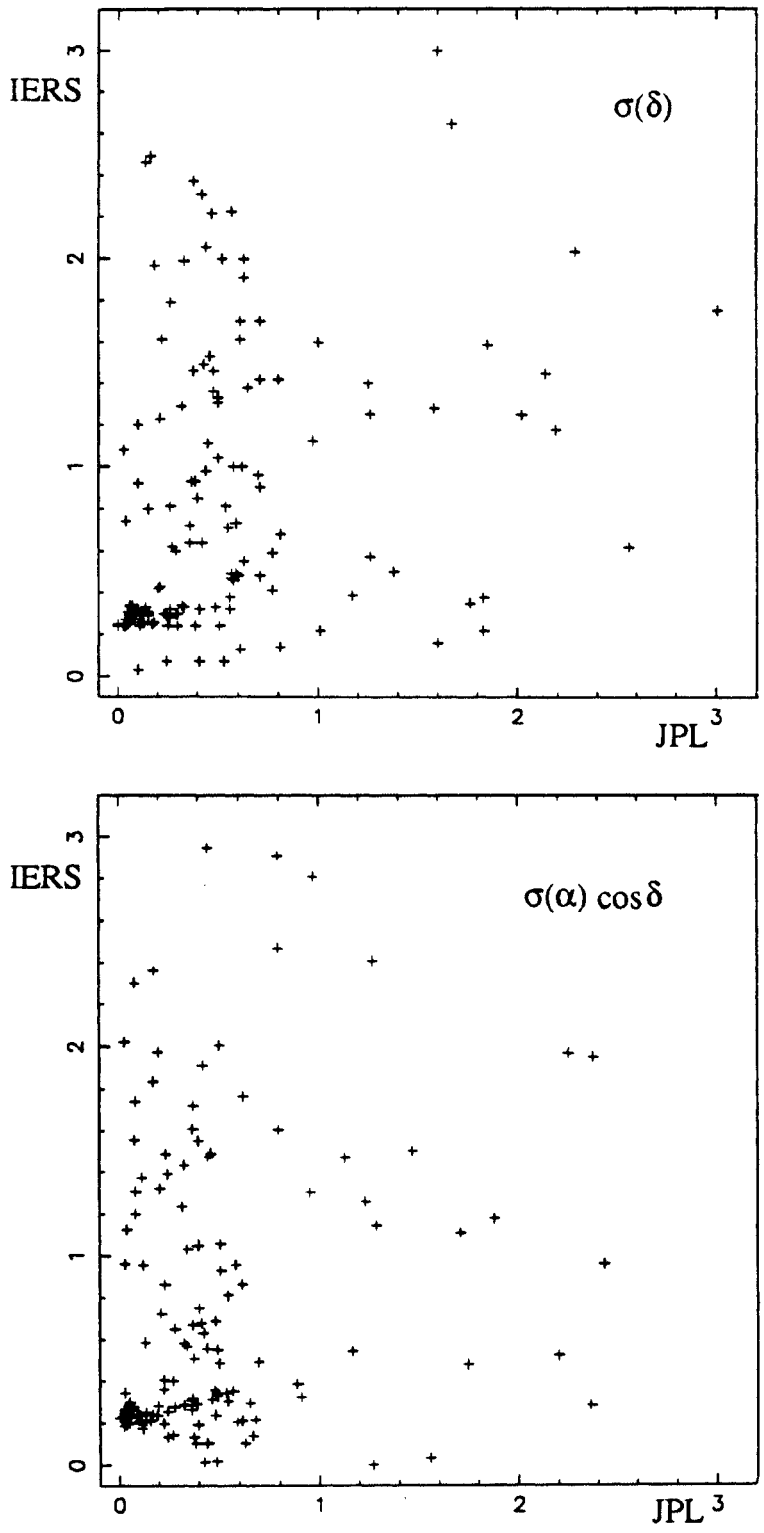

Figure 14. Formal uncertainty of the coordinates of objects in the IERS combined frame versus their value in the JPL combined frame.
Unit: 0.001".

coordinates of the same source in the two combined frames. Apart from a cluster of very small values (around 0.3 mas), the uncertainties in the IERS frame tend to be larger than in the JPL one. They are mostly smaller than 2 mas, while most of the JPL ones are smaller than 1 mas.

The differences in coordinates are investigated after taking out a global rotation between frames on the basis of the 57 primary sources of IERS (1991). The rms weighted residual in the estimation of the rotation is 0.43 mas in $\alpha \cos\delta$, and 0.61 mas in δ; the mean residual in α is negligible (0.01 mas), while it is not in δ (0.10 mas). Figure 15 shows the histogram of the residual differences between the JPL and IERS coordinates. 82% of the differences in right ascension ($\alpha \cos\delta$) are smaller than 1 mas in absolute value, but only 55% declination differences are in this range. The detailed inspection of the residuals will help characterize more precisely the declination discrepancies.

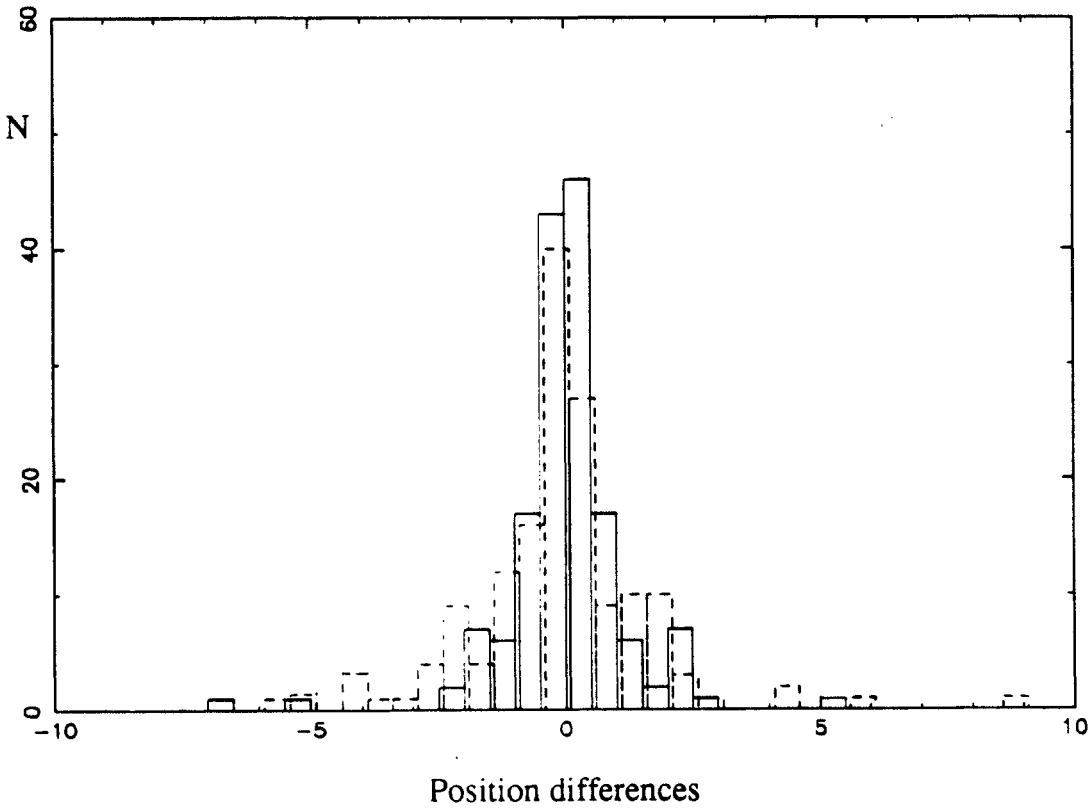

Figure 15. Histogram of position differences between the JPL and IERS combined frames (total of 151 objects). $d\alpha \cos\delta$ (solid line), $d\delta$ (dashed line). Unit: 0.001".

The residual position differences are plotted on figure 16 as a function of declination. Five of the IERS primary sources have residuals larger than 1 mas in declination, one in right ascension. The data available on them is summarized in table 18. The discrepancy in both right ascension and declination for 0016+731 seems to be due to an insufficient number of observations on the JPL side. The declination discrepancies for 0434-188, 1519-273 and 1958-179 correspond to a disagreement between the GSFC and JPL individual solutions, and the one for 1104-445 to a disagreement of the JPL combined solution with both individual solutions.

The inspection of the plot rather suggests the existence of a step of about 0.5 mas amplitude south of -5° for the declinations. Note a cluster of right ascension residuals around $\delta = -10°$ that are shifted by about -1 mas relative to the rest of the plot. The particular network geometries which contributed observations in each of the two analyses might explain this discrepancy. Other models can tentatively describe the discrepancies, using a weighting based on the root-sum-square of the formal uncertainties in the two combined frames, with a lowest value of 0.5 mas. This weighting does not account for a possible correlation between source coordinates in the two frames; it results in discarding the sources which have a large uncertainty in at least one of the frames. The dotted lines are weighted Vondrak (1977) smoothings of the plotted residuals. The smoothed trend in $d\alpha \cos\delta$ does not suggest any systematism in the low declinations; the linear trend estimated with the same weighting is $+5 \pm 2$ μas/degree (0.6 mas over the declination span covered by the common sources). The smoothed trend in declination shows a change for declinations lower than -5°, the estimated linear trend is $+6 \pm 3$ μas/degree (0.8 mas over the total declination span).

Figure 17 shows the same right ascension residuals as figure 16, with the formal uncertainties as given in the two combined frames. 98% of the differences are consistent with 0 in the 2.5 sigma limit when considering the IERS uncertainties, 86% for the JPL ones. The sections south of -20° and north of +50° are characterized by a larger dispersion. The IERS error bars are larger in these sections, reflecting the disagreement of the GSFC and JPL individual frames on which it is based. The error bars are not enlarged in the same manner in the JPL combined frame. The few outliers are associated with numbers of observations lower than 100 in the JPL and the GSFC individual frames.

Figure 18 gives the equivalent plots for the residual differences in declination. Here 73% of values are consistent with 0 in the 2.5 sigma limit in the IERS case, 57% in the JPL case. The above comment on the scale of JPL and IERS uncertainties in the north and south extreme sections is also valid for declinations. All differences larger 3 mas in absolute value are associated with small numbers of observations; they tend to cluster under $\delta = -14°$ and over $\delta = 50$. The only one exception is 1034-293 (marqued with an arrow) which has about 2200 observations. This source is one for which the four 1990 frames compared in the first part of this section give coordinates that are inconsistent at the 1-2 mas level (see table 10, p. 31).

It should be noted that the comparisons made here give information on the consistency and the precision of source coordinates, but not on their accuracy. Further studies should make use of the session per session covariance information and of the astrometric correction for source structure.

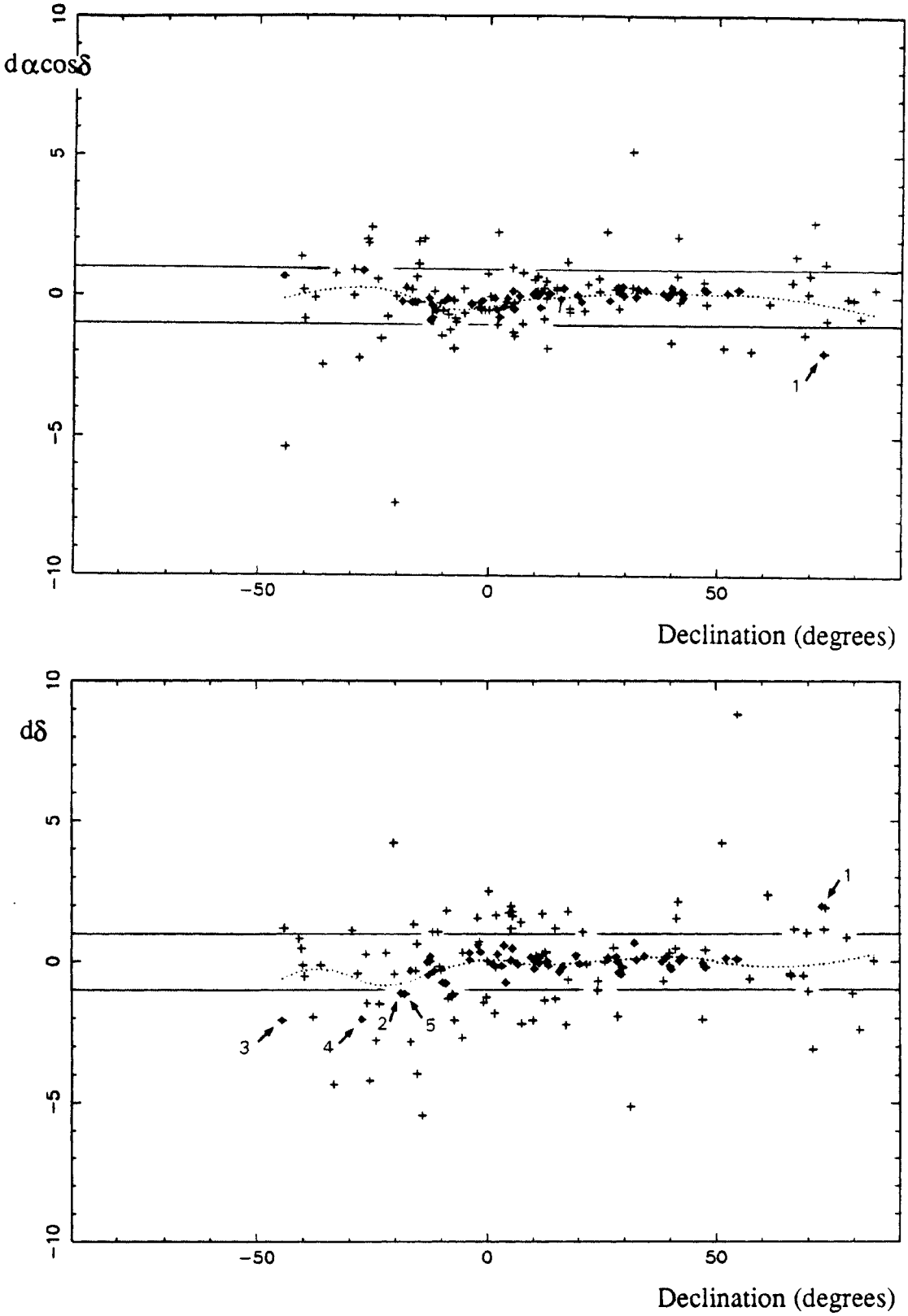

Figure 16. Residual differences in position of objects in the JPL combined frame with the IERS combined frame (JPL-IERS). The diamonds represent the IERS (1991) primary sources. The dotted line is a Vondrak smoothing of the raw differences. Unit: 0.001".

Table 18. Five IERS(1991) primary sources having large position discrepancies with JPL 1990-3

	0016+731	0434-188	1104-445	1519-273	1958-179
Number in figure 16	1	2	3	4	5
Number of observations					
JPL 1990-3	33	100	132	180	119
IERS 1991					
JPL	11	108	141	189	129
GSFC	1583	150	123	61	270
Formal uncertainty (mas)					
$\alpha \cos\delta$					
JPL comb	0.57				
IERS comb	0.24				
JPL ind	0.22				
GSFC ind	0.27				
δ					
JPL comb	0.39	0.29	0.49	0.57	0.33
IERS comb	0.24	0.30	0.33	0.47	0.33
JPL ind	0.16	0.45	0.74	0.87	0.74
GSFC ind	0.12	0.23	0.23	0.37	0.17
Residual differences (mas)					
$\alpha \cos\delta$					
JPL comb.-IERS comb	-1.98				
JPL comb.-JPL ind	-1.91				
JPL comb.-GSFC ind	-1.87				
IERS comb.-JPL ind	+0.08				
IERS comb.-GSFC ind	+0.11				
δ					
JPL comb.-IERS comb	+1.99	-1.14	-2.10	-2.06	-1.17
JPL comb.-JPL ind	+2.08	+0.12	-1.98	-1.18	-0.49
JPL comb.-GSFC ind	+1.79	-1.52	-1.96	-2.24	-1.37
IERS comb.-JPL ind	+0.09	+1.25	+0.12	+0.90	+0.69
IERS comb.-GSFC ind	-0.19	-0.36	+0.14	-0.18	-0.20

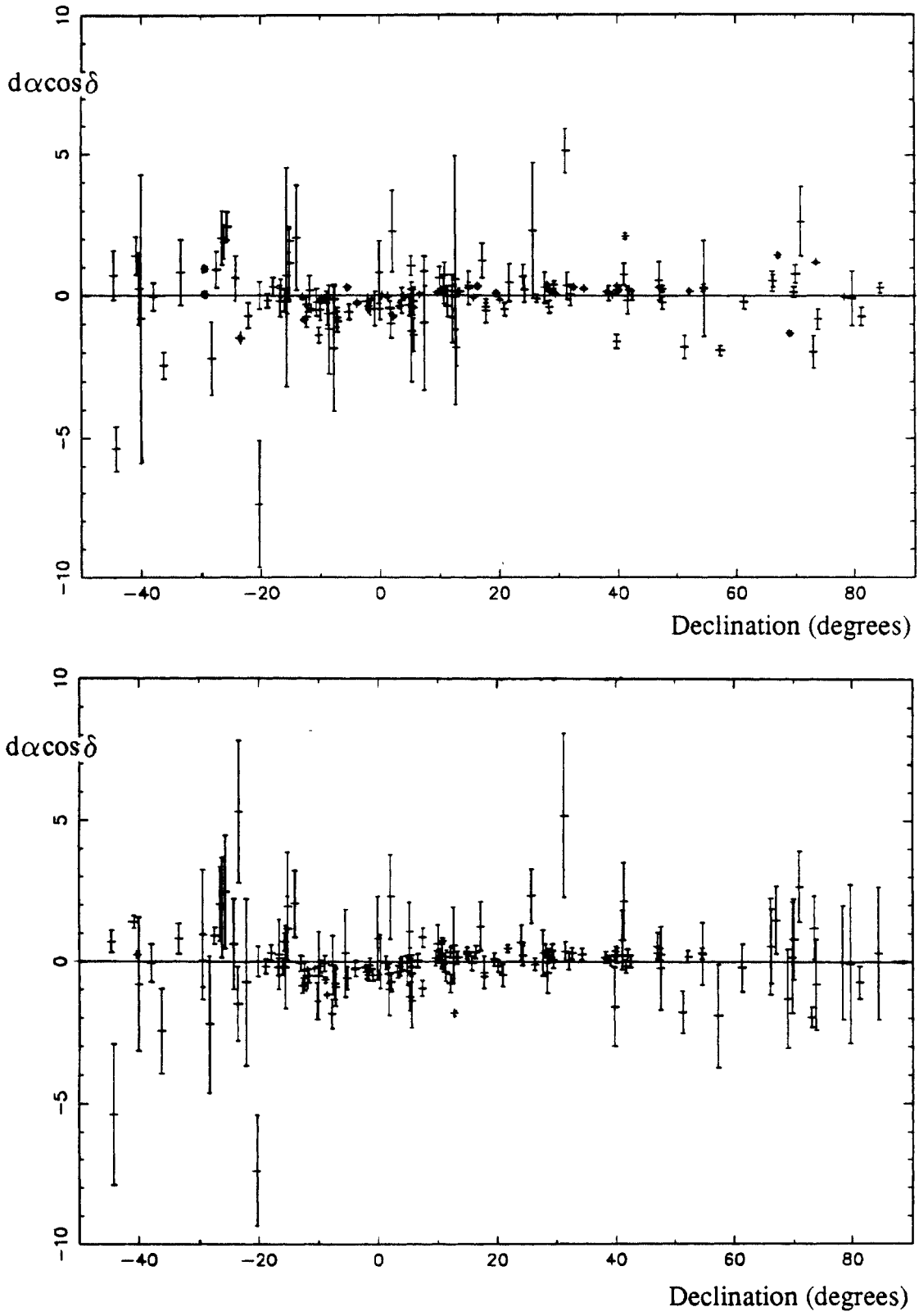

Figure 17. Residual differences in right ascension: JPL-IERS.
Upper part: with JPL error bars. Lower part: with IERS error bars.
Unit: 0.001".

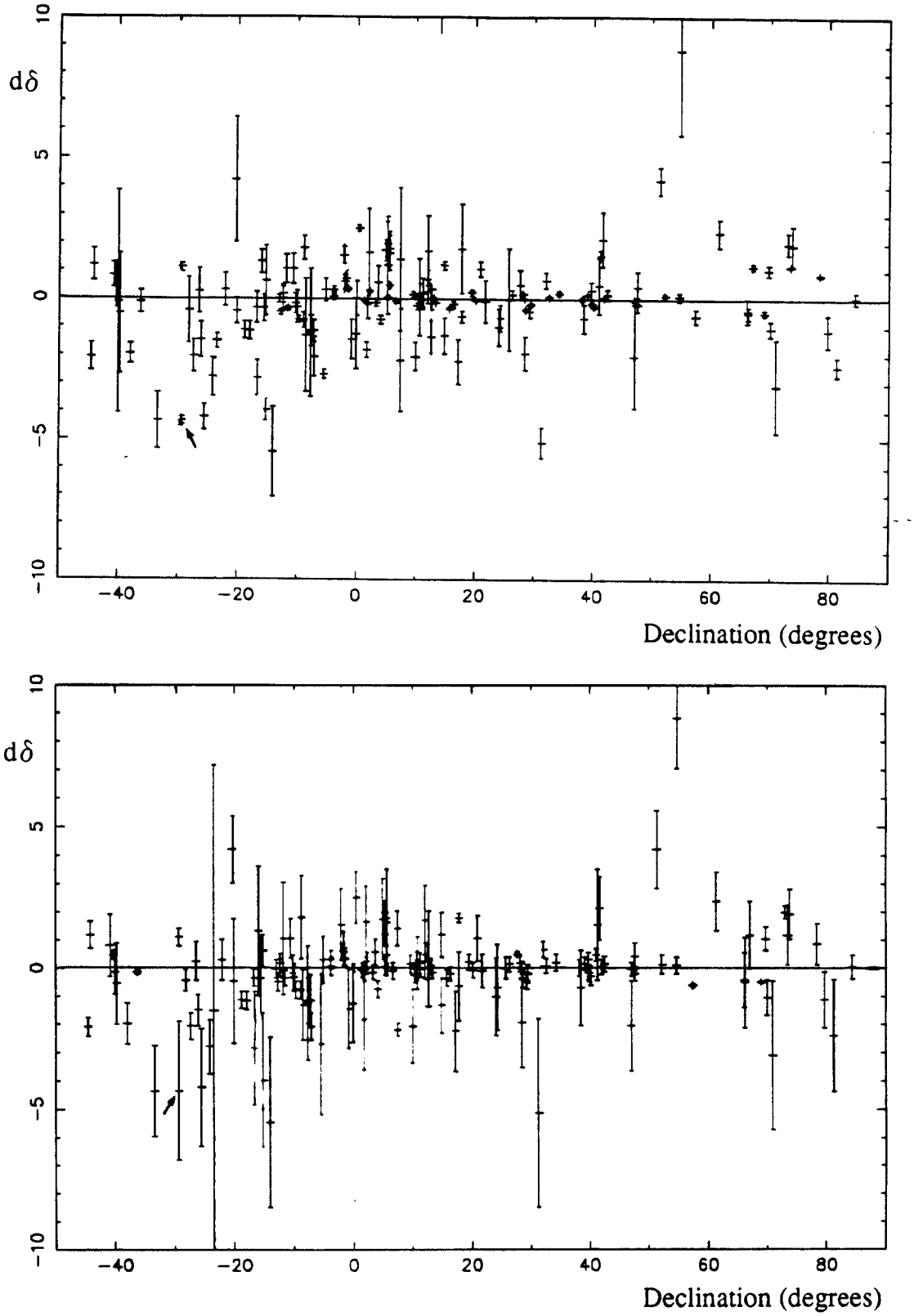

Figure 18. Residual differences in declination: JPL-IERS.
Upper part: with JPL error bars. Lower part: with IERS error bars.
Unit: 0.001".

3. CONNECTION OF THE HIPPARCOS FRAME

The Hipparcos mission

The satellite Hipparcos of the European Space Agency (ESA) was launched in August 1989. The mission will determine the positions, proper motions and parallaxes of about 120000 stars brighter than the 13th magnitude. Hipparcos is the first space astrometric mission. In addition to the advantages of observations made above the atmosphere, the originality of this project lies on the principle of differential measurements over large field which allow to eliminate regional errors affecting ground-based measurements over narrow field. The instrument aboard the satellite, the principle of observations and the method of data analysis are described by Kovalevsky (1980,1984) and Perryman (1989).

In the first step of the data reduction, the star to star angles measured during one or two rotations of the satellite (several hours) are projected on the same mean great circle with an arbitrary origin. In the second step, the reconstruction of the stellar sphere unifies the great circles origins and the coordinates of each star at its epoch of observation are computed in a coordinate system near the ecliptic system. Finally, the astrometric parameters - positions, proper motions and parallaxes - are estimated from these coordinates using a physical model accounting for the motion of the satellite around the Earth and the Sun and the light deflection produced by the gravitational field of the Solar System.

The error budget (ESA 1978) indicates that the precisions should be at the level of 0.002" in positions, 0.002"/year in proper motions and 0.002" in parallaxes of stars brighter than the 9th magnitude. Nevertheless, the astrometric potential of Hipparcos stellar reference frame will be achieved only if it is linked to a non-rotating celestial reference frame, *i.e.*, to the VLBI reference frame and to the planetary dynamical reference system. This link will allow

- to "stop" the rotation of the Hipparcos frame produced by galactic rotation,
- to densify the extragalactic frame by galactic objects accessible at optical wavelengths,
- to directly register the celestial objects structures obtained with radio and optical techniques at the same angular resolution.

Link objects between the Hipparcos and VLBI frames

The VLBI coordinates of extragalactic objects located at cosmological distance define a system of stable directions in space. The proper motions of quasars and active galactic nuclei are undetectable at the level of 20 microseconds of arc per year, as measured in the particular pair, but most probably representative, 3C345/NRAO512 (Bartel *et al.* 1986).

Having quasi point-like structures in the optical domain, quasars are well adapted for precise astrometric measurements but they are too faint for the Hipparcos satellite, and cannot be used to calibrate the proper motions of the stars. The brightest radio source is the quasar 3C273B (m_V = 12.5), but extragalactic objects have generally magnitudes larger than 17.

Froeschle and Kovalevsky (1982) present three methods to connect Hipparcos to the VLBI frame, based on

a) the positions measurements of bright radio stars with both the Hipparcos and VLBI techniques,
b) the observation of quasars with the VLBI technique, and of stars with the satellite, while their angular separations are measured with the Hubble Space Telescope (HST),

c) Hipparcos stars are connected by the HST to extragalactic objects whose radio emission is either non-existing or too weak to perform VLBI precise observations. This method prevents the Hipparcos frame to rotate but it does not contribute to the unification of the radio and the optical frames.

The use of radio stars as common objects (method a) to connect the two frames is the most direct method. However, the flux densities of radio stars are about 100 times weaker than those of the extragalactic radio sources normally observed with VLBI. Thus, radio stars are difficult to detect and their astrometric potential is weak if we use the classical "absolute" positioning VLBI technique with bandwidth synthesis delay observations. But milliarcsecond astrometric precision can be achieved by performing differential VLBI observations with a reference source angularly near the star (Lestrade *et al.*, 1990). The radio link stars must be brighter than magnitude 11 for good observation conditions by the satellite. Their radio components size must be smaller 0.001" in order not to be resolved by the VLBI observations. The flux density must be of at least a few mJy to match the sensitivity of phase-referencing VLBI technique. Besides, the optical and radio counterparts should coincide within 0.002". Following these criteria, Lestrade *et al.* (1982) established an initial list of 22 radio stars candidate for the link. Walter (1977) had also proposed a list of about 30 bright stars selected for their radio emission to link the radio and the optical frames; not all of them have been retained because some presented an extended radio structure. The Input Catalogue of the Hipparcos mission contains 186 radio stars (Argue 1989) but not all of them are suitable for the link. Four link stars (Algol, HR5110, λ And and σ Cr B) are in the FK4 and FK5.

Modelling of the link

As no regional deformations are expected for the Hipparcos frame, the link between the two frames can be mathematically expressed by a global rotation at an arbitrary epoch represented by a matrix [R], and by a matrix [$\dot{R}$] which represents the angular velocity of rotation of one frame relative to the other.

For each radio star the VLBI technique provides a vector $\vec{\sigma}_{vi}$ at an epoch t_{vi} of observation of the star, and the associated proper motion vector $\dot{\vec{\sigma}}_{vi}$. Similarly, the observations of the satellite give the vector $\vec{\sigma}_{Hi}$ at an epoch t_{Hi} of observation, and the associated proper motion vector $\dot{\vec{\sigma}}_{Hi}$.

At an instant t_i, two link equations between the two frames can be written in vectorial form for each star:

$$\vec{\sigma}_{vi}(t_i) = [R(t_i)] \cdot \vec{\sigma}_{Hi}(t_i) \qquad (4)$$

$$\dot{\vec{\sigma}}_{vi} = [R(t_i)] \cdot \dot{\vec{\sigma}}_{Hi} + [\dot{R}]\, \vec{\sigma}_{Hi}(t_i) \qquad (5)$$

The matrices [R] and [$\dot{R}$] are function of the rotation angles A_1, A_2, A_3 around the axes of one of the frames; the angular velocity of rotation is represented by the three time derivatives $\dot{A}_1$, $\dot{A}_2$, $\dot{A}_3$. There are six unknowns (the three rotation angles and their time derivatives), and so in principle two radio stars are sufficient to find a solution with the link equations (4) and (5) written in coordinates form. However, a solution with a larger number of stars to perform a least squares adjustment is preferable.

The director cosine vectors of a star and its proper motion are, in spherical equatorial coordinates

$$\vec{\sigma} = \begin{vmatrix} \cos\alpha \cos\delta \\ \sin\alpha \cos\delta \\ \sin\delta \end{vmatrix} \qquad (6)$$

$$\dot{\vec{\sigma}} = \begin{vmatrix} -\sin\alpha\cos\delta\,\mu_\alpha - \cos\alpha\sin\delta\,\mu_\delta \\ \cos\alpha\cos\delta\,\mu_\alpha - \sin\alpha\sin\delta\,\mu_\delta \\ \cos\delta\,\mu_\delta \end{vmatrix} \qquad (7)$$

The positions, α and δ, and proper motions, μ_α and μ_δ, are measured by the Hipparcos instrument and by VLBI at a variety of times. However the global rotation $[R(t_0)]$ must be determined at an arbitrarily chosen but unique epoch t_0. So the VLBI and Hipparcos positions must be re-writen in more general form:

$$\vec{\sigma}_{vi}(t_0) = \vec{\sigma}_{vi}(t_{vi}) + (t_0 - t_{vi})\,\dot{\vec{\sigma}}_{vi} \qquad (8)$$

$$\vec{\sigma}_{Hi}(t_0) = \vec{\sigma}_{Hi}(t_{Hi}) + (t_0 - t_{Hi})\,\dot{\vec{\sigma}}_{Hi} \qquad (9)$$

Inserting these relations into equations (4) and (5), one finds:

$$\vec{\sigma}_{vi}(t_{vi}) + (t_0 - t_{vi})\,\dot{\vec{\sigma}}_{vi} = [R(t_0)]\,\{\vec{\sigma}_{Hi}(t_{Hi}) + (t_0 - t_{Hi})\,\dot{\vec{\sigma}}_{Hi}\} \qquad (10)$$

$$\dot{\vec{\sigma}}_{vi} = [R(t_0)]\,\dot{\vec{\sigma}}_{Hi} + [\dot{R}]\,\{\vec{\sigma}_{Hi}(t_{Hi}) + (t_0 - t_{Hi})\dot{\vec{\sigma}}_{Hi}\} \qquad (11)$$

We parametrize the matrix $[R(t_0)]$ by three successive individual rotations around each axis. These three rotations are represented by the matrices $[R_X]$,$[R_Y]$,$[R_Z]$, the angle A_1, around the direction of the right ascension origin, the angle A_2 around the axis at 90° in the equator, and the angle A_3 around the direction of the celestial pole.

$$[R_X] = \begin{vmatrix} 1 & 0 & 0 \\ 0 & \cos A_1 & \sin A_1 \\ 0 & -\sin A_1 & \cos A_1 \end{vmatrix}$$

$$[R_Y] = \begin{vmatrix} \cos A_2 & 0 & -\sin A_2 \\ 0 & 1 & 0 \\ \sin A_2 & 0 & \cos A_2 \end{vmatrix}$$

$$[R_Z] = \begin{vmatrix} \cos A_3 & \sin A_3 & 0 \\ -\sin A_3 & \cos A_3 & 0 \\ 0 & 0 & 1 \end{vmatrix}$$

Developing the product of these three matrices, we obtain the rotation matrix

$$[R] = [R_Z].[R_Y].[R_X]$$

$$[R] = \begin{vmatrix} \cos A_2\cos A_3 & \cos A_1\sin A_3 + \sin A_1\sin A_2\cos A_3 & \sin A_1\sin A_3 - \cos A_1\sin A_2\cos A_3 \\ -\cos A_2\sin A_3 & \cos A_1\cos A_3 - \sin A_1\sin A_2\sin A_3 & \sin A_1\cos A_3 + \cos A_1\sin A_2\sin A_3 \\ \sin A_2 & -\sin A_1\cos A_2 & \cos A_1\cos A_2 \end{vmatrix} \qquad (12)$$

This matrix could be used to link the ecliptic coordinate system of Hipparcos to the equatorial VLBI coordinate system. Nevertheless, it is easier to transform the Hipparcos ecliptic coordinates into equatorial coordinates before the link. If we proceed in this way, the angles A_1, A_2, A_3 will be small quantities of the order of some tens of milliarcseconds ($\sim 10^{-7}$ rad), and we can approximate cos A_i ~1, sin $A_i \sim A_i$. The matrix $[R(t_0)]$ becomes:

$$[R(t_0)] = \begin{vmatrix} 1 & A_3 & -A_2 \\ -A_3 & 1 & A_1 \\ A_2 & -A_1 & 1 \end{vmatrix} \tag{13}$$

$[\dot{R}]$ is the matrix of elements $\dot{A}_1$, $\dot{A}_2$, $\dot{A}_3$ which expresses the relative angular velocity between the two frames. Assuming that this velocity is constant, we get

$$[\dot{R}] = \begin{vmatrix} 0 & \dot{A}_3 & -\dot{A}_2 \\ -\dot{A}_3 & 0 & \dot{A}_1 \\ \dot{A}_2 & -\dot{A}_1 & 0 \end{vmatrix} \tag{14}$$

Introducing (6), (7), (13) and (14), equations (10) and (11) can be written, in equatorial coordinates, as:

$$\begin{vmatrix} \cos\alpha_{vi}\cos\delta_{vi} \\ \sin\alpha_{vi}\cos\delta_{vi} \\ \sin\delta_{vi} \end{vmatrix} + \Delta t_{vi} \begin{vmatrix} -\sin\alpha_{vi}\cos\delta_{vi}\,\mu_{\alpha vi} - \cos\alpha_{vi}\sin\delta_{vi}\,\mu_{\delta vi} \\ \cos\alpha_{vi}\cos\delta_{vi}\,\mu_{\alpha vi} - \sin\alpha_{vi}\sin\delta_{vi}\,\mu_{\delta vi} \\ \cos\delta_{vi}\,\mu_{\delta vi} \end{vmatrix} =$$

$$\begin{vmatrix} 1 & A_3 & -A_2 \\ -A_3 & 1 & A_1 \\ A_2 & -A_1 & 1 \end{vmatrix} \cdot \begin{vmatrix} \cos\alpha_{Hi}\cos\delta_{Hi} + (-\sin\alpha_{Hi}\cos\delta_{Hi}\,\mu_{\alpha Hi} - \cos\alpha_{Hi}\sin\delta_{Hi}\,\mu_{\delta Hi})\,\Delta t_{Hi} \\ \sin\alpha_{Hi}\cos\delta_{Hi} + (\cos\alpha_{Hi}\cos\delta_{Hi}\,\mu_{\alpha Hi} - \sin\alpha_{Hi}\sin\delta_{Hi}\,\mu_{\delta Hi})\,\Delta t_{Hi} \\ \sin\delta_{Hi} + \cos\delta_{Hi}\,\mu_{\delta Hi}\,\Delta t_{Hi} \end{vmatrix} \tag{15}$$

$$\begin{vmatrix} -\sin\alpha_{vi}\cos\delta_{vi}\,\mu_{\alpha vi} - \cos\alpha_{vi}\sin\delta_{vi}\,\mu_{\delta vi} \\ \cos\alpha_{vi}\cos\delta_{vi}\,\mu_{\alpha vi} - \sin\alpha_{vi}\sin\delta_{vi}\,\mu_{\delta vi} \\ \cos\delta_{vi}\,\mu_{\delta vi} \end{vmatrix} =$$

$$\begin{vmatrix} 1 & A_3 & -A_2 \\ -A_3 & 1 & A_1 \\ A_2 & -A_1 & 1 \end{vmatrix} \cdot \begin{vmatrix} -\sin\alpha_{Hi}\cos\delta_{Hi}\,\mu_{\alpha Hi} - \cos\alpha_{Hi}\sin\delta_{Hi}\,\mu_{\delta Hi} \\ \cos\alpha_{Hi}\cos\delta_{Hi}\,\mu_{\alpha Hi} - \sin\alpha_{Hi}\sin\delta_{Hi}\,\mu_{\delta Hi} \\ \cos\delta_{Hi}\,\mu_{\delta Hi} \end{vmatrix} + \tag{16}$$

$$\begin{vmatrix} 0 & \dot{A}_3 & -\dot{A}_2 \\ -\dot{A}_3 & 0 & \dot{A}_1 \\ \dot{A}_2 & -\dot{A}_1 & 0 \end{vmatrix} \cdot \begin{vmatrix} \cos\alpha_{Hi}\cos\delta_{Hi} + (-\sin\alpha_{Hi}\cos\delta_{Hi}\,\mu_{\alpha Hi} - \cos\alpha_{Hi}\sin\delta_{Hi}\,\mu_{\delta Hi})\,\Delta t_{Hi} \\ \sin\alpha_{Hi}\cos\delta_{Hi} + (\cos\alpha_{Hi}\cos\delta_{Hi}\,\mu_{\alpha Hi} - \sin\alpha_{Hi}\sin\delta_{Hi}\,\mu_{\delta Hi})\,\Delta t_{Hi} \\ \sin\delta_{Hi} + \cos\delta_{Hi}\,\mu_{\delta Hi}\,\Delta t_{Hi} \end{vmatrix}$$

where $\Delta t_{vi}=t_0-t_{vi}$, $\Delta t_{Hi}=t_0-t_{Hi}$, $(\alpha_{vi}, \delta_{vi})$, $(\alpha_{Hi}, \delta_{Hi})$ are the equatorial coordinates of the i-th radio star obtained with VLBI and Hipparcos respectively, and $(\mu_{\alpha vi}, \mu_{\delta vi})$, $(\mu_{\alpha Hi}, \mu_{\delta Hi})$ are the components of their respective proper motions.

For N radio stars observed with both techniques, the matrix equations (15) and (16) give 4N independent equations with the six unknowns $A_1(t_0)$, $A_2(t_0)$, $A_3(t_0)$, A_1, A_2, A_3, which represent the link between the Hipparcos and the VLBI frames.

Simulation of Hipparcos data

We have simulated Hipparcos and VLBI astrometric data for a realistic set of stars to test the quality of the link. We have made the hypothesis that the parallax effects have been eliminated in Hipparcos as well as in VLBI data.

Equations (10) and (11) can be re-arranged for the simulation of data:

$$\vec{\sigma}_{Hi}(t_{Hi}) = \{[R(t_0)] + (t_{Hi} - t_0)\,[\dot{R}]\}^{-1}\,\{\vec{\sigma}_{vi}(t_{vi}) + (t_{Hi} - t_{vi})\,\dot{\vec{\sigma}}_{vi}\}, \quad (17)$$

$$\dot{\vec{\sigma}}_{Hi} = \{[R(t_0)] + (t_{Hi} - t_0)\,[\dot{R}]\}^{-1}\,\{\dot{\vec{\sigma}}_{vi} - [\dot{R}]\,\vec{\sigma}_{Hi}(t_{Hi})\}. \quad (18)$$

Adopting VLBI positions and proper motions at epochs t_{vi}, one can determine the corresponding Hipparcos coordinates at epochs t_{Hi}, after choosing the rotation angles A_1, A_2, A_3 and the angular velocities $\dot{A}_1$, $\dot{A}_2$, $\dot{A}_3$.

It is expected that less than 14 radio stars will be observed at multiple epochs by the VLBI technique. The initial VLBI observations of 10 stars are presented by Lestrade *et al.* (1988) and White *et al.* (1990). The simulation presented here concerns 14 radio stars. The simulated positions and proper motions used are listed in table 19; their distri-bution on the sky is shown on figure 19.

All these stars have non-thermal radio emission, and most of them belong to the type of spectroscopic close binary systems RSCVn. The extent on the sky of these systems are no more than 2 milliarcseconds and should not limit the VLBI astrometric measurements for Hipparcos. Algol does no belong to the RSCVn type, but it shows rather similar properties. Astrometrically, it is a multiple system formed by a close binary orbiting around a third component with a period of 1.86 years in an orbit of semi-major axis 0.040". The suitability of Algol for the astrometric link is questionable but special treatments of both the VLBI data and the Hipparcos data might make it useful. Cyg XI and LSI 61°303 are close binaries with strong X ray emission that are distant enough and hence point-like to make them good link objects.

The parameter values chosen for the simulation are

$A_1 = +0.030"$, $A_2 = +0.025"$, $A_3 = -0.045"$,

$\dot{A}_1 = +0.002"$/year, $\dot{A}_2 = -0.003"$/year, $\dot{A}_3 = +0.001"$/year, $t_0 = 1991.0$.

The optical coordinates and proper motions simulated for Hipparcos mission with these parameters are in table 20. We have modified the simulated Hipparcos coordinates as well as the simulated VLBI data by introducing gaussian noise. The uncertainties adopted in this simulation are based on ESA estimates of Hipparcos expected accuracy and on the most recent VLBI phase-referenced observations performed on Algol and σ CrB (Lestrade *et al.* 1990, Lestrade *et al.* 1992).

Table 19. Simulated VLBI positions and proper motions of the link stars.

Star	Right. Asc. J 2000.0 h m s	Declination J 2000.0 ° ' "	σ_α (1)	σ_δ (2)	Proper. motion μ_α (s/a)	μ_δ ("/a)	$\sigma\mu_\alpha$ (3)	$\sigma\mu_\delta$ (4)	Epoch -1900	
LSI 61°303	02 40 31.6860	61 13 45.560	1.3	2.0	0.0000	0.000	0.7	1.0	90.5	(w1)
			0.3	0.5			0.2	0.3		(w2)
ALGOL	03 08 10.1308	40 57 20.359	1.3	2.0	+0.0003	+0.002	0.7	1.0	88.5	(w1)
			0.7	1.0			0.5	0.7		(w2)
UX ARI	03 26 35.3375	28 42 56.026	1.3	2.0	+0.0016	- 0.106	0.7	1.0	88.5	(w1)
			0.3	0.5			0.2	0.3		(w2)
HR 1099	03 36 47.3251	00 35 18.600	1.3	20.0	- 0.0020	- 0.161	0.7	1.0	90.5	(w1)
			1.3	5.0			0.2	0.3		(w2)
HD 26337	04 09 40.8640	-07 53 35.640	6.7	10.0	+0.0010	+0.130	4.7	7.0	92.5	(w3)
			3.3	5.0			2.7	4.0		(w4)
HD 32918	04 55 11.0440	-74 56 16.020	6.7	10.0	+0.0072	+0.058	4.7	7.0	92.5	(w3)
			3.3	5.0			2.7	4.0		(w4)
AB Dor	05 28 44.5351	-65 27 02.191	6.7	10.0	+0.0084	+0.133	4.7	7.0	92.5	(w3)
			3.3	5.0			2.7	4.0		(w4)
HD 77137	08 59 42.7650	-27 48 58.110	6.7	10.0	- 0.0036	- 0.049	4.7	7.0	92.5	(w3)
			3.3	5.0			2.7	4.0		(w4)
HR 5110	13 34 47.6893	37 10 56.859	1.3	2.0	+0.0069	- 0.013	0.7	1.0	89.5	(w1)
			0.3	0.5			0.2	0.3		(w2)
σ CrB	16 14 41.2011	33 51 32.470	1.3	2.0	- 0.0221	- 0.080	0.7	1.0	87.5	(w1)
			0.3	0.5			0.2	0.3		(w2)
Cyg X-1	19 58 21.6804	35 12 05.887	1.3	2.0	- 0.0016	- 0.018	0.7	1.0	91.5	(w1)
			0.5	0.5			0.2	0.3		(w2)
AR Lac	22 08 40.8710	45 44 31.510	1.3	2.0	- 0.0028	+0.035	0.7	1.0	89.5	(w1)
			0.3	0.5			0.2	0.3		(w2)
SZ Psc	23 13 23.7645	02 40 31.310	1.3	20.0	- 0.0002	+0.041	0.7	1.0	92.5	(w1)
			0.3	5.0			0.2	0.3		(w2)
II Peg	23 52 29.0891	28 21 17.740	1.3	2.0	+0.0437	+0.038	0.7	1.0	92.5	(w1)
			0.3	0.5			0.2	0.3		(w2)

Units : (1) 0.0001s ; (2) 0.001" ; (3) 0.0001s/a ; (4) 0.001"/a.

Table 20. Simulated Hipparcos positions and proper motions of the link stars.

Star	Right. Asc. J 2000.0 h m s	Declination J 2000.0 ° ' "	σ_α (1)	σ_δ (2)	Proper motion μ_α (s/a)	μ_δ ("/a)	$\sigma\mu_\alpha$ (3)	$\sigma\mu_\delta$ (4)	Epoch -1900
LSI 61°303	02 40 31.685	61 13 45.561	3.3	5.0	+0.0001	+0.004	3.3	5.0	91.0
ALGOL	03 08 10.131	40 57 20.365	1.3	2.0	+0.0004	+0.006	1.3	2.0	91.0
UX ARI	03 26 35.341	28 42 55.762	1.3	2.0	+0.0017	- 0.103	1.3	1.0	91.0
HR 1099	03 36 47.323	00 35 18.521	1.3	2.0	- 0.0019	- 0.158	1.3	2.0	91.0
HD 26337	04 09 40.862	-07 53 35.833	1.3	2.0	+0.0010	+0.133	1.3	2.0	91.0
HD 32918	04 55 11.033	-74 56 16.105	1.3	2.0	+0.0067	+0.061	1.3	2.0	91.0
AB Dor	05 28 44.522	-65 27 02.388	1.3	2.0	+0.0081	+0.135	1.3	2.0	91.0
HD 77137	08 59 42.770	-27 48 58.033	1.3	2.0	- 0.0037	- 0.050	1.3	2.0	91.0
HR 5110	13 34 47.699	37 10 56.840	1.3	2.0	+0.0070	- 0.017	1.3	2.0	91.0
SIG CrB	16 14 41.123	33 51 32.188	1.3	2.0	- 0.0221	- 0.083	1.3	2.0	91.0
Cyg X-1	19 58 21.681	35 12 05.892	1.3	2.0	- 0.0017	- 0.018	1.3	2.0	91.0
AR Lac	22 08 40.866	45 44 31.559	1.3	2.0	- 0.0030	+0.037	1.3	2.0	91.0
SZ Psc	23 13 23.764	02 40 31.246	1.3	2.0	- 0.0001	+0.044	1.3	2.0	91.0
II Peg	23 52 29.023	28 21 17.681	1.3	2.0	+0.0436	+0.041	1.3	2.0	91.0

Units : (1) 0.0001s ; (2) 0.001" ; (3) 0.0001s/a ; (4) 0.001"/a.

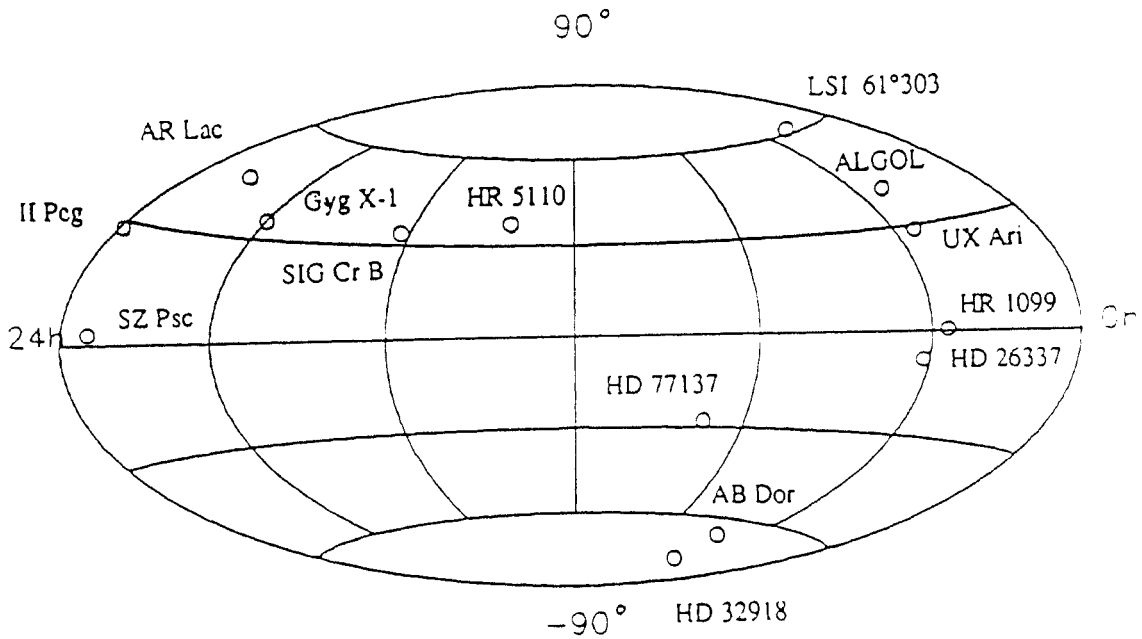

Figure 19. Sky distribution of the 14 radio stars considered in the simulation of the link.

Accuracy of the link

With equations (10) and (11) and the VLBI and Hipparcos simulated coordinates with added noise, we estimate the angles $A_1(t_0)$, $A_2(t_0)$, $A_3(t_0)$ between the axes of the frames, and the components of the angular velocity of rotation $\dot{A}_1$, $\dot{A}_2$, $\dot{A}_3$. We have analysed different cases of link to test the influence of the weighting of data and of the distribution of radio stars. The fit is done by a least squares analysis, with a weithging based on the uncertainties in the VLBI and Hipparcos positions and proper motions. We performed several solutions, assigning different values to the uncertainties in the VLBI data (see table 19).

Tables 21 and 22 present the results obtained by fixing the uncertainties of the positions and proper motions of the northern stars to the values indicated with (w1) in table 19. In case 1 we have adopted the values 0.010" and 0.007"/year for the errors of the coordinates and the proper motions determined with VLBI for the southern stars (values indicated with (w3) in table 19). When these values are reduced to one half (case 2), the precision of the link is 10% better, but the consistency between the adopted and the calculated values of the six link parameters, as well as the correlation coefficients remain unchanged. The parameter R indicates the goodness of the fit normalized by the number of degree of freedom (Bevington, 1969).

In case 3 we have performed the link using only the 10 radio stars in the northern hemisphere. When compared to the solution with the 14 stars, the consistency between the angles A_i and the components of the angular velocity $\dot{A}_i$, the correlation coefficients do not change. The precision of the adjustment, given by the rms post-fit residuals (σ in table 20) is 25% better when only the 10 northern radio stars are included in the link.

Table 21. Results of the simulated VLBI-Hipparcos astrometric link. N is the number of stars used, σ is the standard deviation of the residuals after the fit and R is the goodness of fit. Unit for A_1, A_2, A_3, and σ : 0.001" - Unit for $\dot{A}_1$, $\dot{A}_2$, $\dot{A}_3$, : 0.001"/a.

Case	N	A_1	A_2	A_3	$\dot{A}_1$	$\dot{A}_2$	$\dot{A}_3$	σ	R	Comments
										North and South stars
1	14	+31.33±1.7.	+22.78±1.54	-44.34±1.15	+2.11±1.13	-3.31±1.01	+1.52±0.76	2.10	1.34	VLBI uncertainties of South stars: 0.010" and 0.007"/a
2	14	+31.20±1.65	+22.96±1.40	-44.33±1.13	+2.00±1.09	-3.24±0.90	+1.38±0.74	2.03	1.34	VLBI uncertainties of South stars: 0.005" and 0.004"/a
										North stars only
3	10	+31.44±1.50	+22.96±1.40	-44.34±1.01	+2.14±1.01	-3.70±0.95	+1.65±0.67	1.56	1.01	All
4	9	+31.79±1.34	+23.16±1.19	-44.27±1.07	+1.35±0.83	-3.12±0.75	+1.47±0.70	1.79	1.17	LSI 61°303 deleted
5	9	+32.49±1.17	+22.79±1.03	-43.10±1.10	+1.79±0.77	-3.31±0.67	+1.64±0.70	1.66	0.96	HR 1099 deleted
6	9	+31.41±1.32	+23.13±1.18	-44.13±1.07	+1.03±0.85	-3.27±0.76	+1.70±0.71	1.77	1.10	ALGOL deleted
7	9	+32.18±1.34	+23.32±1.13	-43.83±1.08	+1.20±0.89	-3.02±0.74	+1.43±0.74	1.78	1.11	σCrB deleted
8	9	+32.02±1.17	+22.96±1•04	-44.43±1.03	+1.02±0.75	-3.43±0.70	+0.66±0.70	1.91	0.97	SZ Psc deleted
9	9	+31.18±1.25	+21.54±1.16	-44.32±0.98	+1.57±0.79	-2.48±0.74	+1.58±0.65	1.67	0.96	AR Lac deleted
10	9	+32.33±1.17	+24.65±1.18	-44.57±1.00	+1.30±0.75	-2.77±0.74	+1.54±0.66	1.69	0.97	IIPeg deleted
11	8	+32.21±1.29	+22.94±1.14	-43.15±1.17	+1.85±0.83	-3.38±0.72	+1.67±0.74	1.68	1.07	LSI 61°303, HR 1099 deleted
12	7	+32.03±1.39	+23.17±1.15	-42.19±1.26	+1.63±1.00	-3.56±0.77	+2.08±0.84	1.63	1.01	ALGOL, σCrB, HR1099 deleted
13	8	+32.46±1.10	+22.77±0.97	-43.18±1.13	+1.44±0.73	-3.68±0.67	+0.68±0.73	1.79	0.85	HR1099, SZ Psc deleted
14	5	+30.76±1.29	+23.91±1.34	-42.23±1.17	+1.69±0.94	-2.29±0.86	+2.52±0.77	1.34	0.71	ALGOL, HR1099, HD32918, σCrB, AR Lac, IIPeg deleted
15	5	+31.33±1.78	+22.94±1.65	-42.11±1.49	+1.66±1.32	-4.51±1.13	+1.13±1.01	1.68	1.00	ALGOL,σCrB, HR1099,LSI61°303 deleted

Table 22. Adjustments to the a priori angles, in relative value with respect to their formal uncertainties.

Case	ΔA_1	ΔA_2	ΔA_3	$\Delta \dot{A}_1$	$\Delta \dot{A}_2$	$\Delta \dot{A}_3$	Correlation coefficients					
							A_1, A_2	A_1, A_3	A_2, A_3	$\dot{A}_1, \dot{A}_2$	$\dot{A}_1, \dot{A}_3$	$\dot{A}_2, \dot{A}_3$
1	0.8	-1.4	0.6	0.1	-0.3	0.7	-0.06	+0.31	-0.18	-0.05	+0.27	-0.18
2	0.7	-1.5	0.6	0.0	-0.3	0.5	-0.06	+0.30	-0.21	-0.06	+0.26	-0.22
3	1.0	-1.5	0.7	0.1	-0.7	1.0	-0.01	+0.32	-0.16	-0.04	+0.28	-0.15
4	1.3	-1.5	0.7	-0.8	-0.2	0.7	+0.01	+0.24	-0.13	-0.10	+0.19	-0.09
5	2.1	-2.1	1.7	-0.3	-0.5	0.9	+0.02	+0.28	-0.12	+0.06	+0.23	-0.10
6	1.1	-1.6	0.8	-1.1	-0.4	1.0	-0.03	+0.23	-0.18	+0.06	+0.15	-0.17
7	1.6	-1.5	1.1	-0.9	-0.0	0.7	+0.03	+0.26	-0.10	+0.14	+0.21	-0.06
8	1.7	-2.0	0.6	-1.3	-0.6	-0.9	+0.01	+0.31	-0.08	+0.09	+0.30	-0.02
9	0.9	-2.9	0.7	-0.5	0.7	0.9	+0.11	+0.17	-0.06	+0.19	+0.13	-0.04
10	2.0	-0.3	0.4	-0.9	0.3	0.8	+0.04	+0.20	-0.12	+0.13	+0.15	-0.09
11	1.7	-2.1	1.6	-0.2	-0.5	0.9	-0.01	+0.27	-0.15	+0.05	+0.22	-0.11
12	1.5	-1.6	2.2	-0.4	-0.7	1.3	-0.08	+0.33	-0.19	-0.07	+0.31	-0.16
13	2.2	-2.3	1.6	-0.8	-1.0	-0.9	+0.02	+0.30	-0.12	+0.08	+0.24	-0.08
14	0.6	-0.8	2.4	-0.3	0.8	2.0	+0.06	+0.13	-0.17	+0.06	+0.12	-0.13
15	0.7	-1.2	1.9	-0.3	-1.3	0.1	-0.15	+0.43	-0.33	-0.11	+0.43	-0.25

Seven other cases of link have been analysed including nine radio stars at positive declinations (cases 4 to 10). Here, we intend to test the influence of individual objects on the link. In each case, one object has been eliminated, because its physical and/or astrometric characteristics make it a particular case. The precision of the adjustement given by the rms of the post-fit residuals and by the values of the parameter R indicates that the quality of the link in either of these cases is comparable to that of case 3 (only northern stars).

Table 23 presents the mean adjustment to the a priori angles and rates when the lowest values of the VLBI uncertainties are considered (indicated with (w2) in table 19), and the errors in Hipparcos data are fixed to the values indicated with (w4) in table 19. In this analysis we have considered two cases of link: all 14 radio stars and only the 10 stars at positive declinations. Comparing these results with cases 2 and 3 of table 22 we find that, when the uncertainties of the VLBI data are four times better than the Hipparcos astrometric uncertainties the precision of the link given by the 14 radio stars is more than 50% higher for the angles A_i, and that the error in the components $\dot{A}_i$ of the relative velocity of rotation is between 10% to 30% better than the Hipparcos astrometric uncertainties. When only the 10 northern radio stars are considered, the best estimates of the VLBI data errors lead to a solution 40%-80% more precise in the angles A_i, and 2%-30% more precise in their time derivatives $\dot{A}_i$.

Table 23. Accuracy of the simulated link between Hipparcos and VLBI reference frames via radio stars. Units of A_k = 0.001", units of $\dot{A}_k$: 0.001"/year, σ are the post-fit residuals, in units of 0.001", R is the goodness-of-fit parameter.

N	14 All stars	10 Northern stars
A1	+ 1.09 ± 0.91	+ 1.45 ± 0.87
A2	- 1.67 ± 0.91	- 1.73 ± 0.79
A3	+ 0.07 ± 0.73	+ 0.35 ± 0.71
$\dot{A}1$	- 0.51 ± 0.82	- 0.56 ± 0.79
$\dot{A}2$	+ 0.22 ± 0.77	+ 0.02 ± 0.72
$\dot{A}3$	+ 0.08 ± 0.67	+ 0.55 ± 0.66
σ	1.92	1.55
R	1.55	1.25

CONCLUSION

The celestial system of the International Earth Rotation Service (IERS) is maintained for the study of the Earth's orientation and geodynamics studies at the level of 0.0001". The direction of its axes relative to physical directions related to the Earth rotation (mean celestial pole) and orbit (dynamical equinox) are known within ±0.001" and ±0.005" respectively. Its 1991 realization contains 396 objects in the declination range -84° to +85°, nearly 100 objects have positions that are known within ±0.0005". Its largest systematic errors are smaller than 0.002", associated with low declinations.

The International Astronomical Union recommends that efforts be made to elaborate a list of primary radio sources which will define the direction of axes of the primary celestial frame, and a list of secondary sources candidate to become primary in the future. In agreement with these recommendations, and using the wealth of observations accumulated in the Earth rotation and other programs, the Central Bureau of IERS processes VLBI results from IERS analysis centres and evaluate their astrometric quality on a regular basis.

From the analysis of the differences between five pairs of independent VLBI catalogues of extragalactic radio sources available in 1990 from GSFC, JPL, NGS, and USNO, we can make the following comments. The formal uncertainties on the source coordinates in the catalogues follow a law in $N^{-0.5}$ for numbers of observations up to a few thousands. A limit is reached at the level of 0.0001" in the case of GSFC. The dominant source of dispersion in the source coordinates seems to be the low declinations, an effect already mentionned by several analysts. This effect is not reflected in full scale by the formal uncertainties. The source coordinates uncertainty, estimated from the comparisons on the 39 sources common to the four catalogs, is at the level of 0.0002" in the northern hemisphere, and not larger than 0.0009" in the southern hemisphere. The influence, if any, of the total flux, the spectral index, the type of object, and the redshift of the sources is presently overruled by the low declination effect.

The comparison of global frames obtained either by combining the observations of various networks, or by combining the partial frames based on these various networks shows a good statistical agreement of the two sets of coordinates. The distribution of the differences is consistent with the formal uncertainties evaluated by IERS.

The contribution of Earth rotation observations to the extragalactic celestial frame includes the monitoring of the sources. The data available to IERS in 1991 concern 179 sources monitored in at least two programs of observations. The histogram of their position uncertainties, derived from the agreement of coordinates in the GSFC and JPL analyses, after taking out a global relative rotation, is plotted in figure 20. Also available to IERS are 217 objects (113 in the northern hemisphere, 104 in the southern hemisphere) with coordinates in only one frame (GSFC: 153 objects; JPL: 64 objects). The networks are operated in parallel by groups which tend to extend their lists of observed objects both with common and non common sources, in order to perpetuate their celestial references on a sound basis; this results in a progressive improvement in precision and distribution of the global celestial frame. In the near future, as a consequence of the extension of the networks in the southern hemisphere for a better coverage of the planet, the sky coverage in the southern hemisphere will be improved, and the systematic errors due to unsatisfactory latitude distribution of stations will be diminished.

The link between the extragalactic VLBI and the galactic Hipparcos frames via radio stars has been evaluated, based on a realistic simulation of the Hipparcos mission and on the distribution of stars likely to be measured by VLBI. It is shown that the rotation at the initial epoch can be determined with an accuracy at the milliarcsecond level. The accuracy of the relative rotation velocity is in the range 0.0007"/year - 0.0015"/year. Although the number of link stars is relatively small, the tests have shown that the solution for the rotation angles is robust.

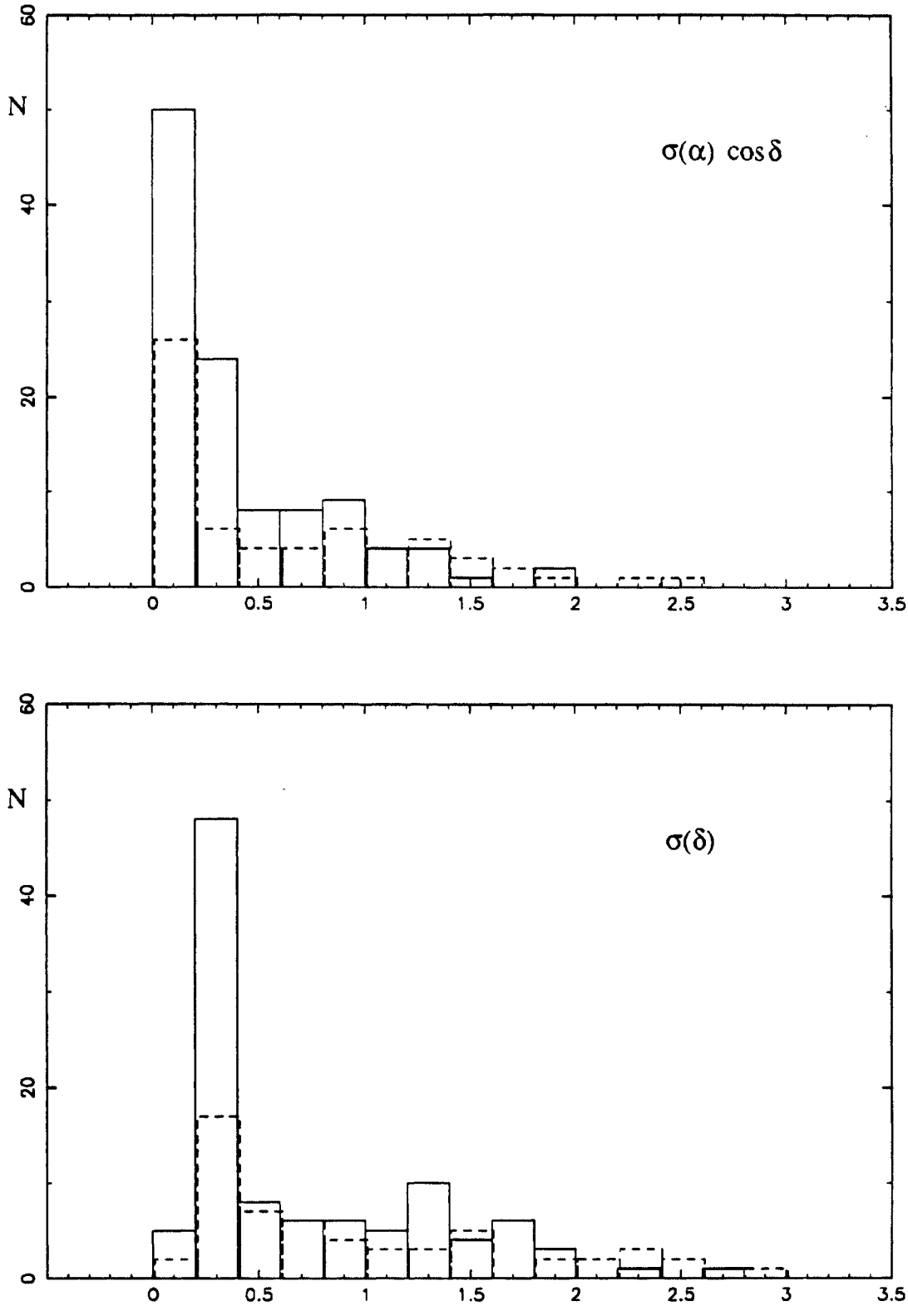

Figure 20. Histogram of the precision of source coordinates in the IERS celestial reference frame for 170 objects available from two programs; northern hemisphere (solid line) and southern hemisphere (dashed line). Unit: 0.001".

References

Argue, A.N., 1989: Coordinating Optical and Radio Reference Frames, Impact of Hipparcos.

Arias, E.F., Feissel, M., Lestrade, J.-F., 1988: *BIH Annual Report for 1987*, D-113.

Arias, E.F., Feissel, M.,1990: *Proc. IAU Symp.* ***141***, 119, Kluwer.

Bartel, N., Herring, T.A., Ratner, M.I., Shapiro, I.I., Corey, B.E., 1986: *Nature* **319,** 733.

Bevington, P.R., 1969: *Data Reduction and Error Analysis for the Physical Sciences*, Ch. 10, McGrow-Hill Book Company.

Carter, W.E., 1987: *Internal. memo.* IERS, December 1987.

Carter, W.E., Robertson, D., 1990: *IERS Technical Note* ***5***, 25.

Carter, W.E., Robertson, D., 1991: *IERS Technical Note* ***8***, 87.

Charlot, P., 1990: *Astron. Astrophys.*, **299**, 51.

Charlot, P., 1991: Private communication (work in collaboration with W.M. Folkner, J.G. Williams, O.J. Sovers, XX Newhall).

Eubanks, T.M., Carter, M.S., Josties, F.J., Matsakis, D.N., McCarthy, D.D., 1991: *Proc. IAU Coll. 127,* Hughes, J.A., Smith, C.A., Kaplan, G.H. (eds), 256.

Eubanks, T.M., Carter, M.S., Josties, F.J., Matsakis, D.N., McCarthy, D.D., 1991: *IERS Technical Note* ***8***, 95.

ESA, 1978: European Space Agency, DP/PS (78) 13, Paris 26 April 1978.

Feissel, M., 1991: *Proc. IAU Coll. 127,* **101**, US Naval Observatory, 101.

Finger, M.H. and Folkner, W.M., 1992: *TDA Progress Report,* Jet Propulsion Laboratory (in press).

Fricke, W., 1982: *Astron. Astrophys.*, **107**, L13 - 16.

Fricke, W., Schwan, H., and Lederle, T., 1988: *Fifth Fundamental Catalogue, Part I.* Veröff. Astron. Rechen Inst. Heidelberg.

Froeschle, M., Kovalevsky, J., 1982: *Astron. Astrophys.* **116**, 89.

Hazard, C., Sutton, J., Argue, A.N., Kenworthy, C.M., Morrison, L.V., Murray, C.A., 1971: *Nature*, **233**, 89.

IERS, 1989: *Annual Report for 1988.* Observatoire de Paris.

IERS, 1990: *Annual Report for 1989.* Observatoire de Paris.

IERS, 1991: *Annual Report for 1990.* Observatoire de Paris.

Kovalevsky, J., 1980: *Cel. Mech.* **22**, 153.

Kovalevsky, J., 1984: *Space Sci. Rev.* **39**, 1.

Lestrade, J.-F., Preston, R.A., Slade, M.A., 1982: *Very Long Baseline Interferometry Techniques, Conf. CNES*, Toulouse, France, F. Biraud (ed.), Ed. Cepadues, 199.

Lestrade, J.-F., Niell, A.E., Preston, R.A., Mutel, R.L., 1988: *Astron. J.* **96**, 1746.

Lestrade, J.-F., Rogers, A.E.E., Whitney, A.R., Niell, A.N., Phillips, R.B., Preston, R.A., 1990: *Astron. J.*, **99**, 1663.

Lestrade, J.-F., Phillips, R.B., Preston, R.A., Grabuzda, D.C., 1992: *Astron. Astrophys.*, (in press).

Ma, C., Ryan, J.W., Caprette, D.S., 1990: *IERS Technical Note 5*, 1.

Ma, C., Ryan, J.W., Caprette, D.S., 1991: *IERS Technical Note 8*, 47.

Ma, C. and Shaffer, D.B., 1991: *Proc. IAU Coll. 127*,.U.S. Naval Observatory.135.

McCarthy, D.D., (ed.), 1989: IERS Standards (1989). *IERS Technical Note No 3.*

Perryman, M.A.C., 1989: *Nature*, **340**, 111.

Preston, R.A., Morabito, D.D., Williams, J.G., Faulkner, J., Jauncey, D.L., Nicolson, G.D., 1985: *Astron. J.*, **90**, 1599.

Schwan, H., 1988: *Astron. Astrophys.*, **198**, 116 - 124.

Sovers, O.J., 1990: *Proc. IAU Symp.* **141**, 261, Kluwer.

Sovers, O.J., 1991a: *Proc. IAU Coll.* **127**, 130, U.S. Naval Observatory..

Sovers, O.J., 1991b: *TDA Progress Report* 42-106. Jet Propulsion Laboratory, 364.

Steppe, J.A., Oliveau, S.H., Sovers, O.J., 1990: *IERS Technical Note 5*, 13.

Steppe, J.A., Oliveau, S.H., Sovers, O.J., 1991: *IERS Technical Note 8*, 9.

Vondrak, J., 1977: *Bull. Astron. Czechosl.* **28**, 84.

Walter, H.G., 1977: *Astron. Astroph. Supplement* **30**, 381.

White, G.W., Lestrade, J.-F., Jauncey, D.L., Phillips, R.B., Preston, R.A., Reynolds, J.E., 1990: A. J. 99, 405.